

*In vivo* evaluation of gene editing and prosthetic strategies to restore vision in small and large animal models of retinal degeneration

Présentée le 24 janvier 2020

à la Faculté des sciences et techniques de l'ingénieur  
Chaire Medtronic en Neuroingénierie  
Programme doctoral en neurosciences

pour l'obtention du grade de Docteur ès Sciences

par

**Paola VAGNI**

Acceptée sur proposition du jury

Prof. F. Schürmann, président du jury  
Prof. D. Ghezzi, directeur de thèse  
Prof. Y. Arsenijevic, rapporteur  
Prof. S. Kleinlogel, rapporteuse  
Prof. M. Herzog, rapporteur

*So long, and thanks for all the fish*

## ***Acknowledgments***

Foremost, I would like to express my sincere gratitude to my advisor Prof. Diego Ghezzi, who helped me during all the steps of this PhD: from applying to the doctoral school to writing the final thesis. I feel the pressure of being the first PhD student to graduate from the lab, but I hope I lived up to the expectations.

Besides my advisor, I would like to thank the rest of my thesis committee, Prof. F. Schürmann, Prof. Y. Arsenijevic, Prof. S. Kleinlogel, and Prof. M. Herzog, for taking the time out of their busy schedules to evaluate my work and be present to my defense.

A sincere thanks to the people from the Italian Institute of Technology in Genova for their precious help and advice, without which the gene editing project would not have been successfully concluded: Dr. Laura Cancedda, Dr. Andrea Contestabile, and Dr. Laura Perlini. I am also grateful to Laura Perlini and Andrea Contestabile for teaching me everything I know (still not enough) about molecular biology, which made me decide that I do not like it that much. A special thanks go to Tommaso, who helped me with the experiments during his Master's thesis and is now doing his PhD in Zurich.

The microscopy facility of the Campus Biotech was essential during these years. Specifically, the help and feedback of Dr. Laura Batti was instrumental for my work and very much appreciated.

Serendipity made some incredibly nice and interesting people collide into the LNE micro-environment. I would like to thank all of them for making this journey possible. Doing a PhD can be tough at times, but working in a nice and supportive environment is surely part of the recipe for success. Nevertheless, I am aware of your demand for personal acknowledgments. Therefore, without further ado, thanks to (in no particular order): Laura for teaching me a lot about the royal family; Marta for explaining me more than I would have liked to know about rabbits; Naïg for showing me how to pour (and more importantly drink) absinthe; Vivien for the random, and not always called for, coffee-time insights; Adele for bringing a lot of amazing food (and not eating it herself); Eleonora for teaching me how to fall gracefully; Giulia for keeping me alive the first time I climbed outside; Enrico for being generally oddly knowledgeable; Elodie for being a boss at bending metal; Charles for his enthusiasm about, well, anything; Jake for teaching me how to properly pronounce the word "gin".

An immense thank you goes to the friends who were always there for me during these years, especially Marta and Barbara, for the emotional support. I am grateful to the 21st-century technology which allows them to check up on me, despite living in different countries. I want to additionally thank Marta (and Andrea) for hosting me in their apartment in London many times, especially when they were not there. A personal thank you to: Mél for making me discover how delicious vegan food can be and for the patience and support, to Jas for wanting to hang out with me even if I do not like people that much, and to Andreas without whom I would not have a bed in my apartment.

Last but not the least, I would like to thank my parents, first of all for giving me the opportunity to pursue my studies and as well for always believing in me and helping me when I needed it the most.

I would finally like to remind everyone that I find it incredibly difficult to write this kind of content, which I am aware might have turned out not especially brilliant. Please, be gentle.

*Paola*

## Abstract

Inherited retinal diseases (IRDs) form a group of diverse disorders that lead to the degeneration of the light-sensing cells of the retina: the photoreceptors. IRDs are among the leading causes of blindness in working-age adults living in industrialized countries and their treatment has been a long-term challenge in medicine. Given the heterogeneity of IRDs in terms of causative genes and symptoms, finding a common therapy is not a real possibility. Conversely, it is important to research as many different approaches as possible so as to have the opportunity to decide which one to use for a specific patient. The outcome of clinical interventions depends in large part on the preclinical research conducted on animal models. As an example of this, this thesis illustrates two preclinical approaches to the treatment of retinal degenerations that lie at the opposite ends of the spectrum of available therapies.

The first approach discussed is gene editing. This strategy is most effective during the development of the retina and can be used to correct genetic mutations causing the degeneration of photoreceptors on the progenitor cells. Here, we used a tailored gene editing system based on clustered regularly interspaced short palindromic repeats (CRISPR)/CRISPR-associated protein 9 (Cas9) to prevent photoreceptor death in the retinal degeneration 10 (Rd10) mouse model of retinitis pigmentosa. The construct was delivered in the photoreceptor cells by electroporation and targets the mutated gene, editing its sequence with the help of a DNA repair template. This technique for gene editing has shown promising results in terms of visual function preservation in mice, inspiring further research into viral-free gene editing approaches.

On the opposite side of the range of therapeutic options, prosthetic devices are generally used for late-stage retinal degeneration since they bypass the photoreceptor layer and rely on the retinal internal circuits to perform visual stimulation. In this work, I describe a series of experiments performed to test the POLYRETINA photovoltaic epiretinal visual prosthesis, previously developed by our laboratory, in a minipig model of chemically induced retinal degeneration. First, the visual responses were carefully characterized in the animal model before and after the injection of the toxin. Then, preliminary results were obtained using the prosthesis to stimulate the blind retina. Although the experiments are still ongoing, the results are encouraging and demonstrate that we could indeed use a completely photovoltaic prosthesis to restore visual perception in blind patients.

In conclusion, this thesis displays preclinical research concerning two ways to restore vision, each adapted to a different stage of retinal degeneration. The overarching goal is to improve as much as possible the outcome of the therapy for the benefit of blind patients. To this end, we need to continue to test all the approaches that have so far showed promising results, such as the ones presented herein, while continuing to develop new ones. This outlook, implemented at the preclinical level, can lead to the best chances of a successful clinical intervention. At the same time, the diagnostic tools need to be perfected and precisely utilized to determine which therapeutic option is best suited for a specific patient.

**Keywords:** retinal degeneration, retinitis pigmentosa (RP), gene editing, vision restoration, visual function preservation, CRISPR/Cas9, retina, photoreceptors, retinal prosthesis, POLYRETINA, rd10, electroporation, animal model, inherited retinal diseases (IRDs).

## Sommario

Le degenerazioni retiniche ereditarie sono un gruppo diversificato di patologie che portano alla degenerazione dei fotorecettori, le cellule fotosensibili della retina. Il trattamento di questi disturbi, tra le maggiori cause di cecità nella popolazione adulta dei paesi industrializzati, è da sempre una sfida per la medicina. Data l'eterogeneità delle patologie, in termini di mutazioni genetiche coinvolte e sintomi, non è possibile trovare una terapia comune. Al contrario, è importante sviluppare e testare il maggior numero possibile di soluzioni terapeutiche, in modo da avere la possibilità di scegliere quale applicare basandosi sulla specifica situazione del paziente. L'esito della terapia nei pazienti dipende dalla ricerca preclinica che viene condotta sui modelli animali. Questa tesi ne è un esempio, presentando due approcci preclinici differenti che si possono collocare ai due poli opposti dello spettro delle terapie al momento disponibili.

Il primo approccio che viene discusso è l'editing genomico (correzione genetica). Questa strategia è efficace durante lo sviluppo della retina e può essere utilizzata per correggere le mutazioni genetiche che causano la degenerazione dei fotorecettori direttamente sulle cellule progenitrici della retina. La tecnica presentata, basata sull'uso di CRISPR/Cas9 (proteina associata (Cas9) a brevi sequenze palindrome di DNA ad intervalli regolari (CRISPR)), permette la modificazione genetica mirata di una mutazione nel DNA che causa la degenerazione dei fotorecettori in un modello murino di retinitis pigmentosa (topo Rd10). Il costrutto viene inserito nei fotorecettori tramite elettroporazione e si lega, taglia e infine modifica il gene di interesse con l'aiuto di una sequenza modello di DNA. I risultati ottenuti nel modello murino per quanto riguarda la preservazione funzionale della vista suscitano interesse nei confronti della ricerca sui metodi di editing genetico che non si basano su vettori virali.

Dall'altro estremo dello spettro terapeutico troviamo le protesi retiniche che vengono normalmente usate in situazioni in cui la degenerazione dei fotorecettori è molto avanzata. Le protesi aggirano totalmente lo strato dei fotorecettori, stimolando elettricamente i circuiti interni della retina. In questa tesi vengono presentati i risultati ottenuti utilizzando la protesi retinica fotovoltaica sviluppata precedentemente dal nostro laboratorio (POLYRETINA) in un modello animale di minipig con cecità indotta chimicamente. Per prima cosa, la risposta visiva degli animali viene caratterizzata prima e dopo l'iniezione della tossina. In seguito, vengono presentati i risultati preliminari relativi alla stimolazione della retina degli animali ciechi, ottenuti utilizzando la protesi retinica. Gli esperimenti sono tuttora in fase di realizzazione, ma i risultati sono incoraggianti e fanno pensare che questo approccio possa essere utilizzato in futuro anche sui pazienti.

Per concludere, questo lavoro mostra due approcci alla ricerca preclinica, ognuno adattato a una differente fase di degenerazione della retina. Dal momento che l'obiettivo globale è di ottenere il miglior risultato possibile nei pazienti, è importante testare le terapie che si dimostrano promettenti, come quelle qui presentate, continuando allo stesso tempo a sviluppare nuovi approcci terapeutici. I migliori risultati in ambito clinico si possono ottenere tenendo questa prospettiva in mente a partire dalla fase preclinica. Inoltre, è necessario perfezionare e utilizzare correttamente gli strumenti diagnostici per determinare quale opzione sia la migliore per ogni specifico paziente.

**Parole chiave:** degenerazioni retiniche ereditarie (DREs), retinitis pigmentosa (RP), editing genetico, preservazione della vista, CRISPR/Cas9, retina, fotorecettori, protesi retiniche, POLYRETINA, rd10, elettroporazione, modelli animali.

# Contents

<b>1 Introduction</b>	<b>1</b>
1.1 The Visual System and the Retina . . . . .	2
1.2 Inherited Retinal Diseases (IRDs) . . . . .	4
1.3 Animal Models of Retinal Degeneration . . . . .	6
1.4 Therapeutic Approaches to Restore Vision . . . . .	7
1.4.1 Neuroprotection . . . . .	8
1.4.2 Retinal Prostheses . . . . .	8
1.4.3 Optogenetics . . . . .	11
1.4.4 Cell Transplantation and Retinal Regeneration . . . . .	12
1.4.5 Gene Therapy . . . . .	12
1.5 Delivering Therapeutic Agents to the Retina . . . . .	14
1.5.1 The Current Gold Standard: Viral Delivery . . . . .	15
1.5.2 Alternatives to Viral Delivery: Non-Viral Methods . . . . .	16
1.6 Assessing Vision: Tests of the Visual System . . . . .	18
1.6.1 Electrophysiological Measurements . . . . .	18
1.6.2 Behavioural Assessment: Optomotor Test . . . . .	21
1.7 Open Challenges and Motivation . . . . .	23
1.8 Synopsis and Objectives . . . . .	24
<b>2 A CRISPR/Cas9-based Gene Editing Approach to Preserve Visual Functions in a Mouse Model of Photoreceptor Degeneration</b>	<b>25</b>
2.1 Introduction . . . . .	26
2.2 Methods . . . . .	28
2.3 Results and Discussion . . . . .	38
2.4 Conclusions . . . . .	52
<b>3 Development of a minipig chemically-induced model of photoreceptor degeneration for the <i>in vivo</i> testing of retinal prostheses</b>	<b>54</b>
3.1 Introduction . . . . .	55
3.2 Methods . . . . .	59
3.3 Results and Discussion . . . . .	63
3.4 Conclusions and Future Work . . . . .	79
<b>4 Discussion and Outlook</b>	<b>81</b>
References . . . . .	85
<b>List of Abbreviations</b>	<b>101</b>
<b>List of Publications with Detailed Contribution</b>	<b>104</b>
<b>Curriculum Vitae</b>	<b>106</b>

# List of Figures

1.1	The eye and the retina. . . . .	3
1.2	Overview of the phototransduction cycle in the rod photoreceptors of the healthy retina. . . . .	4
1.3	Strategies for treating retinal degeneration based on the stage of the disease. . . . .	9
1.4	Retinal Prostheses. . . . .	10
1.5	Available approaches for retinal repair. . . . .	13
1.6	Routes of injection: subretinal and intravitreal. . . . .	15
1.7	Delivery of therapeutic agents to the retina by electroporation. . . . .	17
1.8	Electroretinography. . . . .	20
1.9	Visually evoked potentials. . . . .	21
1.10	The optomotor system. . . . .	22
2.1	Screening of gRNAs targeting the Rd10 locus. . . . .	40
2.2	Electroporation of photoreceptor progenitor cells <i>in vivo</i> at P3. . . . .	42
2.3	Editing efficiency <i>in vivo</i> . . . . .	44
2.4	Preservation of <i>ex vivo</i> microelectroretinograms at P60 and <i>in vivo</i> electroretinograms at P30. . . . .	46
2.5	Preservation of the visual acuity in Rd10 treated mice. . . . .	48
2.6	Electroporation <i>in vivo</i> of photoreceptor progenitor cells at P8. . . . .	49
2.7	Optomotor reflex upon electroporation at P8. . . . .	50
2.8	Preservation of visually evoked potentials at P90. . . . .	51
2.9	Probability density function for the VEP recordings. . . . .	52
3.1	The POLYRETINA photovoltaic epiretinal prosthesis. . . . .	58
3.2	Example of quantification of the retinal thickness with OCT in one subject. . . . .	64
3.3	Quantification of the retinal thickness in control and treated eyes before and one month after the injection of IAA. . . . .	65
3.4	H & E staining on retinal sections in the visual streak. . . . .	66
3.5	H & E staining on retinal sections in the zone adjacent to the optic nerve. . . . .	67
3.6	IHC/IF for L/M opsin on retinal sections in the visual streak. . . . .	68
3.7	IHC/IF for L/M opsin on retinal sections in the zone adjacent to the optic nerve. . . . .	69
3.8	IHC/IF for Rho on retinal sections. . . . .	70
3.9	ERG recordings in control and blind animals after dark adaptation. . . . .	71
3.10	ERG recordings in control and blind animals following light adaptation. . . . .	73
3.11	Flicker ERG in control and blind animals. . . . .	74
3.12	VEP recordings from the primary visual cortex. . . . .	75
3.13	Surgical procedure for the implantation of the POLYRETINA epiretinal prosthesis. . . . .	77

3.14 ERG/corneal potentials and VEP responses 2 weeks after POLYRETINA  
implantation. . . . . 78



# **Introduction**

This introductory chapter is meant to give an overview of the concepts that are relevant to understand the work I performed during my PhD, which focuses on preclinical research in the field of vision restoration. First, I will introduce the visual system, the retina, and the diseases that can affect them. I will then talk about animal models used in preclinical research and the main therapeutic options available at the moment to cure degenerative diseases of the retina. To conclude, I will present some behavioural and electrophysiological tests, commonly used to measure the functionality of the visual system, which are particularly relevant for this work. The diseases affecting the visual system are very diverse and the list of causative genes is extremely lengthy. As a consequence, this is by no means a comprehensive account of all the diseases and therapies for vision restoration. Conversely, all the concepts that are touched upon in this chapter were specifically chosen because of their importance for my research.

## **1.1 The Visual System and the Retina**

Vision is a sense of central importance for humans, who rely on it for a great number of everyday tasks. Given this premise, it does not surprise that decreased vision correlates with a lower quality of life and can lead to unemployment, reduced independence, and depression [1–4]. Furthermore, blindness not only has a significant impact on the well-being of the affected person, but has also a very high global cost, consistently increasing with the constant aging of the population [5–7].

It is estimated that 216 million people worldwide suffer from some sort of visual impairment that interferes with their daily activities and 36 million are totally blind (for a detailed meta analysis see [8], data from 2015). As of 2015, the principal causes of blindness were uncorrected refractive errors and cataracts, followed by glaucoma and macular degeneration. Among the less common causes of blindness, there are several degenerative diseases, a lot of which are hereditary.

Restoring vision to the blind has been a long term goal of medicine and many efforts have been put in finding out more about the causes of retinal diseases and developing new therapies. While refractive errors and cataract can now easily be corrected, at least in industrialized countries, a lot remains to be understood regarding other causes of vision loss, especially hereditary diseases.

The process of vision starts in the eye where the light, after passing through the cornea and the pupil, is focused on the retina by the lens and eventually absorbed by the photosensitive molecule opsin in the outer segment of photoreceptor cells, which transforms it into electrical signals [9]. The internal part of the eye is filled with vitreous humor, a viscous substance that helps keeping the eye's round shape and maintaining the retina in place (Fig. 1.1A). The retina, a sheet of light-sensitive tissue, is sitting at the back of the eye and comprises five types of neurons involved in the process of vision [11], which are organized in layers (Fig. 1.1B-C). The innermost layer is formed by the ganglion cells, which serve as

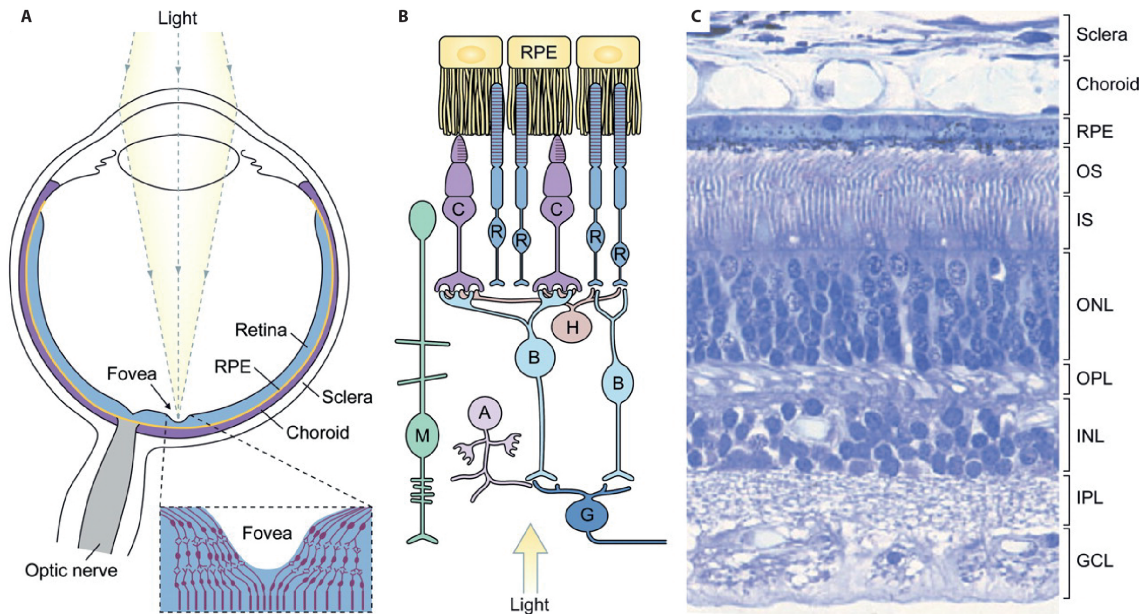


Figure 1.1: The eye and the retina. A, Schematic representation of the structures composing the human eye. B, Schematic representation of the retinal layers. C, Histological image of a retinal section in which all the layers are identifiable [10].

the output of the retina, while the outermost one is formed by the light-sensitive cells, the rod and cone photoreceptors. While cones are mostly contributing to day and color vision, rods are very sensitive to small amounts of light, thus enabling vision in dim conditions.

The retinal pigmented epithelium (RPE) lies beneath the photoreceptor layer and absorbs byproducts emitted by rods and cones during the phototransduction process, while also sustaining them with nutrients, water, ions, and essential factors for the preservation of the structural integrity of the retina. The RPE has many other functions, namely the absorption of light, protection against photo-oxidation, the reisomerization of all-trans-retinal into 11-cis-retinal to start over the visual cycle, and phagocytosis of dead photoreceptor membranes [12].

Another important component of the retina is the fovea, an area specialized for high acuity vision in conditions of bright light, which forms a depression in the surface of the retina, approximately 1.0 mm in diameter [13]. At the centre of the fovea, the inner retinal layers are absent and there is a peak in cone density in the photoreceptor layer.

The process of phototransduction is a series of biochemical reactions, taking place in the outer segment of photoreceptors, by which photons are converted into cellular membrane potentials [14]. The opsin photopigment is activated by a photon and triggers a cascade of events that ultimately lead to hyperpolarization, initiating the process of vision (Fig. 1.2).

The hyperpolarization occurring in photoreceptors triggers a signal which travels through the retinal internal circuitry, formed by bipolar, horizontal, and amacrine cells, and is finally conveyed to the retinal ganglion cells, whose axons

form the optic nerve [10]. The optic nerve carries the action potentials generated in the retina to various relay nuclei in the brain. A part of the signal, which passes through the lateral geniculate nucleus, is forwarded to the visual cortex, where it is extensively computed and transformed in the images forming our perception of the world [15].

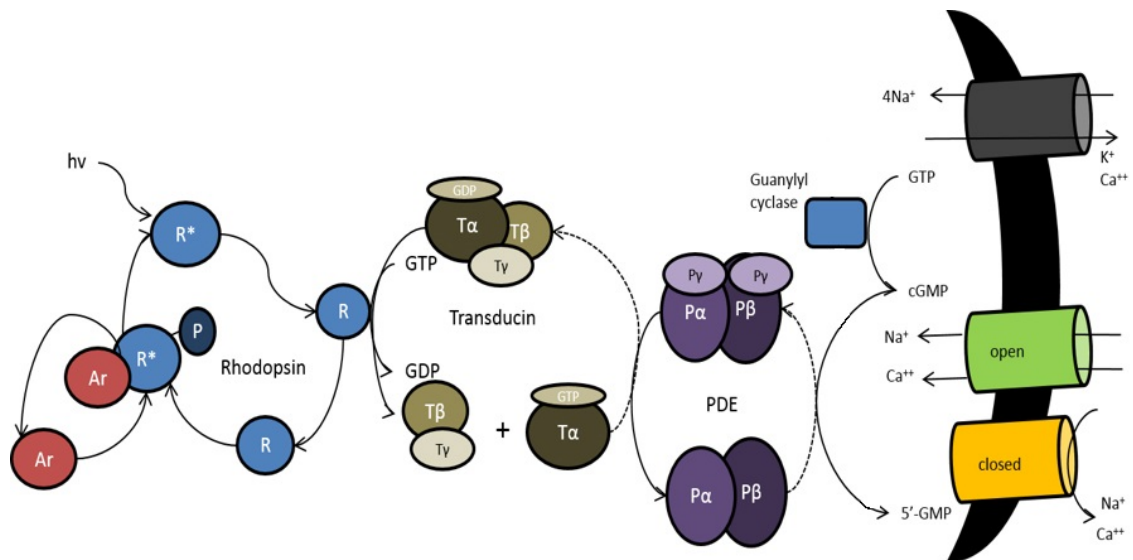


Figure 1.2: Overview of the phototransduction cycle in the rod photoreceptors of the healthy retina. A photon is absorbed by the photopigment rhodopsin and activates cGMP-PDE and transducin. cGMP-PDE catalyzes the degradation of cGMP to guanosine-5-monophosphate (5'-GMP). The ionic channels gated by cGMP are then closed and the membrane of the photoreceptor hyperpolarizes, initiating the process of vision.

Vision loss can result from problems in the phototransduction cycle, as well as at the level of any other structure of the eye or the entire visual system. For the purpose of this work, the next section focuses on inherited retinal diseases (IRDs), a group of rare eye disorders caused by inherited gene mutations.

## 1.2 Inherited Retinal Diseases (IRDs)

IRDs, a heterogeneous group of disorders that lead to the degeneration of photoreceptor cells in the retina, are among the leading causes of blindness in working-age adults living in industrialized countries [16], with millions of people affected. More than 250 genes are known to be involved in the onset of IRDs (RetNet).

The classification of these disorders can be challenging since they exhibit a wide range of phenotypes, but they can be divided into three main groups: diseases primarily affecting the periphery of the retina (e.g. retinitis pigmentosa (RP)), those affecting the macula (e.g. age-related macular degeneration (AMD)), and those affecting both the centre and the periphery of the retina (e.g. cone-rod or rod-cone dystrophies) [17]. Another possible classification of IRDs relies on

the cell type targeted by the disease. Although, IRDs that primarily target cone photoreceptors are overall quite rare compared to diseases that target rod photoreceptors or both types of photoreceptors. Moreover, in cone dystrophies, age of onset, type of symptoms, and the progression of symptoms vary substantially between individuals and patients tend to develop rod dystrophies later in life, which contributes to the overlap of symptoms with other IRDs [18].

RP and AMD are the two most prevalent forms of retinal degenerative diseases and, together, they account for millions of cases of blindness in elderly patients, young adults, and children.

AMD affects people 50 years old or older and is a very slowly progressing degeneration that starts in the central part of the retina (macula) and progresses towards the periphery. Although the loss of central vision interferes with daily activities, AMD does not by itself provoke complete blindness, especially after the discovery of some extremely efficient treatments, like the delivery of antibodies against growth factors, such as the anti-vascular endothelial growth factor (anti-VEGF) for wet AMD [19]. Although AMD is historically considered an IRD, it is most likely caused by the interaction of environmental, genetics, and life-choices factors rather than by the mutation in a single gene [20].

The term RP refers to a group of IRDs that cause the progressive death of rod photoreceptors [21]. The first symptoms are decreased night vision and loss of peripheral vision, after which the patient is going to experience tunnel vision as the cells in the retinal periphery progressively disappear. Contrarily to AMD, the treatment of RP presents additional challenges due to the time-course of the disease: rod photoreceptor death starts very early, but the symptoms do not appear until most of the cells are already lost. Cone photoreceptors, on which day-light vision relies in humans, degenerate only at a later stage, but this is likely related to their metabolic dependence from rods [22]. Most of the genes associated with RP are expressed in photoreceptors or in the RPE. Therefore, acting at the level of rod photoreceptors is the most explored therapeutic approach to preserve vision in RP [23].

Other common IRDs include Leber congenital amaurosis (LCA), cone-rod dystrophy (CRD), juvenile macular degeneration (JMD), and choroideremia (CHD).

Twenty-three causative genotypes have been related to the onset of LCA and the implicated genes are mostly involved in the phototransduction process and in the development of photoreceptors. Hence, depending on the genes involved, the disease can be characterized by either severe retinal dysfunction or photoreceptor degeneration. The symptoms generally start during the early life of the patient [24].

CRDs reflect the opposite sequence of events than RP, with cone degeneration preceding rod degeneration. The course of CRDs is generally rapid and leads to early vision loss. Retinal pigment deposits are visible on fundus examination, predominantly localized in the macular region [25].

JMDs typically present during childhood, when vision is still developing and affect primarily the central retinal region (macula). The principal symptoms are low vision and nystagmus. The most common JMDs are Stargardt disease, X-linked retinoschisis, and Best vitelliform macular dystrophy [26].

CHD manifests as a progressive degenerative disorder of the photoreceptor layer, RPE, and choroid. The symptoms start with night blindness and evolve into peripheral vision loss and, finally, legal blindness in late adulthood. Since CHD is inherited in an X-linked recessive pattern, male patients are predominantly expressing the characteristic features of the disease [27].

### **1.3 Animal Models of Retinal Degeneration**

In order to understand retinal disorders and develop cures, it is crucial to have animal models that approximate the time-course and genetic causes of the disease in humans. To this end, researchers have historically used rodent models, which are really easy to breed and manipulate genetically [28].

There are already several commercially available mouse lines with disorders affecting different parts of the eye, such as lid, cornea, iris, lens, and retina. These animals are good models for human diseases like cataract, glaucoma, and retinal degeneration [29]. The first animal identified with a retinal degeneration was the Royal College of Surgeons rat [30]. During the years, sixteen naturally occurring mouse models of photoreceptor degeneration have been identified [31]. Spontaneous canine models also exist for several inherited retinal dystrophies [32]. Moreover, many transgenic animals carrying mutation in the rhodopsin gene have been produced, including rats [33], rabbits [34], and minipigs [35].

Rodent models are useful preclinical tools for developing potential therapies for human IRDs, such as RP. Mutations in the  $\beta$ -domain of the phosphodiesterase 6 (PDE6B) gene, which hydrolyses cyclic guanosine monophosphate (cGMP) and initiates phototransduction, are among the most commonly identified causes of autosomal recessive RP [36, 37]. Missense mutations in PDE6B lead to photoreceptor death, triggered by the toxic accumulation of cGMP [38], resulting in a progressive loss of visual function, which starts from the peripheral retina and progresses towards the centre. The retinal degeneration 1 (Rd1) mouse was the first described natural occurring model of rod-less retina used to study RP in rodents [29, 39]. In this mouse strain, the degeneration starts at the postnatal day 8 (P8) and by 4 weeks of age no photoreceptors are left [40]. Elseways, the Rd10 mouse, another natural occurring model of human RP, presents a more gradual degeneration, closely mimicking the time-course of recessive RP in humans. It carries an autosomal recessive loss-of-function missense point mutation in the *Pde6b* gene (exon 13; C1678T to R560C), leading to the progressive degeneration of photoreceptor cells. The slower progression of the disease makes the Rd10 mouse a better model to test time sensitive therapies by reason of the larger therapeutic window left by the slower degeneration process.

On the other hand, translational research typically requires to validate the hypothesis being tested in larger mammals, with relevant characteristics similar to humans. As a consequence, even if rodents are still widely used in ocular research, scientists also started to employ larger non-rodent mammalian species, for instance rabbits, pigs, sheeps, and non-human primates, as appropriate models for specific human diseases [41]. Non human primates have a fovea which is not found in rodents, but is essential for human vision [42]. In addition, colour vision in mice is limited because of the lack of a red-green chromatic system, which in primates is based on L-M cone projections opponency in the parvocellular retinogeniculate pathway. Pigs and miniature pigs also have a cone rich part of the retina, the area centralis [43, 44]. These characteristics are extremely valuable in the context of translational studies, for instance to test new implantation techniques, evaluate the safety of new ocular drugs, and test new biomaterials and implantable ocular devices [45, 46].

Alongside the above mentioned animal models, some non-animal models have started to be used in retinal research, namely retinal organoids and post-mortem human retinas. Organoids can be produced using cells obtained from the patient, which opens up great opportunities for personalised medicine [47]. Moreover, post-mortem human retinas permit direct access to normal and pathological tissue to better understand the time-course of retinal pathology in humans [48].

## **1.4 Therapeutic Approaches to Restore Vision**

Some ophthalmological procedures, such as lens replacement after cataract and the control of fluid leakage from retinal vessels, have become standard in clinical care. More recently, gene therapy proved to be efficient in improving visual performance for patients suffering from LCA and few other hereditary blinding diseases [49]. In spite of these incredible achievements, from the point of view of the patient, ophthalmological improvement might appear extremely slow. This is due to the intrinsic challenges presented by the retina: its high complexity and lack of regenerative potential.

Although the therapeutic options are currently limited and mostly aim at slowing down the degeneration, an increasing number of studies is appearing every year about novel therapeutic approaches. Diverse approaches to the treatment of IRDs include slowing down cell degeneration (e.g. neuroprotection), stimulating the remaining retina (e.g. retinal prostheses), or providing the cells with a functional copy of the gene of interest (e.g. gene therapy). Some of the aforementioned methods have already entered clinical trials (for a review of the clinical trials, concluded and ongoing, see [50]). The therapeutic strategy of choice greatly depends on the stage of the disease (Fig. 1.5) [51], but none of those can currently completely re-establish normal vision once it is lost. For instance, in the late stages of retinal degeneration, there are few remaining photoreceptor cells, which rules out interventions relying on the presence of healthy cells. In such advanced cases,

the only suitable procedures might be cell transplantation, retinal prostheses, and optogenetics.

A series of strategies that can be used alone or in combination to target retinal and, more specifically, photoreceptor degeneration will be outlined in this section.

#### **1.4.1 Neuroprotection**

Neuroprotective therapies aim at increasing neuronal survival by either directly blocking cell death pathways or by indirectly strengthen the cell's intrinsic survival mechanisms. They are generally used to maintain the visual function of the patient intact for as many years as possible, even if there is the possibility that it will eventually decline in the long run. Notably, antibodies against VEGF, such as the commercial drugs LUCENTIS® (Ranibizumab) and MACUGEN® (Pegaptanib), have been proven successful for the treatment of AMD. Other examples of successful neuroprotection approaches include synthetic bile acids, progesterone, dopamine, exercise, and electrical stimulation (for a complete review see [53]).

Up to now, neuroprotective strategies have proven difficult to translate to the clinics. In fact, attempts to use neuroprotection in clinical trials have mostly led to failure. The principal problems are related to the low reproducibility of pre-clinical studies, often performed on animal models that are too different from humans, and to the difficulty in finding meaningful endpoints for clinical trials because of the slow progression of the disease [54]. Even with its limits, neuroprotection could be very advantageous when used jointly with other strategies, as for instance retinal prostheses or gene replacement and supplementation: preserving the retinal circuits healthy for longer could boost the effect of other therapies.

#### **1.4.2 Retinal Prostheses**

Despite the retina undergoes extensive reorganization and cell loss as a result of retinal degeneration, the inner layers remain relatively well preserved for a long time after the onset of the disease [55]. The remaining bipolar and retinal ganglion cells can thus be directly stimulated, bypassing the thinning photoreceptor layer. Electrical stimulation of the retina is achieved by implantation of devices (retinal prostheses) which contain electrodes that contact the remaining cells in the patient retina. The stimulation can be targeted directly to the ganglion cells or can be network mediated, in which case the electrical impulse stimulates the internal retinal circuits and is transmitted to the ganglion cells. In the latter case, the retinal reorganization has to be especially taken into consideration, since the networks formed by the cells of the degenerating retina can greatly differ from the ones observed in the healthy tissue.



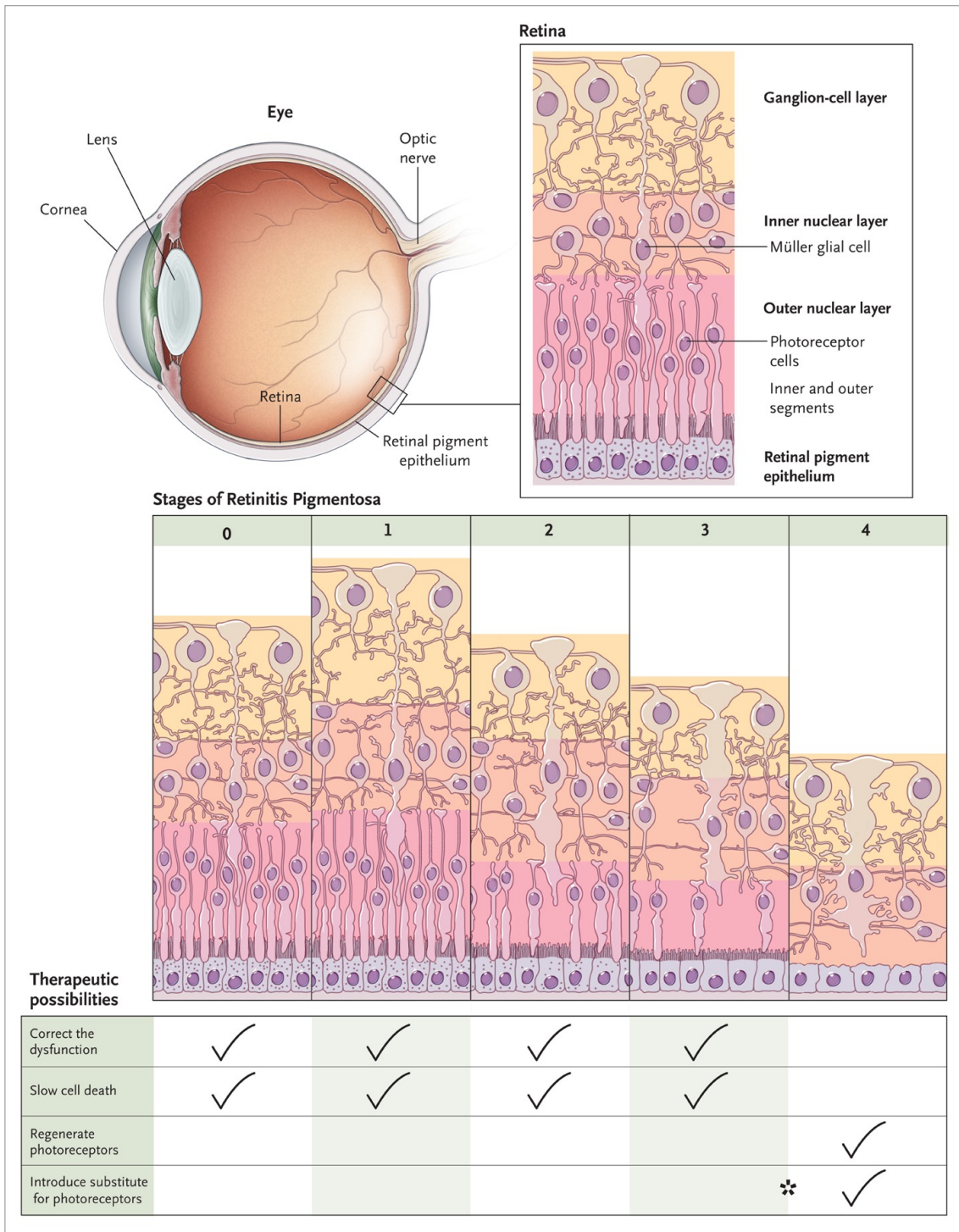


Figure 1.3: Strategies for treating retinal degeneration based on the stage of the disease. The normal retina is depicted in stage 0. Stage 1 represents the first evidence of the disease in RP patients, where the retina is functional, but appears slightly thickened. The symptoms of RP become clear when there is loss of photoreceptor nuclei and shortening of their outer segments (stage 2 and 3). Stage 4 is the most advanced stage of the disease, characterized by major neural loss, gliosis, and prominent reorganization of the retinal circuits. Between stage 3 and 4, the photoreceptors lose completely their outer segments (asterisk). With the progression of the disease, therapies that rely on photoreceptor viability (gene editing and neuroprotection) lose their practicality and the only options available are to stimulate the remaining retinal layers using prosthetic devices, restore light sensitivity with optogenetics or, alternatively, to perform cell transplantation [52].

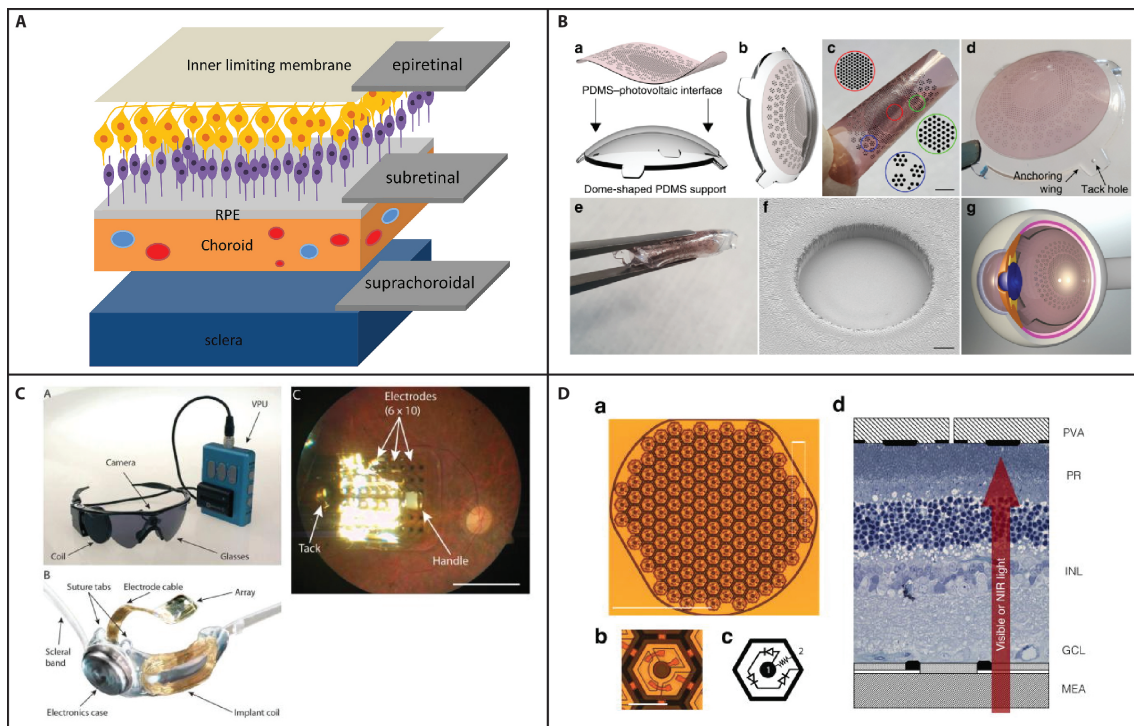


Figure 1.4: Retinal Prostheses. A, Different positions for retinal prostheses implantation [56]. Epiretinal prostheses aim at stimulating ganglion cells directly, while subretinal prostheses stimulate the remaining circuit of the retina from the photoreceptor side. B, The foldable epiretinal photovoltaic prosthesis POLYRETINA [57]. C, The Argus II retinal prosthesis developed by Second Sight. D, The photovoltaic subretinal prosthesis (PRIMA) [58].

Typically, a retinal prosthesis is formed by multiple components: a miniature camera, an image processing unit, a stimulator chip, and an intraocular electrode array. The camera, mounted on a pair of glasses, captures the images from the visual field and sends them to the processing unit, where they are translated into the appropriate stimulation patterns. The patterns are subsequently delivered to the extraocular stimulator chip, which finally sends the stimulation to the intraocular electrode array. The extraocular and intraocular parts are interconnected via a trans-scleral cable [56].

Different types of stimulations are generally achieved by implanting the device in different positions: subretinal for network mediated responses and to contact remaining bipolar cells and epiretinal for stimulating ganglion cells either directly or, as recent evidence suggests, by network-mediated activation and the recruitment of the excitatory and lateral inhibitory networks [59] (Fig. 1.4A). The waveform of the stimulation is another key factor to achieve focalized activation of retinal ganglion cells [56].

Examples of retinal prosthesis include the Argus II (Fig. 1.4C), for which some result from clinical trials are already available, and epiretinal (POLYRETINA, Fig. 1.4B) or subretinal (PRIMA, Fig. 1.4D) photovoltaic prostheses.

Human trials already proved that the patients can recover some form of vision with the aid of retinal prostheses [60]. Although normal visual functions are far from being restored using prosthetic devices, even a slight enhancement of vision can greatly improve the patient's quality of life, especially since at the moment there are not many suitable therapeutic options for late-stage retinal degeneration.

### 1.4.3 Optogenetics

Optogenetics is a technique consisting in the introduction of light-sensitive proteins into cells in order to enable the control and monitoring of neural activity with light. Light-sensitive proteins encoded by opsin genes (opsins) can function as light-responsive ion pumps or sensory receptors. The most used for this purpose are microbial opsins such as channelrhodopsin, halorhodopsin, and archaerhodopsin [61].

Optogenetic tools can be used to restore blindness caused by the degeneration of photoreceptors: as long as some other cell types, such as remaining foveal cones, bipolar, or retinal ganglion cells, are present in the retina, they can be targeted by the optogenes and become light-sensitive [51]. For instance, the expression of halorhodopsin in light-insensitive cone photoreceptors was shown to activate the phototransduction cascade in a mouse model of photoreceptor degeneration and in *ex vivo* human tissue [62], which translated into photoreceptor functionality in the RP mouse model [63].

Optogenetic therapies are a very promising approach to treat retinal degeneration without the need for invasive surgeries, although the final results will

depend on the status of the retinal degeneration and the cell type targeted by the opsin. Also, similarly to retinal prostheses, it is necessary to use a set of goggles that project onto the retina the visual scene in a spectrum and intensity range matching the one of the chosen opsin. This is required since the engineered proteins, contrarily to photoreceptors that can adapt to broad intensity distributions, can only respond to a narrow range of light intensities [64].

#### **1.4.4 Cell Transplantation and Retinal Regeneration**

In invertebrates, e.g. zebrafish, retinal stem cells can be activated by injuries and efficiently regenerate the lost photoreceptors [65]. Conversely, although adult mammals also have some stem cells in their retina, those do not have the same power to spontaneously re-enter the cell cycle in adult age. A lesion can still force stem cells to re-differentiate, but the resulting neurogenesis is limited [66]. Moreover, the injury could lead to more cell degeneration than the proliferation of stem cells.

The delivery of retinal progenitor cells or reprogrammed stem cells to degenerated retinas holds great potential for the treatment of retinal pathologies [67], but it remains unclear how to improve cell survival, differentiation, and integration within the host retina [68–70]. Interestingly, recent research showed that it is possible to restore vision in an animal model of retinal degeneration by reprogramming Müller glial cells to become photoreceptors [71].

A compelling approach to the problem of regeneration in the central nervous system consists of trying to recapitulate the conditions in which the organism naturally develops [73] to provide the new cells with an environment in which they can thrive, differentiate, and eventually integrate into the host tissue. Bioscaffolds offer a unique opportunity to recreate said environment and increase cell viability, allowing network formation in an extracellular matrix-like substrate [74]. Among the different materials that can be used, hydrogels seem to be the most promising tool for the delivery of cells to the retina [75–77].

To conclude, stem cell transplantation and cell reprogramming are attractive strategies for late-stage retinal degeneration. One thing that has to be taken into account is the level of reorganization in the retina of the patient. Indeed, a high level of reorganization could prevent new cells from forming functional networks in the host retina. It is possible though that the retina would be able to undergo further reorganization to integrate the new cells in the circuit.

#### **1.4.5 Gene Therapy**

The term gene therapy refers to any kind of treatment using genes to treat diseases, including gene addition, silencing, disruption, and editing. Ophthalmology is at the forefront of gene therapy techniques for various reasons: the eye is easily accessible and relatively immune-privileged, constant monitoring after the treatment can be easily done using non-invasive techniques, and many in-

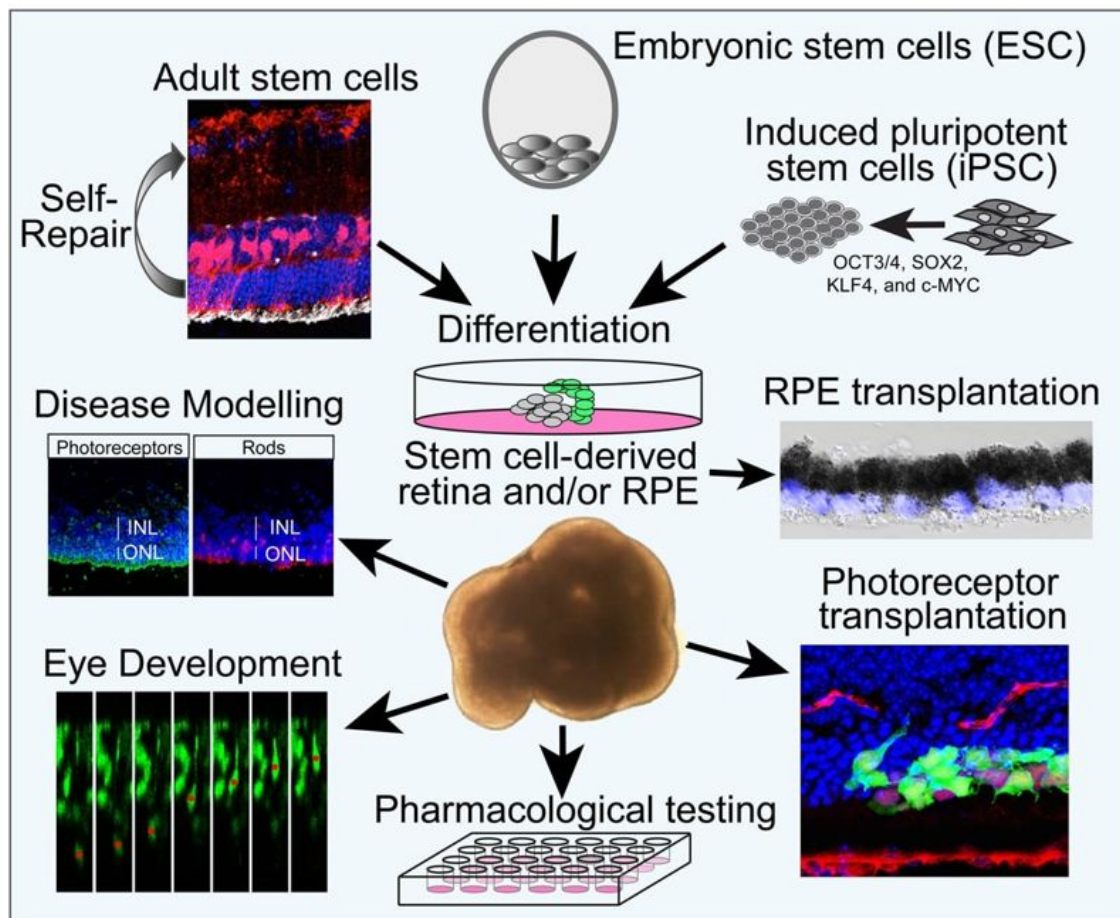


Figure 1.5: Available approaches for retinal repair. Retinal stem cells, embryonic stem cells, and induced pluripotent stem cells can be differentiated into retinal cells with a wide range of applications [72].

herited retinal diseases are caused by a single-gene mutation. The latter offers an opportunity to target a wide variety of different mutations [78].

Gene addition is the simplest option to address a single loss-of-function recessive mutation: it consists of supplementing the cells with a functional copy of the mutated gene, so that they can produce the missing protein themselves. The first gene supplementation therapy was developed for the treatment of LCA: in 2008 three groups successfully deliver an adeno-associated virus (AAV) containing the RPE65 gene to the retina of three patients [79–81].

A problem that has been reported is that the effects of the therapy decline after few years [82, 83]. The issue might be addressed by increasing the dosage of the therapeutic DNA, repeating the administration, or combining gene supplementation with other therapies, such as neuroprotective strategies.

The term gene surgery is sometimes used when talking about very specific gene editing techniques, such as zinc fingers, transcription activator-like effector nucleases, and clustered regularly interspaced short palindromic repeats (CRISPRs)-associated (Cas) genes. Recently, gene editing tools based on CRISPR/Cas9 have completely revolutionised gene therapy [84]. The Cas9 nuclease utilises a guide RNA (gRNA) to induce DNA double-strand breaks (DSBs) at a precise location in the target genomic site. Specifically, the use of the endonuclease Cas9 for precise genome targeting has risen fast in the last few years because of its ease of use and the capacity to finely tune it to target a specific mutation [85]. Since the early 90's it is known that the introduction of a DSB in the genomic DNA can lead to DNA repair through a process called non-homologous end joining (NHEJ). NHEJ can be exploited to disrupt a gene and can be therefore used to treat gain-of-function mutations fairly easily. This mechanism is very active in all cells, but being extremely error prone, it normally results in random insertions and deletions (indels) of some nucleotide in the sequence. More recently, researchers have tried to use another internal mechanism of cells called homologous direct repair (HDR), which is more active in dividing cells and can precisely repair a specific mutation in the genome when a DNA template is present [86]. A template carefully designed to repair a mutation can be introduced in the cells and this triggers the HDR mechanism, which will use the endogenous DNA to correct the mutated sequence.

Although several gene therapy approaches have reached clinical trials [87], a lot of research is still needed in this field to increase the duration of the benefits, principally for the correction of recessive loss-of-function mutations that are more difficult to address than gain-of-function ones since the gene of interest needs to be actively corrected instead of just disrupted.

## **1.5 Delivering Therapeutic Agents to the Retina**

As already mentioned, the eye provides a number of advantages when it comes to *in vivo* gene therapy, mainly in the domain of safety, efficacy, and potential for

clinical application.

Unfortunately, naked DNA does not enter into cells efficiently because of its large size and is very susceptible to degradation. Accordingly, it needs a vector to penetrate its target. Many successful proof-of-concept studies have been carried out in animal models, using diverse delivery methods. Still, preclinical data alone cannot predict the outcome of the therapy in humans and further optimization and testing is needed to reach the clinical stage.

To date, the gold standard for the delivery of therapeutic agents to the retina is the use of viral vectors, although a complete safety evaluation is still missing for most diseases. Alternative methods, not requiring cell infection, have been developed in the past, although they did not enter clinical trials yet. In the following sections, the advantages and limitations of viral and non-viral delivery methods will be outlined.

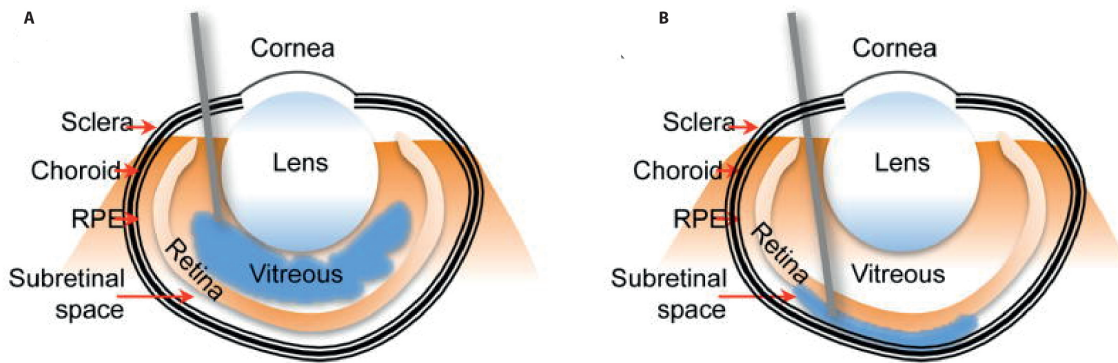


Figure 1.6: Routes of injection: subretinal and intravitreal. A, A subretinal injection allows the therapeutic agent to be delivered to photoreceptors. B, Conversely with an intravitreal injection the target is the inner retina [88].

### 1.5.1 The Current Gold Standard: Viral Delivery

Viral delivery has been proven efficient for the retina, leading to several clinical trials (reviewed in [50]). There are two principal routes of injection to administer viral vectors to the eye: intravitreal injection to target the ganglion cell layer and the inner retina (Fig. 1.6A) and subretinal injection to target the photoreceptor layer (Fig. 1.6B).

The vectors of choice for the posterior segment of the eye are AAVs, although their major drawback is their cargo capacity, limited to 5 kb, which is an issue in the case of large gene delivery [89]. Possible workarounds include using either combined AAVs, as already attempted with success by some research groups [90, 91], or less safe viral vectors with larger cargo capacity [92]. Among the alternatives to AAVs, there are adenoviruses and lentiviruses. Adenoviruses do not integrate into the host genome, thus possibly needing multiple administrations in order to reach a therapeutic level of the protein of interest [93]. Lentiviruses are enveloped retroviruses with high cargo capacity, but it is still not clear to which

extent their use is safe, especially with regard to the generation of replication-competent viruses that can self-propagate within the host. In fact, retroviruses can insert into the genome of the host, but their low precision can lead to insertional mutagenesis [94].

As stated above, although viruses are at the moment the gold standard for gene transfer to the eye, their use does not cease to raise concerns, especially regarding long-term safety and limited opportunity for repeated administration, although this last feature could be achieved by immunosuppression, which can lead to side effects [95–98]. The ongoing clinical trials have also highlighted some additional challenges that have to be overcome in order to effectively transfer gene therapy to the clinic. First, subretinal administration can damage the already thinned retinal tissue of patients with retinal degeneration, but viral vectors cannot reach the photoreceptor layer when administered in the vitreous. In addition, a large amount of different genes is involved in the pathology of IRDs and, although there have been some attempts to develop a generic therapy using viral vectors, this is not suitable for the vast majority of patients. Conversely, the development of a mutation-specific therapy would be an extremely time and resource consuming process.

### **1.5.2 Alternatives to Viral Delivery: Non-Viral Methods**

Several strategies are available for the non viral delivery of therapeutic agents to the retina, generally using synthetic or natural materials or, alternatively, physical forces, to deliver DNA into a cell. They have the advantage of permitting multiple administration of large therapeutic agents using less toxic reagents [99]. On the other hand, the resulting gene expression is often short lived [100–102], which normally is not an appealing characteristic for clinical applications.

Some interesting non-viral delivery methods are sonoporation, chemical-based vectors such as inorganic nanoparticles, and electroporation [103].

Sonoporation is the use of ultrasound waves to create acoustic cavitations in the cell membrane, which is generally combined with contrast agents or microbubbles [104]. Upon absorbing ultrasound waves, the microbubbles start to oscillate and finally break up, disrupting the nearby cell membrane. This promotes the formation of pores, availing DNA transfer. Sonoporation is non-invasive and safe, however it is not directional, contrarily to electroporation.

Among the chemical-based vectors, inorganic nanoparticles are probably the most interesting for retinal gene therapy applications [105]. They are prepared from metals, inorganic salts, and ceramic and have a typical size of 10-100 nm in diameter. Besides, they can be coated to facilitate DNA binding and targeted gene delivery. The small size of nanoparticles allows them to pass through most barriers and they have been proven efficient in transfecting cells both *in vitro* and *in vivo*. However, additional studies to characterize their efficiency and long term safety are still needed.



Electroporation (also known as electrotransfer) is a non-viral delivery method that uses an electric field to alter the permeability of cells. In addition, the DNA is negatively charged and this can be used to drive it inside the cells, according to the orientation of the electric field. The promising therapeutic potential of electrotransfer was demonstrated by several *in utero* [106–109] and cancer studies [110, 111]. Further, as reported *in vitro*, the size of the DNA does not have an impact on the efficiency of the transfer, allowing larger DNA molecules to be delivered [112].

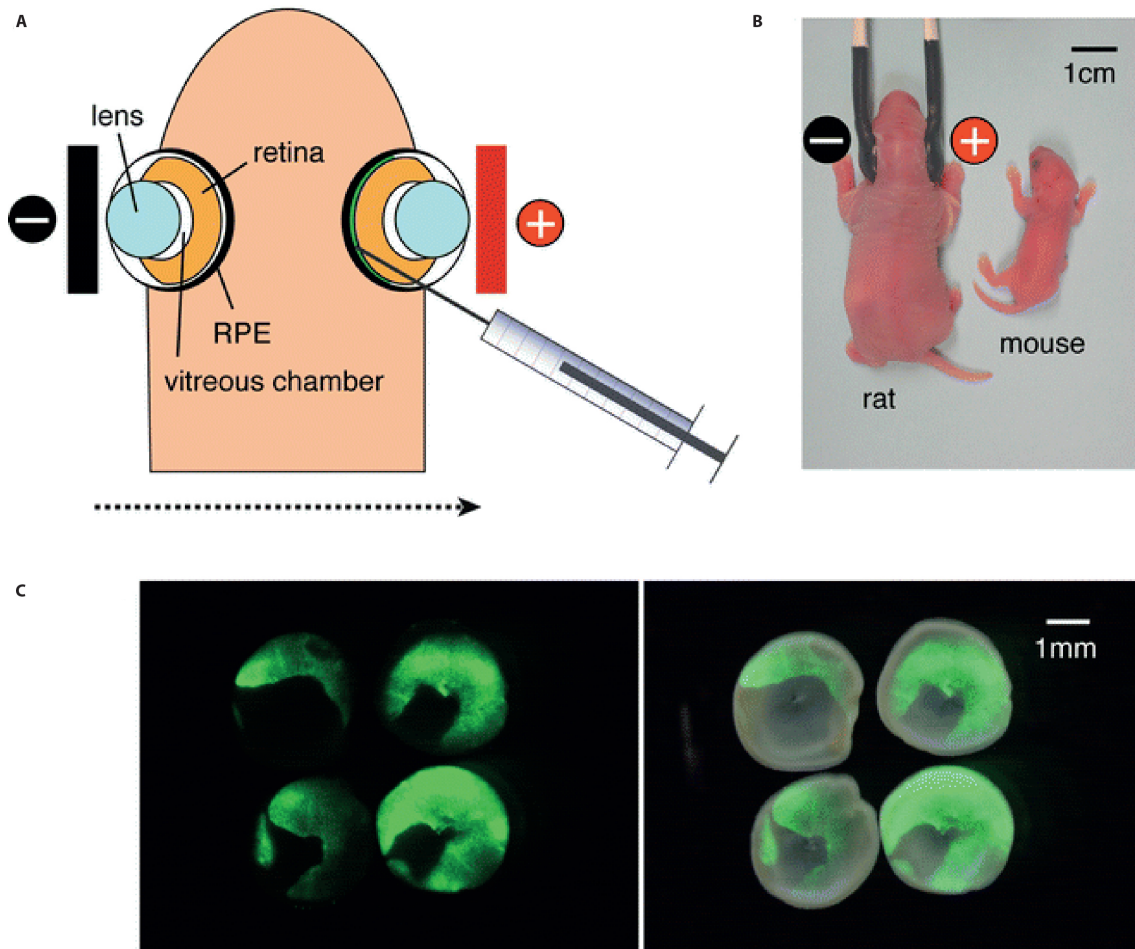


Figure 1.7: Delivery of therapeutic agents to the retina by electroporation. A, Example of electroporation, a non-viral delivery method, in the mouse developing retina. A DNA plasmid expressing GFP is injected into the subretinal space of mouse pups. B, The electric field is used to open pores into the cell membrane and guide the DNA, which is negatively charged, inside the photoreceptor cells. C, GFP expression can be then detected in the retina, starting from 48 hours after the injection. [113].

In the retina, electroporation has been used multiple times to study the development of the visual system in mice [113, 114] (Fig. 1.7A-C), but it is still not adopted for clinical applications, even if it has been tried on the human ciliary muscle [115]. In the same way as for viral-mediated transfer, the injection can be done from the two usual routes in the eye: subretinal and intravitreal.

All considered, viral vectors are the standard delivery method for gene therapy and further research is undoubtedly needed to optimize the non-viral strategies mentioned above. Nonetheless, recent research has shown that it is definitely worth to further look into non-viral approaches and the eye is a very good model system to do so given its accessibility.

## **1.6 Assessing Vision: Tests of the Visual System**

In order to identify the symptoms of diseases and evaluate the effects of new therapies, both in animals and humans, it is necessary to measure vision in a quantitative way, which can be achieved using a number of visual tests. On account of the wide variety of complex behaviours for which the visual system is responsible, no single visual test can be considered a comprehensive measurement of all visual aspects. Indeed, a few are often used in combination to obtain the most exhaustive result.

Electrophysiological measurements allow us to assess neural activation in response to visual stimuli, while behavioural tests use visual-driven behaviours to estimate the visual performance of the subject [116, 117].

With these tests, it is also possible to measure the visual acuity, which can be defined as the spatial resolving capacity of the visual system. Visual acuity is normally measured by target resolution thresholds: the smallest angular size at which the subject can discriminate the separation between critical elements of a stimulus pattern, such as a grating or a checkboard.

For the purpose of this thesis, only the visual tests that were used to obtain the results described in the following chapters will be presented in detail. Therefore, this section is by no means a complete report of all the options.

### **1.6.1 Electrophysiological Measurements**

Neuronal activation in response to visual stimuli can be recorded at different levels in the visual system, from the retina up to the visual cortex. While recording from the retina gives a precise assessment of the functionality of different cell populations, the activity of the visual cortex grants an overview of the functionality of the entire visual system.

#### **Electroretinography**

The term electroretinography (ERG) refers to the measurement of the variation of the retinal resting potential in response to light stimulation. It is a non-invasive way to directly and quickly assess the functionality and integrity of the retina. The electrodes are generally placed on the cornea in order to pick up the signal generated by the activation of retinal cells [118].

Upon flash light stimulation (flash(f)-ERG), the first negative wave (a-wave) is caused by the hyperpolarization of rod and cone photoreceptors and is propor-

tional to the intensity of the light used for the stimulation. The a-wave is followed by the b-wave (generated by cell postsynaptic to photoreceptors, most likely the ON-bipolar cells) and by the c-wave (generated by the RPE and Müller glial cells). The oscillatory potentials, sometimes visible on the b-wave, originate from the inner retina [119]. Although being postsynaptic to photoreceptors, the b-wave can be used to assess the functionality of rods and cones themselves, especially in the case of cone photoreceptors, which generate a very small a-wave. fERGs can be recorded in two different conditions which isolate the contribution of cones and rods respectively: with the eye adapted to light (photopic) or to darkness (scotopic). Scotopic responses to dim light are completely rod-driven, while increasing the intensity of the light elicits mixed rod-cone responses. Contrarily, responses recorded in photopic conditions are cone-driven. Moreover, the light can be directed to the entire retina or just to a part of it, enabling the experimenter to analyse the functionality of retinal portions separately.

When the stimulation is delivered using a checkboard or grating stimulus (pattern reversal(pr)-ERG), the response is correlated to the functionality of the retinal ganglion cells. Lower visual acuity is associated with smaller responses at higher spatial frequencies of the stimulus. It is also possible to record fERG and prERG responses on explanted retinas using a multielectrode array (MEA) to record the evoked potentials from the ganglion cell layer. The retina has to be carefully cleaned from the vitreous and placed flat on the array with the retinal ganglion cells facing down in order to have the best result [120].

In humans, ERG standard techniques have a high clinical relevance [121]. Even if ERGs from humans and mice have few differences, most notably the latency of the b-wave and the amplitude of oscillatory potentials [122] (Fig. 1.8), in general the polarity and shape of the different waves are preserved.

### **Visually Evoked Potentials**

Visually evoked potentials (VEPs) can be recorded from the visual cortex in response to a stimulation applied to the eye. They can be evoked either by full field light stimulation (fVEP), which activate neurons in the geniculo-cortical pathway and in the visual cortex [123], or by pattern reversal stimuli (prVEP), which mostly activate neurons in the visual cortex [124].

The complex shape of the VEP response can be divided into several waves, but the cellular origin of each of them has not been studied as much as for ERGs. The first negative wave of the response correlates with the intensity of the light in the fVEPs (Fig. 1.9A) and with the spatial frequency of the stimulus in prVEPs (Fig. 1.9B). Considering that any abnormality affecting the visual pathways or visual cortex could, in turn, affect the VEPs [125], they can be used to measure the functional integrity of the visual system in its entirety, from the retina, through the optic nerve and subcortical nuclei, and up to the visual cortex.

Since the cellular origin of VEPs is not completely known, they are a use-

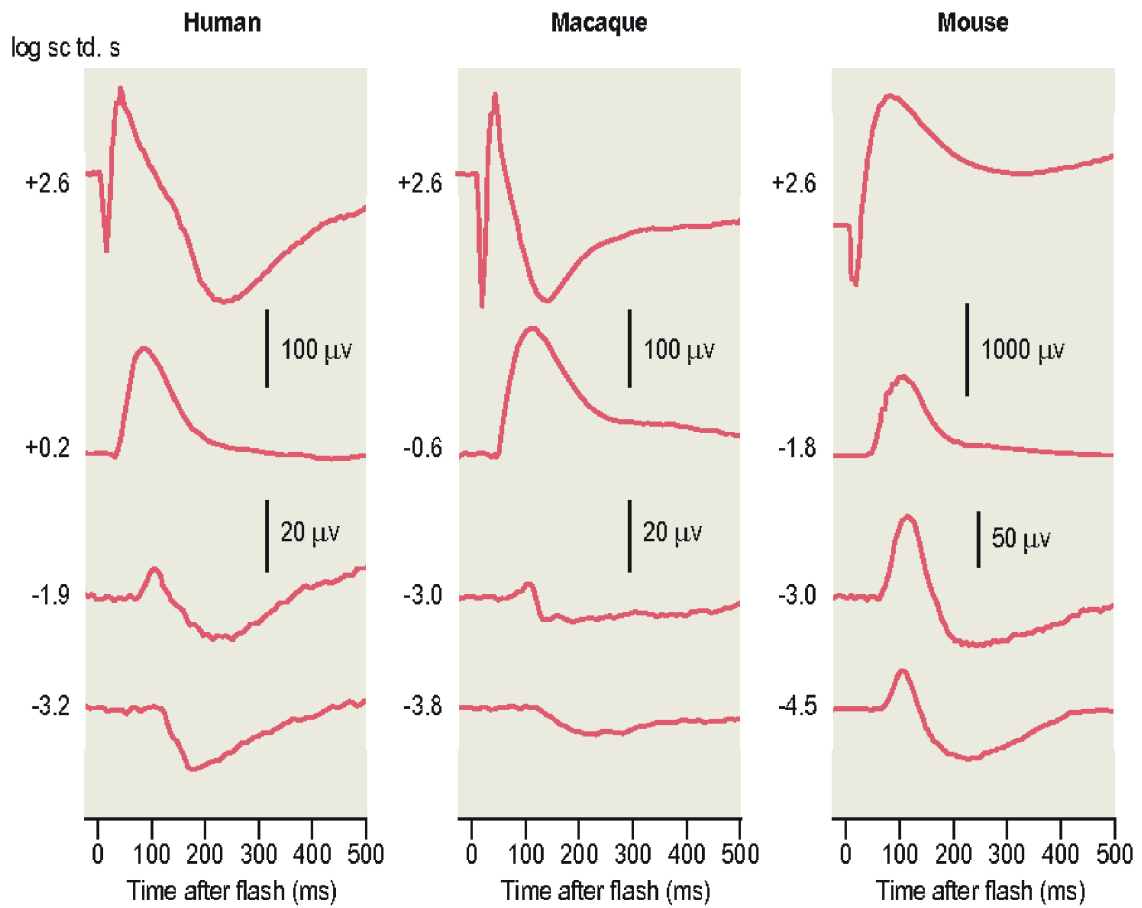


Figure 1.8: Electretinography. Comparison between human, macaque, and mouse fERGs recorded in dark adapted (scotopic) conditions in response to brief (< 5 ms) light stimuli. The responses to the weakest stimuli are rod-driven, whereas stronger stimuli elicit compound rod-cone responses. Vertical axis:  $\log \text{ cd s m}^{-2}$  [118].

ful screening test, but do not provide information on the specific causes of the disease. Indeed, VEPs are often used conjointly with ERGs to obtain a global assessment of the visual performance of the subject.

For instance, VEPs can be recorded in mice with subdermal electrodes (e.g. Fig. 1.9), intracranial screws placed above the visual cortex (identified using stereotaxic coordinates, e.g. Fig. 2.8) or, alternatively, with penetrating electrodes. The shape of the recorded compound potentials generated by the activation of neurons in the visual cortex varies depending on the position of the electrode with respect to the origin of the response, as well as with the depth at which the electrode is implanted. This reliable measurement allows us to screen the visual capability of different groups of rodents in 20-30 minutes per animal. In addition, prVEP can be also used to measure visual acuity varying the spatial resolution of the grating stimuli [126].

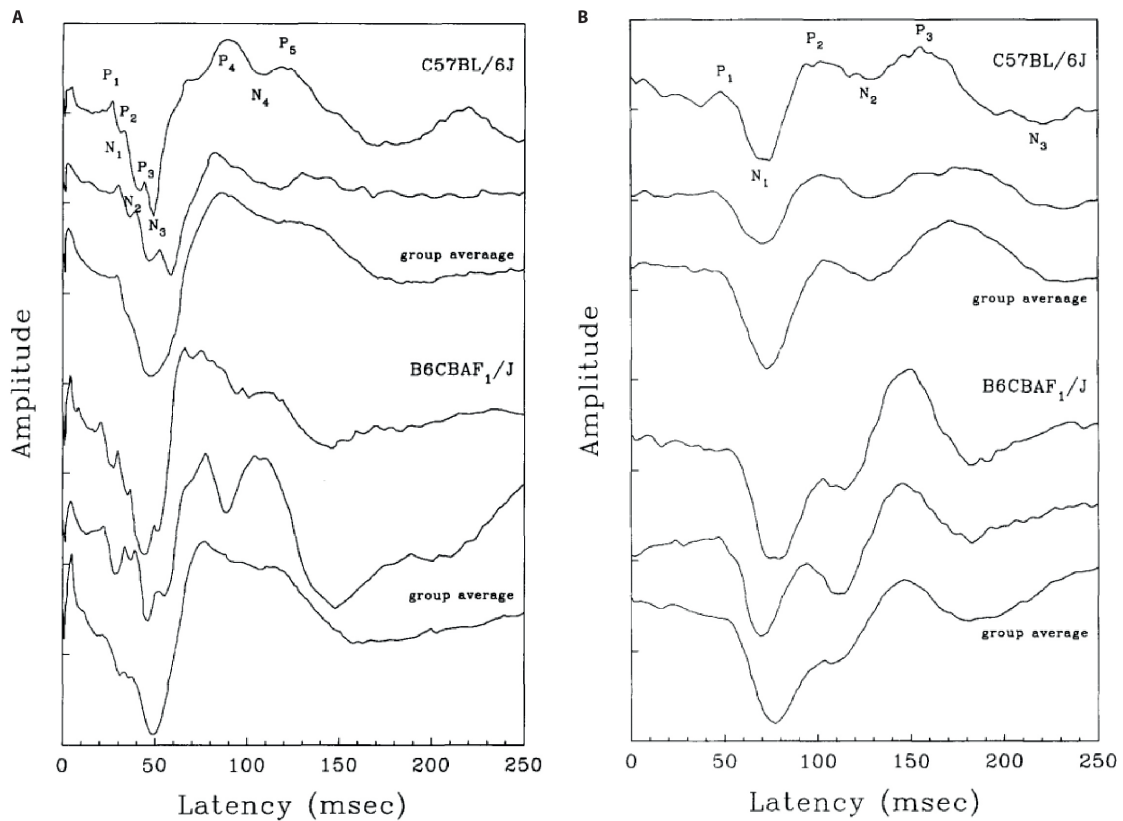


Figure 1.9: Visually evoked potentials. Comparison between the A, fVEP and B, prVEP in the mouse strains C57BL/6J and B6CBAF<sub>1</sub>/J. Each trace is the average of 200 responses. Vertical axis: group averages 10  $\mu$ V/div, other tracings 20  $\mu$ V/div [126].

### 1.6.2 Behavioural Assessment: Optomotor Test

The optomotor (OM) test is a widely adopted behavioural test that allows researchers to measure the visual threshold of rodents and other animals [127]. It is routinely used in mice to test the visual performance of different strains or the

effect of certain therapies on visual functions. Moreover, using the OM test, it is possible to determine the visual acuity and/or the contrast sensitivity of each eye independently [127, 128]. This makes it a great candidate to assess the differences in performance between control and treated eye in the same individual, allowing researchers to have an internal control on the same animal.

The main advantage of this test is that it support the quantification of the visual acuity in rodents and other animals [127], while other visual tests only measure visual functions, namely the subject ability to use vision to achieve a certain task. Moreover, this test is not reward-dependent, which is the best way to exclusively isolate the contribution of the visual system in the behaviour measured.

The OM test is based on the optokinetic (movement of the eyes) and optomotor (movement of the head/neck) reflexes, which happen involuntarily when an animal perceives a movement in the visual environment [129]. The optomotor arena is formed by a closed box with a platform in the center, surrounded by screens, with a camera on top. The mouse is placed on the platform and can freely move on it, while stimuli rotating in either direction are projected onto the screens. The movement of the head can be detected by the camera and the stimulus is controlled by a computer (Fig. 1.10A). Fig. 1.10A shows the visual threshold for two different strains of mice, obtained using the optomotor setup [130]. The threshold is calculated in cycles over degrees, which means how many couples of bars (black + white) of the stimulus fit in a degree of rotation. Higher numbers correspond to smaller bars, hence a higher visual acuity for the mouse.

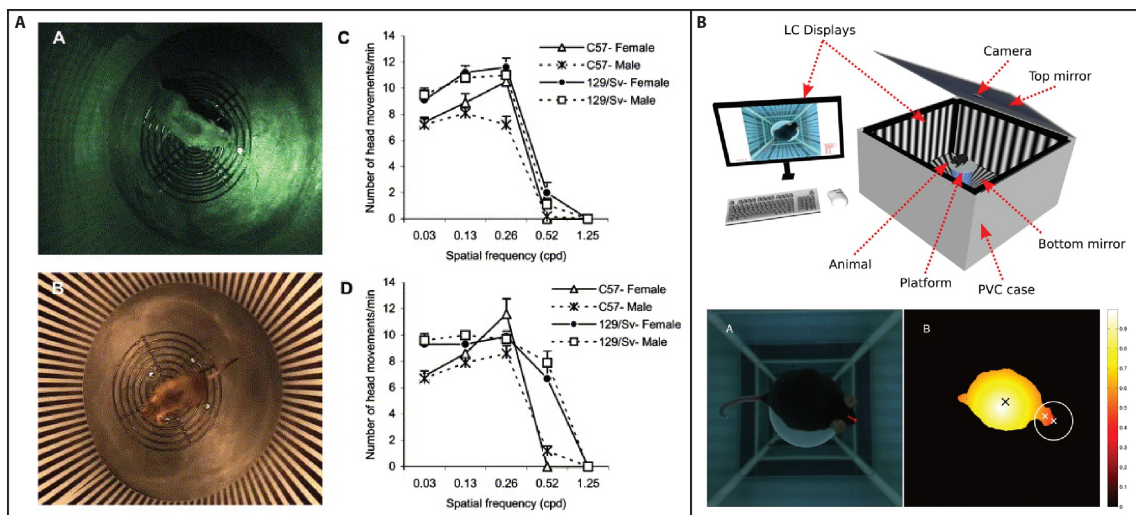


Figure 1.10: The optomotor system. A, Setup of the classic computerized optomotor system and characterization of the mouse visual acuity in two different mice strain [130]. B, Setup of the automatic optomotor system [131].

The OM test usually relies on the judgment of an expert observer to evaluate the behaviour of the animal, which could lead to biased results. As a matter of fact, the test should be performed in blind conditions, the experimenter not

knowing the group to which each animal is allocated.

More recently, completely automatic OM setups have been developed [122, 131]. In this case, the mouse is tracked by an algorithm based on the shape and color of the body (Fig. 1.10B). At the end of the experiment, the software produces a curve of the visual threshold that can be easily analysed and compared among different animals. Although the standard OM setup gives comparable results to this new automated machine, the use of the algorithm-based detection can be extremely useful since it does not rely on the judgment of the experimenter.

Importantly, the OM test measures the functionality of subcortical visual pathways, as demonstrated by the fact that the response is not lost in the presence of a lesion of the visual cortex [128].

## 1.7 Open Challenges and Motivation

The treatment of IRDs remains a major challenge because of the high number of diverse genes involved in their pathology (section 1.2). The vast majority of IRDs is caused by gene defects in photoreceptors or the RPE, thus considered the best targets for therapeutic approaches.

Although viruses still represent the gold standard for gene delivery to the retina, there are some unsolved concerns regarding their use (section 1.5.1). In addition, the limited cargo capacity of certain viruses limits the delivery of big genes, such as the CRISPR/Cas9 system (section 1.4.5). The CRISPR/Cas9 system, which is steadily gaining popularity because of its versatility, can either be used to disrupt the target gene by NHEJ of DSBs or to edit the target gene by HDR in the presence of a DNA donor sequence (repair template), unlocking a number of possibilities in gene therapy.

Oppositely to viral vectors, non-viral gene delivery strategies permit the multiple administration of large therapeutic agents using less immunogenic and toxic vectors. Electroporation (section 1.5.2) is one of the most efficient non-viral delivery methods and holds a promising therapeutic potential, without imposing limits on the size of the DNA to deliver. CRISPR/Cas9 constructs have already been successfully delivered by electroporation to photoreceptor cells to target autosomal dominant mutations. Nevertheless, loss-of-function mutations are more difficult to address since the faulty sequence has to be actively edited by HDR to restore the correct gene product and not just disrupted.

Given the high potential of non-viral delivery strategies and the limitations of viral vectors, more research is needed on the feasibility of non-viral gene delivery systems for the treatment of retinal diseases. All considered, experimentation in mouse models has a pivotal role in selecting the most promising therapeutic approaches and devise new strategies for gene correction and supplementation.

On the other hand, although historically mice have been largely used for ocular research, translational studies need animal models closer to humans for the validation of therapeutic approaches (section 1.3). For instance, in the field of

implantable devices there is a necessity for animal models in which eye size and retinal physiology fit the one of humans. This is indeed the case for the pre-clinical *in vivo* testing of the POLYRETINA prosthesis developed by our lab [57]. Unfortunately, especially in Europe, there is no availability of large mammals with the relevant genetic modifications to study retinal diseases. Alternatively, chemical compounds could be used to induce light-insensitiveness in animals. This strategy is often tricky to implement, but there are few examples of toxins (e.g. iodoacetic acid) that can be successfully used for this purpose.

## 1.8 Synopsis and Objectives

This work tackles two aspects of research in the field of preclinical visual therapy that can be summarized in two aims, which motivated the research undertaken in the following chapters:

- **Aim 1: to test a non-viral method for the delivery of a gene editing construct which takes advantage of HDR to correct, directly on photoreceptors, the mutation causing retinal degeneration in a mouse model of RP** (see chapter 2).
- **Aim 2: to characterized the timecourse of visual function loss in a big animal model of chemically-induced retinal degeneration and apply it to the testing of the POLYRETINA epiretinal prosthesis [57]** (see chapter 3).

In chapter 2, a proof-of-concept study using CRISPR/Cas9 to correct the loss-of-function point mutation in the Rd10 mouse model of RP will be presented. This line of research addresses a specific question: whether a non-viral delivery method can be utilized to correct *in vivo* an autosomal recessive point mutation causing retinal degeneration. This was previously achieved only by gene supplementation or using viruses to deliver the DNA into the cells. The results from behavioural and electrophysiological experiments will be presented, along with a discussion about the advantages and limitations of this approach.

In chapter 3, a model of chemically-induced light-insensitive minipig will be characterized for applications in the *in vivo* testing of photovoltaic retinal prostheses. Minipigs present some favourable characteristics, compared to swines, which will be addressed in this chapter. The preliminary results obtained testing the POLYRETINA photovoltaic epiretinal prosthesis (section 1.4.2) on the light-insensitive minipig model will also be showed and discussed. This prosthetic device has several advantages since it is foldable (minimizing the surgical aperture needed to implant it in the eye) and photovoltaic (limiting the use of cables).



2

# **A CRISPR/Cas9-based Gene Editing Approach to Preserve Visual Functions in a Mouse Model of Photoreceptor Degeneration**

---

*\*Adapted from:* Paola Vagni, Laura E. Perlini, Naïg A. L. Chenais, Tommaso Marchetti, Martina Parrini, Andrea Contestabile, Laura Cancedda, Diego Ghezzi. **Gene editing preserves visual functions in a mouse model of retinal degeneration.** Front. Neurosci. 2019.  
*Contribution:* I performed all the experiments and wrote the manuscript.

## 2.1 Introduction

RP is a group of IRDs that cause the progressive death of retinal photoreceptors and eventually blindness [21]. The treatment of RP is still a major challenge because of the early death of rod photoreceptors and the late onset of the symptoms. Moreover, there is a huge number of diverse mutations implicated in the pathology of RP, which further complicates the use of generic therapeutic approaches (section 1.2).

Although daily vision in humans mainly depends on cone photoreceptors, which in RP degenerate only at a late stage, cone cells likely metabolically depend on rods, which provide them with nutrients [22]. Notably, rod-rich photoreceptor transplantations can halt cone loss in degenerating retinas [132], demonstrating that rod degeneration is indeed the leading cause of the disease. For this reason, rod photoreceptors are considered a much more suitable therapeutic target than cones for the treatment of RP.

Mutations in the PDE6B gene, which hydrolyses cGMP and initiates phototransduction, are among the most commonly identified causes of autosomal recessive RP [36, 37]. Missense mutations in the human gene PDE6B lead to photoreceptor death, triggered by the toxic accumulation of cGMP [38], and result in a progressive loss of visual function, starting from the peripheral retina and progressing towards the centre.

The discovery of naturally occurring mouse models carrying mutations on the Pde6b gene [29, 39] has provided a better understanding of the mechanisms underlying retinal degeneration and prompted the development of new therapies. The Rd10 mouse carries an autosomal recessive loss-of-function missense point mutation in the Pde6b gene (exon 13; c.1678C>T to R560C), leading to the progressive degeneration of photoreceptor cells. Rd10 mice are particularly useful as an animal model for autosomal recessive RP since the slow degeneration of photoreceptor cells recapitulates the time course of the disease in patients, as opposed to the very fast degeneration happening in the Rd1 model (section 1.3). In the Rd10 mouse the degeneration starts at around P18 and peaks between P20 and P25. By this time the ERG response is almost undetectable and the outer nuclear layer appears thinned with only two rows of cells remaining [133].

The first genetic approaches to vision restoration in the Rd10 mouse were based on virus-mediated supplementation of the Pde6b gene [134–137]. Similarly, viral gene transfer therapies have led to promising results for LCA type 2 and some other retinal diseases, as demonstrated by the several ongoing clinical trials [50].

Recently, gene editing tools based on CRISPRs/Cas genes have completely revolutionised gene therapy [84]. The Cas9 nuclease utilises a gRNA to induce DNA DSBs at a precise location in the target genomic site. The CRISPR/Cas9 system is easily tunable, versatile, and enables the precise correction of genetic defects directly on the patient genome. The CRISPR/Cas9 system can either be used

to disrupt the target gene by NHEJ of DSBs or to edit the target gene by HDR in the presence of a DNA donor sequence (repair template) [85]. Importantly, the expression of the CRISPR/Cas9 system is only needed for the relatively short period necessary to correct the genetic mutation (a few days, rather than continuously as in the case of gene supplementation therapies) (section 1.4.5).

Some of the biggest limitations of delivering a big therapeutic agent, such as the Cas9 coding plasmid, using viruses are related to the limited cargo capacity of viral vectors. In fact, AAV vectors are the most efficient at transducing cells in the posterior segment of the eye [89], in particular in the photoreceptor layer, but their cargo capacity is limited to 5 kb. Workarounds include combine more than one AAV vector [90, 91] or use other less safe viral vectors with larger cargo capacity [92]. A smaller Cas9 variant, delivered using AAVs, was recently used to disrupt and thus inactivate the P23H mutated allele in a mouse model of dominant RP, but the authors reported a poor cleavage efficiency [138].

Moreover, there are several safety concerns regarding the use of viral vectors which are still far from being resolved (section 1.5.1)[95–98]. For instance, viral vectors can cause inflammatory reactions that have not yet been monitored in a consistent manner in clinical settings. Considering the current situation, research in the field of non-viral delivery methods as a viable alternative to the use of viruses appears extremely interesting and valuable.

Non-viral gene delivery strategies [99, 103], on the other hand, permit the multiple administration of large therapeutic agents using less immunogenic and toxic plasmid vectors (section 1.5.2). While the fact that the resulting short-lived gene expression can be in general unappealing for clinical applications, it is important to remember that this does not represent a concern when editing tools need to be active only for a short period required to correct the sequence of the gene of interest. [100–102].

Electroporation is an attractive non-viral method for the delivery of large therapeutic plasmids in the eye. CRISPR/Cas9 constructs were already successfully delivered by electroporation in photoreceptor cells to target and disrupt by NHEJ the rhodopsin mutated allele in heterozygous P23H mice [138, 139] and in S334ter rats, both model of autosomal dominant RP [140]. Nevertheless, loss of function mutations (like the one affecting Rd10 mice) are more difficult to address since the faulty sequence has to be actively edited by HDR to restore the correct gene product and not just disrupted as in the examples cited above. This is particularly true for non-viral delivery methods that are generally considered less efficient than their viral-based counterpart.

To fill this gap, here we present a proof-of-concept study in which we designed a CRISPR/Cas9 gene editing system that can repair the genetic loss-of-function point mutation in the Rd10 mouse model taking advantage of the increased activity of the HDR mechanism in dividing progenitor cells [86]. Retinal electroporation was exploited to deliver the therapeutic DNA mixture to photoreceptor

cells during and after the proliferation peak of rod photoreceptors. We used a CRISPR/Cas9-based gene editing strategy to prevent retinal degeneration and assessed the preservation of visual functions *in vitro* and *in vivo*, in both sub-cortical visual-driven behavioural responses (optomotor reflex) and electrophysiological analyses (ERGs and VEPs) until as late as P90.

## 2.2 Methods

### Construct design and cloning

#### pCAGGS-Cas9(BB)-2A-GFP-gRNA

The online CRISPR Design Tool (<http://tools.genome-engineering.org>; [85]) was used to design gRNAs targeting the mouse gene *Pde6b* at the level of the mutation c.1678C>T. The sequence of the gene *Pde6b* was used as input sequence and the first three best scoring gRNAs were selected. gRNA #1 and gRNA #3 flanked the mutation c.1678C>T (mapping respectively upstream and downstream the mutation) while gRNA #2 and its mutated counterpart gRNA #4 mapped on the mutation. The online CRISPR Design Tool was also used to predict off-target sites.

The gRNA sequences are the following:

gRNA #1: gtggtaggtgattcttcgat

gRNA #2: tgaagccgtggcgccagttg and gRNA #4: tgaagccgtggcaccagttg

gRNA #3: tctgggctacattgaagccg

The necessary oligos for generating the gRNAs fragments to be cloned into pSpCas9(BB)-2A-GFP were designed as follows: the top strand and the bottom strand contained overhangs for ligation into the BbsI sites in pSpCas9(BB)-2A-GFP (Addgene Plasmid 48138) with the top and bottom strand orientations matching those of the genomic target. The top and bottom sequences are listed in table 2.1.

gRNA	top	bottom
1	caccggtggtaggtgattcttcgat	aaacatcgaagaatcacctaccacc
2	caccgtgaagccgtggcgccagttg	aaaccaactggcgccacggcttcac
3	caccgtctgggctacattgaagccg	aaaccggcttcaatgtagcccagac
4	caccgtgaagccgtggcaccagttg	aaaccaactggtgccacggcttcac

Table 2.1: gRNA sequences

The oligos were purchased from Sigma and then annealed *in vitro*. The plasmid pSpCas9(BB)-2A-GFP was then digested with the restriction enzyme BbsI and the annealed oligos were ligated into the BbsI restriction site. The CBh promoter was then replaced with a CAGGS promoter that is routinely used to obtain efficient gene expression in the retina. Briefly, the CAGGS promoter fragment obtained from the plasmid pCAGGS-mCherry (Addgene) cut with Sal and

AgeI restriction enzymes was ligated into the plasmid pSpCas9(BB)-2A-GFP cut with KpnI and AgeI. All the restriction enzymes were purchased from Promega. Before the ligation, Sall- and KpnI-generated ends were blunted with the DNA Polymerase I Large (Klenow) Fragment (Promega) to obtain compatible ends. The obtained plasmid pCAGGS-Cas9(BB)-2A-GFP-gRNA was subsequently used for the *in vitro* experiments.

### Repair Oligos

The restriction site of the enzymes BanI (GGYRCC, where Y= C or T and R = A or G) maps on the mutation c.1678C>T and is present both in the wild type (WT, GGCGCC) and in the mutated (GGTGCC) sequence. We took advantage of this shared restriction site to develop a screening assay that allowed us to distinguish between the edited and the non-edited sequences. The oligos for repair were manually designed as follows: the mutation site was flanked by approximately 100 bps on each side; a silent mutation was inserted in order to alter the PAM site (TAC to TAT), and a silent mutation was inserted in order to reintroduce the codon coding for the Arginine (mutated into a Cystein in the Rd10 mice, R560C) and destroy the BanI restriction site at the same time (TGC to AGA). The oligo repair sequences (Ultramers™ DNA oligo) are listed in table 2.2 and were purchased from IDT (Coralville, Iowa). The repair oligos are antisense to the Pde6b sequence.

Oligo	gRNA	sequence
1	1	ccc tct gat tca tct agc cca tcc aat tta cat acg tac cat gag tag ggt aaa cat ggt ctg ggc tac att gaa gcc gtg TcT cca gtt gtg gta ggt gat tct tcg ata Tgc ttt gct gac aga gaa tag aaa gcg cac caa gac ctg ggg agc aga gta cat gtg ggt tct gag atc cac ata tga gcc tac aca gc
2	2 and 4	gct gtg gtc ctt gcc cca gcc ctc tga ttc atc tag ccc atc caa ttt aca tac gta cca tga gta ggg taa aca tgg tct ggg cta cat tga agc cgt gTc Tcc agt tgt gAt agg tga ttc ttc gat agg ctt tgc tga cag aga ata gaa agc gca cca aga cct ggg gag cag agt aca tgt ggg ttc tga gat cc
3	3	aga aga tag tta gct gtg gtc ctt gcc cca gcc ctc tga ttc atc tag ccc atc caa ttt aca tac gta cca tga gta ggg taa aca tgg tct ggg cta cat tga agc cgt gTc Tcc agt tgt ggt agg tga ttc ttc gat agg ctt tgc tga cag gaa tag aaa gcg cac caa gac ctg ggg agc aga gta cat gtg g

Table 2.2: Repair oligo sequences

### N2A cell culture and transfection

Neuro 2A cells (N2A, ATCC® CCL-131™) were cultured in Dulbecco's MEM (DMEM, GIBCO-Life Technologies, Waltham, MA) supplemented with 10 % fetal calf serum (GIBCO), 1 % L-glutamine, 100 U ml<sup>-1</sup> penicillin, and 100 mg ml<sup>-1</sup> streptomycin

(Biowhittaker-Lonza). They were maintained at 37 °C in a 5 % CO<sub>2</sub> humidified atmosphere. The cells were transfected with Fugene 6 (Roche, Basel, Switzerland). The day before transfection 5 x 10<sup>5</sup> N2A cells were plated on 6 cm plates. The medium was replaced with fresh medium 1 h before the transfection. The DNA/Fugene mix (ratio 1:2) was prepared in Optimem medium (GIBCO). N2A cells were co-transfected with 1.5 µg of pCAGGS-Cas9(BB)-2A-GFP-gRNA and 2,2 µg of repair template. Cells were incubated at 37 °C in a 5 % CO<sub>2</sub> humidified atmosphere for 48 h following transfection, then detached using Trypsin-EDTA 0.25 % (Sigma-Aldrich), and prepared for fluorescent activated cell (FAC)-sorting.

### **FAC-sorting and DNA extraction from cell cultures**

Cells in Hibernate-A medium were filtered and analyzed using the FACSaria FAC-sorter (BD-Biosciences). Green fluorescent protein (GFP) positive cells were collected in a tube containing PBS + FBS 2 % . FAC-sorting was performed at the Flow Cytometry Facility of the University of Lausanne by specialized operators. The genomic DNA of the sorted cells was extracted with the Genomic DNA - Tissue MiniPrep kit (Zymo Research) following the protocol of the manufacturer for single cell layer samples. The DNA was eluted in 30 µl of RNase-free water. Following measurement of the DNA concentration, the sample was either immediately used for further analyses or stored at -20 °C.

### **Animals handling**

Animal experiments were approved by the Service de la consommation et des Affaires vétérinaires (SCAV) of the Canton de Vaud (Switzerland, authorization VD3044), the Département de l'emploi, des affaires sociales et de la santé (DEAS), Direction générale de la santé of the République et Canton de Genève (Switzerland, authorization GE3217), and the Italian Ministry of Health (authorization 726/2015-PR).

Mice pups and adult mice (male and female) from a homozygous colony of B6.CXB1-Pde6brd10/J mice (The Jackson Laboratory) were used for the experiments. C57BL/6J mice (Charles River) were used as control group. All animals were kept in a 12 h day/night cycle with access to food and water ad libitum. The mice were kept under white light with spectrum similar to natural light (300 ± 50 lux) from 7 AM to 7 PM and under red light (600 - 700 nm, 80 - 100 lux) from 7 PM to 7 AM. The light intensity was measured at 1 m above the floor. All pups were kept with the mother until weaning, except for the time necessary to perform the subretinal injection. All the experiments were carried out during the day cycle. All experiments were approved by the relevant organizations.

### **Preparation of neurospheres and nucleofection**

Primary cultures of neural stem cells (NSCs) were prepared from P2 WT and Rd10 mice as described in [141], with slight modifications. Briefly, P2 mice were

decapitated and the brain was removed from the skull. The cortex and the hippocampus were isolated in the tissue dissection solution (2 M NaCl, 1 M KCl, 1 M MgCl<sub>2</sub>, 155 mM NaHCO<sub>3</sub>, 1 M glucose, and 108 mM CaCl<sub>2</sub>, Sigma-Aldrich) and cut in small cubes. The enzyme mix (trypsin 0.04 g, Type 1-S Hyaluronidase, and kynurenic acid 0.004 g, Sigma-Aldrich), dissolved in 30 ml of tissue dissection solution, was added, the tissue was incubated for 40 min in a water bath at 37 °C and triturated with a pasteur pipette every 20 min. After centrifugation, the enzyme mix was removed and the trypsin inhibitor (Sigma-Aldrich) 1 mg ml<sup>-1</sup> dissolved in serum free medium (SFM) was added. The tissue was then triturated and incubated in the water bath for additional 10 min. After centrifugation, the tissue was resuspended in SFM (DMEM/F12, Life Technologies, Carlsbad, California) with 20 ng ml<sup>-1</sup> EGF (Peprotech, London, UK), 20 ng ml<sup>-1</sup> FGF (Peprotech), 2 % v/v B-27 (Life Technologies), 1,83 µg ml<sup>-1</sup> Heparin (Sigma-Aldrich), 1 mM Putrescine (Sigma-Aldrich), 2 µM Progesterone (Sigma-Aldrich), 10 µg ml<sup>-1</sup> ITSS (Sigma-Aldrich), 6 mg ml<sup>-1</sup> glucose (Sigma-Aldrich), and 1 % Pen/Strep (Life Technologies) and triturated to obtain a single-cell solution.

The cells were counted with the vital dye trypan blue (Sigma-Aldrich) and then plated at 100.000 cells in each well of a 12-well non-coated plate. We obtained neurospheres that were maintained in SFM at 37 °C in a 5 % CO<sub>2</sub> humidified atmosphere and passed 1:3 three times a week. Cells passaged 3 - 4 times were electroporated via Nucleofection with the AMAXA nucleofection device (LONZA, Basel, Switzerland). The Neurospheres were dissociated with Accutase (Sigma-Aldrich) and 5 x 10<sup>6</sup> NSCs were electroporated with 2 µg of pCAGGS-Cas9(BB)-2A-GFP-gRNA and 2 µl of repair template (10 µM) following the protocol suggested by the manufacturer [85]. Cells were then incubated at 37 °C in a 5 % CO<sub>2</sub> humidified atmosphere for 30 hours, dissociated with Accutase and then sorted for green fluorescence via FACS.

### **DNA amplification and restriction analysis**

125 ng of purified genomic DNA were used for PCR amplification. A region of approximately 700 bps, containing the edited region of the Pde6b gene, was amplified via PCR using the following primers (Sigma-Aldrich):

- FW primer: TTTCTGCTCACAGGCCACAT
- RV primer: GCTCCAGAAGGCAGTGGTTA

Details about the PCR program and mix can be found in table 2.3 and 2.4 respectively. The DNA fragment obtained by amplification was purified with the PCR purification kit (QIAGEN, Hilden, Germany) and quantified as previously explained. For restriction analysis of PCR products from WT, Rd10 control, and Rd10 edited retinas, 100 ng of the purified genomic DNA were digested with 1 unit of the restriction enzyme BanI (NEB, Ipswich, Massachusetts) for 20 minutes at 37 °C in a 10 µl reaction volume. The enzyme was subsequently inactivated

Step	time	temperature	reps
1	3 min	95 °C	1
2	1 min	95 °C	35
4	30 sec	65 °C	35
5	1 min	72 °C	35
6	5 min	72 °C	1
7	inf	4 °C	1

Table 2.3: PCR program

quantity	reagent
0.725 $\mu$ l	GoTaqG2 5 u/ $\mu$ l
10 $\mu$ l	5X GoTaq Buffer
1 $\mu$ l	dNTPs 10 Mm
2.5 $\mu$ l	RV primer 10 $\mu$ M
2.5 $\mu$ l	FW primer 10 $\mu$ M
50-125 ng	DNA
to 50 $\mu$ l	water

Table 2.4: PCR mix

for 20 min at 65 °C, following the instructions of the manufacturer. For the restriction analysis of PCR products from cells we used 300 ng of DNA in a 25  $\mu$ l reaction volume and digested with 5 units of enzyme for 1 hour. The digestion of the PCR fragment obtained amplifying unedited genomic DNA with the BanI restriction enzyme generated two fragments of about 470 and 230 bps respectively that were resolved on agarose gel 2 %. The PCR fragments obtained amplifying edited genomic DNA could not be digested by BanI enzyme, enabling the visualization of the undigested 700 bps fragment on agarose gel. The optical density of the 700 bps band was measured using the gel tool of ImageJ.

The DNA sequence is described in detail hereafter. The sequences in capital letters represent the gRNAs and the sequences highlighted in yellow represent the silent mutation that restores the Arginine.

#### PCR product WT DNA

```

1 TTTCTGCTCA CAGGCCACAT gtgaatcaaa cactcaggcc ttaaaccaat gggttttttt
61 gttgttgttg ttggtggttg gttggttatt tagttggttt tggtttttgc tttctcaaaa
121 gatctcacat gccagggggtc ctctttccat tgtgagtctg aaccttggga agagagaggc
181 atcaaattcc caagggtgtg tctttgttct ggtgtgagag cccttcccaa acaggaaggg
241 gccagtgaga acaaggaaca agggctctga gaccaacaag atagaagtgg agaaataggt
301 ataacagact ctaatgcaag cagtatgaga ggcttgata ggctctgata tggtgctgtg
361 taggctcata tgtggatctc agaaccaca tgtactctgc tcccagggtc ttggtgctgt
421 ttctattctc tgtcagcaaa gcctatcgaa gaatcaccta ccacaactgg Cgccacggct
481 tcaatgtacg ccagaccatg tttaccctac tcatggtacg tatgtaaatt ggatgggcta
541 gatgaatcag agggctgggg caaggaccac agctaactat cttctggccc aaggatgcc

```



601 attgtgtgta tccagtccta gcaatgagtg gaagggacct gggtagggcaa agggatgggt  
 661 ttgggacacc ccacatcccc ttTAACCACT GCCTTCTGGA GC

#### PCR product Rd10 DNA

1 TTTCTGCTCA CAGGCCACAT gtgaatcaaa cactcaggcc ttaaaccaat gggttttttt  
 61 gttgtttgtt ttgtttgttg gttggttatt tagttggttt tggtttttgc tttctcaaaa  
 121 gatctcacat gccagggggtc ctctttccat tgtgagtctg aaccttggga agagagaggc  
 181 atcaaattcc caagggctgt tctttgttct ggtgtgagag cccttcccaa acaggaaggg  
 241 gccagtgaga acaaggaaca agggctctga gaccaacaag atagaagtgg agaaataggt  
 301 ataacagact ctaatgcaag cagtatgaga ggcttggata ggctctgata tgggtgctgtg  
 361 taggctcata tgtggatctc agaaccaca tgtactctgc tcccagggtc ttgggtgcgct  
 421 ttctattctc tgtcagcaaa gcctatcgaa gaatcaccta ccacaactgg Tgcacggct  
 481 tcaatgtagc ccagaccatg tttaccctac tcatggtacg tatgtaaatt ggatgggcta  
 541 gatgaatcag agggctgggg caaggaccac agctaactat cttctggccc aaggatgccca  
 601 attgtgtgta tccagtccta gcaatgagtg gaagggacct gggtagggcaa agggatgggt  
 661 ttgggacacc ccacatcccc ttTAACCACT GCCTTCTGGA GC

#### PCR product edited DNA

1 TTTCTGCTCA CAGGCCACAT gtgaatcaaa cactcaggcc ttaaaccaat gggttttttt  
 61 gttgtttgtt ttgtttgttg gttggttatt tagttggttt tggtttttgc tttctcaaaa  
 121 gatctcacat gccagggggtc ctctttccat tgtgagtctg aaccttggga agagagaggc  
 181 atcaaattcc caagggctgt tctttgttct ggtgtgagag cccttcccaa acaggaaggg  
 241 gccagtgaga acaaggaaca agggctctga gaccaacaag atagaagtgg agaaataggt  
 301 ataacagact ctaatgcaag cagtatgaga ggcttggata ggctctgata tgggtgctgtg  
 361 taggctcata tgtggatctc agaaccaca tgtactctgc tcccagggtc ttgggtgcgct  
 421 ttctattctc tgtcagcaaa gcctatcgaa gaatcaccta ccacaactgg AgAcacggct  
 481 tcaatgtagc ccagaccatg tttaccctac tcatggtacg tatgtaaatt ggatgggcta  
 541 gatgaatcag agggctgggg caaggaccac agctaactat cttctggccc aaggatgccca  
 601 attgtgtgta tccagtccta gcaatgagtg gaagggacct gggtagggcaa agggatgggt  
 661 ttgggacacc ccacatcccc ttTAACCACT GCCTTCTGGA GC

### Plasmids and DNA preparation for *in vivo* delivery

We purchased nanoplasms expressing enhanced green fluorescent protein (EGFP) and Cas9/GFP from Nature Technology (Lincoln, Nebraska), the guide plasmid was obtained as previously described, and the template repair was ordered from Integrated DNA Technologies. We decided to use nanoplasms instead of regular plasmids because Cas9 is a big molecule and we wanted to maximise the chances of it entering effectively the cells upon electroporation. Table 2.5 gives an overview of the different plasmids used for the experimental procedures, with their respective suppliers.

The concentration of each plasmid was adjusted in order to have the same number of copies of guide- and Cas-coding plasmid, taking into account the rel-

Component	Name	Length	Supplier
EGFP plasmid	NTC9385R-EGFP	2391 bps	NTC
Cas9 plasmid	NTC9385R-CAG-Cas9-T2A-GFP	6500 bps	NTC
gRNA plasmid	CAG-Guide4	3000 bps	Addgene
Repair template	ssDNA	200 nts	IDT

Table 2.5: plasmids

ative number of base pairs. The repair template concentration is in accordance to what previously described for CRISPR/Cas9 editing systems in [85].

Details on plasmid preparation:

- *GFP construct preparation:* a solution of  $1 \mu\text{g } \mu\text{l}^{-1}$  EGFP-coding plasmid in PBS + Fast Green 0.1 %.
- *Cas9 construct preparation:* a solution of  $1 \mu\text{g } \mu\text{l}^{-1}$  Cas9-coding plasmid +  $0.45 \mu\text{g } \mu\text{l}^{-1}$  guide-coding plasmid +  $2 \mu\text{l } \mu\text{g}^{-1}$  Cas9 of template repair in PBS + Fast Green 0.1 %.
- *Sham construct preparation:* a solution of  $1 \mu\text{g } \mu\text{l}^{-1}$  Cas9-coding plasmid +  $2 \mu\text{l } \mu\text{g}^{-1}$  Cas9 of template repair in PBS + Fast Green 0.1 %.
- *Cas9 + EGFP construct preparation 1.5:1 ratio:*  $1.5 \mu\text{g } \mu\text{l}^{-1}$  Cas9-coding plasmid +  $0.8 \mu\text{g } \mu\text{l}^{-1}$  guide-coding plasmid +  $0.9 \mu\text{g } \mu\text{l}^{-1}$  EGFP-coding plasmid +  $2 \mu\text{l } \mu\text{g}^{-1}$  Cas9 of template repair in PBS + Fast Green 0.1 %.

### Subretinal injection and electroporation

Subretinal injections were performed in mice pups at P3 and/or P8. A glass capillary (ORIGIO, Måløv, Denmark) was backfilled with the previously prepared DNA solution (GFP, Cas or sham, prepared as previously described). The pups were anaesthetised using isoflurane some minutes prior to the procedure, then placed onto a clean paper towel under the dissecting microscope while the anaesthetics was constantly delivered using a custom-made breather. The skin over the eyelid was disinfected with Betadine and a sterile 30 gauge needle was used to cut the skin on the mark of the future eyelid aperture. If performed properly, the incision will not result in bleeding, as this region is undergoing cell death in young pups. The skin was gently pushed to the side with a pair of sterile forceps to expose the eyeball and insert the pipette into the subretinal space, maintaining a  $45^\circ$  inclination with respect to the surface of the eye.

The DNA was injected into the subretinal space for 3 seconds at 300 bar using an automatic injector (Eppendorf, Hamburg, Germany). Two injections were performed in the following directions: dorsal to nasal and ventral to nasal. Since the eye of the pups are really small, two injections should be sufficient to spread the liquid in most of the retina. Additional injections could result in too

much liquid in the subretinal space, with subsequent retinal detachment. Given the internal pressure of the subretinal space, a sudden extraction of the pipette could result in leakage of the previously injected liquid, for this reason it is better to wait few seconds prior to remove the needle from the eye.

Immediately after the DNA injection, an electric field was applied to the area using a tweezer electrode pre-soaked in PBS (P5, Sonidel, Dublin, Ireland). The Platinum/Iridium sheet (anode, +) was attached to the sclera of the injected eye, while the other side of the tweezer (cathode, -) was placed on the not-injected eye. The pulses were delivered using a CUY21SC electroporator (Sonidel). This configuration allows the DNA to go from the subretinal space to the photoreceptor cells [142]. A conductive gel was placed between the electrode plate and the eye to maximize the conductivity and minimize problems on the cornea. This proved to be a very important step in our experience, given that 90 % of the mice electroporated using conductive gel presented a treated eye undistinguishable from the control, whereas when skipping the conductive gel, this percentage would go down to 50 % in some cases. We applied 2 square pulses of 5 ms at 100 V with 0.1 Hz frequency (poring pulses), followed by 5 pulses of 50 ms at 30 V with 1 Hz frequency (transfer pulses). After the procedure the eyelid was closed gently with a cotton swab and the pup was placed onto a warm heating mat (37 °C) until fully recovered, then returned to the mother. In all the groups the injection was performed monolaterally in order to keep the other eye as internal control.

### **Retinal sections, wholemounts, and immunohistochemistry**

After euthanasia by CO<sub>2</sub> inhalation, the eyes of the mice were extracted from the ocular cavity using forceps, washed in PBS, and fixed in 4 % PFA overnight. For wholemount preparation, the retina was extracted and cut in 4 points in order to flat it on a microscope slide. For section preparation, the samples were cryoprotected in sucrose 30 % and frozen in optimal cutting temperature compound (Tissue-Tek). 20  $\mu$ m thick sections of the retina were obtained using a Histo-com cryostat (Thermo Scientific) and placed on microscope slides. The wholemounts were washed in PBS, permeabilised with PBS + Triton 0.1 % (Sigma-Aldrich), counterstained with DAPI 1:300 (Sigma-Aldrich), and mounted for imaging with Fluoromount (Sigma-Aldrich). Retinal sections were washed in PBS, permeabilised with PBS + Triton 0.1 %, left for one hour at room temperature in blocking buffer (Triton 0.1 % + 5 % normal goat serum), and incubated overnight at 4 °C with primary antibodies: anti-rhodopsin 1:300 (ab221664, Abcam) and anti-GFP 1:1000 (ab13970, Abcam). The day after the sections were incubated for two hours at room temperature with secondary antibodies 1:500 (Alexa Fluor 647 and 488, Abcam), counterstained with DAPI 1:300, and mounted for imaging with Fluoromount solution. Image acquisition was performed with a confocal microscope (LSM-880, Zeiss).

### **Droplet-digital PCR (ddPCR)**

The eyes of P6 mice electroporated at P3 were enucleated, and the retina was immediately isolated in ice-cold PBS and quickly inspected under a fluorescence microscope to verify EGFP expression. The genomic DNA (gDNA) was extracted using the Genomic DNA™ - Tissue MiniPrep kit (Zymo Research) following the protocol of the manufacturer for solid tissues. The DNA was eluted in 30  $\mu$ l of DNase-free water. To avoid possible false-positive signals in ddPCR from unintegrated single-stranded oligonucleotide (ssODN) repair template, we optimised a nested-ddPCR assay. We first pre-amplified from extracted gDNA by conventional PCR a fragment of 700 bps containing the edited region of the Pde6b gene with primers mapping outside the ssODN sequence (same as for the BanI restriction assay). The amplified DNA fragment was purified and quantified as above. Next 2.5 fg of the purified template (corresponding to 3500 copies of target DNA) was used in the ddPCR assay with internal primers (Fwd: CAGCAAAGCCTATC-GAAGAATCA; Rev: CATGGTCTGGGCTACATTGAAG) and detected with an edited-specific TaqMan® probe (FAM- TATCACAACCTGGAGACAC-MGB) and an unedited-specific TaqMan® probe (VIC-TACCACAACCTGGTGCCA-MGB). Reactions were assembled with ddPCR™ Supermix for Probes (Bio-Rad Laboratories) and partitioned into nanoliter-sized droplets with QX200 Droplet Generator (Bio-Rad Laboratories). After PCR thermal cycling, droplets for each sample were individually read on a QX200 Droplet Reader (Bio-Rad Laboratories) and assigned as positive or negative based on fluorescence amplitude.

### **Recording of microelectroretinograms *ex vivo***

P60 animals were dark-adapted overnight before tissue collection. Retinas were explanted after animals' sacrifice by injection of Sodium Pentobarbital (150 mg  $\text{kg}^{-1}$ ). All procedures were performed under dim red light. The retinas were dissected in carboxygenated (95 %  $\text{O}_2$  and 5 %  $\text{CO}_2$ ) Ames' medium (A1420, Sigma-Aldrich). After dissection of the sclera, the retina was detached from the pigment epithelium and the vitreous humor removed. The retina was then cut into pieces ( 5  $\text{mm}^2$ ), attached to filter paper, and transferred on a 16x16 microelectrode array (256MEA200/30iR-ITO, Multichannel systems, Reutlingen, Germany) with the ganglion cells layer down. Explanted retinas were continuously superfused with carboxygenated Ames's medium at 32 °C. Data acquisition, amplification, and digitalization were performed with a USB-MEA256-System (Multichannel system) recording system placed on the microscope stage of a Nikon Ti-E inverted microscope (Nikon Instruments, Egg/ZH, Switzerland). The microscope was equipped with a dichroic filter (FF875-Di01-25x36, Semrock) and a 4x objective (diameter of the illumination spot 5.5 mm; CFI Plan Apochromat Lambda). Light stimuli were provided by an attached Spectra X system (Emission filter 560/32, Lumencor, Beaverton, Oregon). Sequences of 10 consecutive 4 ms pulses were delivered at 1 Hz for sequentially increasing irradiance conditions:

LED at 0 % ( $0 \mu\text{W mm}^{-2}$ ), 5 % ( $186.88 \mu\text{W mm}^{-2}$ ), 10 % ( $481.51 \mu\text{W mm}^{-2}$ ), 20 % ( $1.0131 \text{ mW mm}^{-2}$ ), 40 % ( $2.0456 \text{ mW mm}^{-2}$ ), 60 % ( $3.0389 \text{ mW mm}^{-2}$ ), 80 % ( $3.9186 \text{ mW mm}^{-2}$ ), and 100 % ( $4.6762 \text{ mW mm}^{-2}$ ). Extracellularly recorded signals were digitalized at 10/25 kHz and stored for offline analysis. Filtering and spike sorting have been performed by MCRack V 4.6.2 Multi-Channel Systems software. To ensure the reliability of the recording, spikes were first sorted from 300 - 3000 Hz filtered signals.  $\pm 100$  ms peri-stimulus time window of 0.5 - 100 Hz filtered signal was then further data processed in Matlab (MathWorks, Natick, Massachusetts). ERG a-wave amplitude and delay were estimated from average detrended signals of each individual channel. Channels with prominent peaks lower than  $5 \mu\text{V}$  for the 100 % intensity stimulation were discarded.

### **Recording of electroretinograms *in vivo***

Before the recording sessions, P30 mice were dark-adapted overnight. The mice were then anaesthetised with isoflurane ( $0.8 - 1.5 \text{ l min}^{-1}$  at 4 % for induction and  $0.8 - 1.5 \text{ l min}^{-1}$  at 1.5 % for maintenance). The depth of anaesthesia was assessed with the pedal reflex, and artificial tears were used to prevent the eyes from drying. The temperature was maintained at  $37^\circ\text{C}$  with a heating pad. The pupils were dilated with a drop of Atropine 1 %. The recordings were performed in both eyes simultaneously using two custom-made platinum loop electrodes placed in contact with the eyes and kept in place with a small drop of conductive gel. A needle electrode was placed subcutaneously in the dorsal area near the tail as ground. Five light flashes (4 ms,  $30 \text{ cd s m}^{-2}$ , 0.1 Hz repetition rate) were delivered with a Ganzfeld stimulator (BM6007IL, Biomedica Mangoni) positioned close to the mice and the corresponding retinal potentials were amplified, filtered (0.1 - 500 Hz), and digitalized for 500 ms (50 ms pre-stimulus and 450 ms post-stimulus) at 8 kHz (BM623, Biomedica Mangoni). The data were analysed using Matlab.

### **Measurement of the visual acuity**

The optomotor system (Cerebral Mechanics) was used for the measurement of the visual acuity. Control and treated mice were habituated for 5 min placing them in the centre of the virtual arena the day before the beginning of the test. On the day of the test, each mouse was placed on the platform, and the program started. The mouse in the arena was presented with a grating stimulus rotating in either direction, and the operator had to decide if the mouse was tracking or not the rotating stimulus with a movement of the head in the same direction of the rotation. The program uses a built-in algorithm based on a staircase method to evaluate the visual threshold of the two eyes independently. Since each eye can be effectively tracking a rotating stimulus only with a temporal-to-nasal movement, the visual acuity can be measured independently for each eye by controlling the direction of rotation of the stimulus. Shortly, clockwise movements represent the

left eye-driven tracking behaviour (hence the visual acuity of the left eye), while anticlockwise movements represent the right eye-driven tracking behaviour [96, 128]. The performance of any single mouse was assessed during three subsequent days, and the resulting average was considered the value of the mouse visual threshold. Mice were tested at P30, P60, and P90.

### **Electrode implantation and recording of visually evoked potentials**

P60 mice were anaesthetised with isoflurane and placed on a stereotaxic apparatus. The skull was exposed for the visualization of lambda and the skin was glued on the side so not to interfere with the drilling procedure. Two screw electrodes were implanted 3 mm lateral to lambda over the left and right visual cortices. A reference electrode was placed in the rostral side of the cranium, outside of the visual cortex. The craniotomy was closed using dental cement. An extra layer of dental cement was applied to secure the electrodes. The screws were then left in place for 30 more days in order to let the electrodes to stabilise.

At the moment of the recording, P90 mice anaesthetised with isoflurane were placed on a stereotaxic apparatus in front of a Ganzfeld flash generator. The pupils were dilated with a drop of Atropine 1 % and a needle electrode was placed subcutaneously in the dorsal area near the tail to serve as ground. The recordings were acquired simultaneously in two channels connected to the two electrodes implanted on both visual cortices and normalized by the signal recorded from the reference electrode. The signals were recorded for 1000 ms after the onset of the light stimulus and the responses were band pass filtered (0.1 – 500 Hz), digitized using an I/O board in a personal computer, and averaged with the WinAver software (Biomedica Mangoni, Pisa, Italy). The signal was amplified by a factor of 10000. Following overnight dark adaptation, rod-mediated responses were recorded in response to 3 sweeps with a flash intensity of  $10 \text{ cd m}^{-2}$ , keeping an interval of two minutes between each sweep.

### **Statistics**

Statistical analysis and graphical representation were performed with Prism (Graph-Pad Software Inc.). The normality test (D'Agostino and Pearson omnibus normality test) was performed in each dataset to justify the use of a parametric (t-test and One-Way ANOVA) or non-parametric (Kruskal-Wallis and Mann-Whitney) test. The fitting of the VEPs was performed with the non-parametric Kernel distribution in Matlab. In each figure p-values were represented as: \*  $p < 0.05$ , \*\*  $p < 0.01$ , \*\*\*  $p < 0.001$ , and \*\*\*\*  $p < 0.0001$ .

## **2.3 Results and Discussion**

The eye is considered to be a preferential target for the delivery of gene therapies due to its accessibility and immune privilege [78]. Gene defects affecting

photoreceptors cause the vast majority of IRDs; therefore, the development of neuroprotective, gene supplementation, and gene editing therapies has focused primarily on gene transfer to photoreceptors [143–145].

As a first step in the development of the gene editing system, we designed and screened different gRNAs for their ability to induce CRISPR/Cas9-mediated editing of the Pde6b gene. We selected three candidate gRNAs and tested them in mouse N2A cells to determine which one was the best at targeting the sequence coding for the WT Pde6b. We transfected N2A cells with a single plasmid, containing Cas9, one of the three gRNAs, and GFP, along with a DNA ssODN repair template specific for each gRNA, containing flanking sequences of 100 bp on each side of the insertion site that were homologous to the target region. The gRNA #1 and gRNA #3 mapped upstream and downstream to the Rd10 locus, while the gRNA #2 mapped directly on it (Fig. 2.1A).

Each repair template for HDR-mediated editing was designed to edit the gDNA sequence at the Rd10 locus and simultaneously remove an adjacent cutting site for the restriction enzyme BanI (by introducing a silent mutation), allowing the assessment of the editing efficiency by BanI restriction analysis (Fig. 2.1A). Moreover, each repair template also carried a second specific silent mutation in the PAM sequence of the corresponding gRNA to avoid further Cas9-mediated cutting on the edited genomic sequence (Fig. 2.1A). One day after transfection, we isolated GFP-expressing cells by FAC-sorting, extracted the gDNA and PCR-amplified a 700 bp fragment containing the Pde6b target region with primers mapping outside the ssODN homology arm sequence. After BanI digestion and agarose-gel electrophoresis, the edited DNA appeared as a single uncut band (700 bp), while non-edited DNA was digested in two fragments (230 and 470 bp) (Fig. 2.1B). The quantification of the percentage of edited versus non-edited DNA for each gRNA showed that gRNA #2 had the highest editing efficiency and was the best performing gRNA (Fig. 2.1C). Based on this result, we next designed for the final editing tool gRNA #4 which differ from gRNA #2 only in a single base pair (Fig. 2.1D), corresponding to the C to T mutation found in the mutated Pde6b gene of Rd10 mice.

We further verified gRNA #4 editing efficiency in NSC derived from Rd10 homozygous pups. The transfected Rd10 cells were selected for GFP-expression with FACS and the editing efficiency was evaluated by BanI restriction assay, as described above for N2A cells. We found a mean ( $\pm$  s.d.,  $n = 3$ ) net editing efficiency of  $39.3 \pm 6.4$  % in NSC harbouring the Rd10 mutation (Fig. 2.1E-F).

These data indicate that the selected gRNA #4 efficiently targets the Rd10 mutation in the Pde6b gene and that the correct sequence can be restored with high efficiency by CRISPR/Cas9-mediated HDR editing.

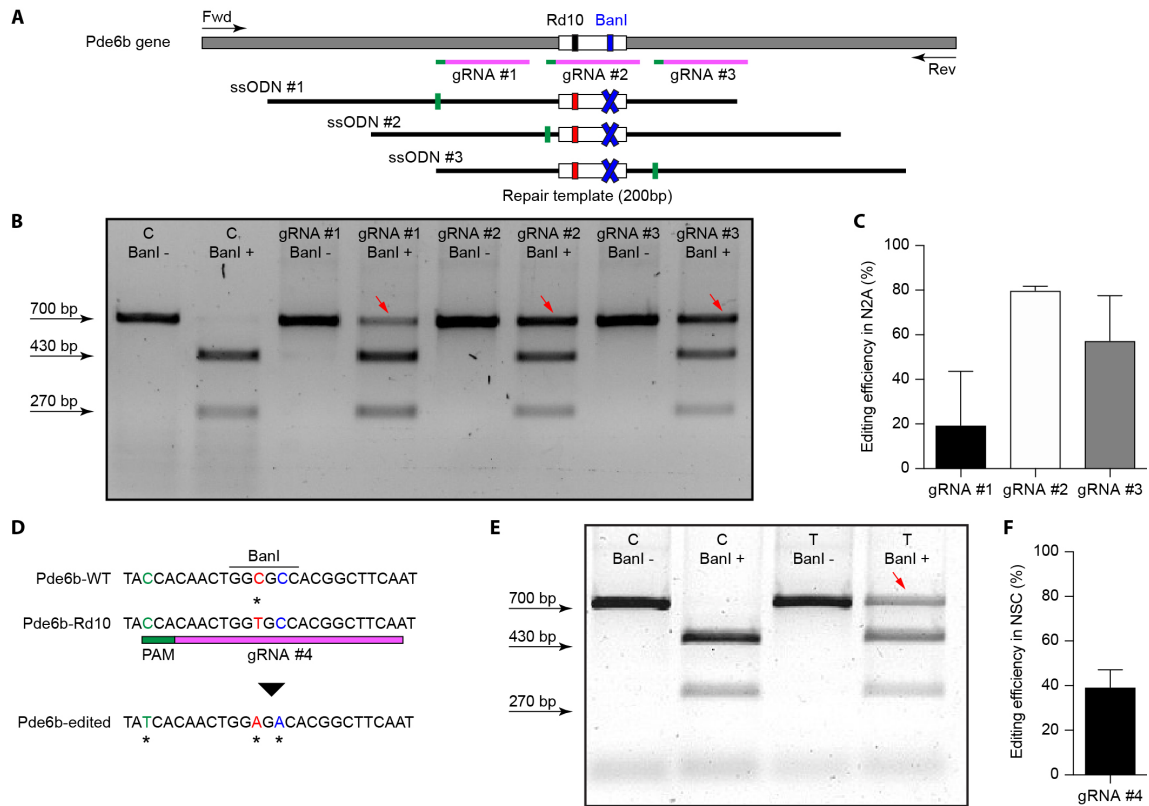


Figure 2.1: Screening of gRNAs targeting the Rd10 locus. A, Schematic representation (not in scale) of the mouse *Pde6b* gene showing the position of the three gRNAs tested (in magenta with green PAM sequence), the ssODN repair templates (black), and the PCR primers used for screening (arrows). The white rectangle represents the target editing region with Rd10 mutation (black/red) and the *BanI* cutting site (blue). Each ssODN also carries a silent mutation in the corresponding gRNA PAM sequence (green). B, Representative example of an agarose gel electrophoresis of the *BanI* restriction assay from transfected (T) and control (C) mouse N2A cells. Unedited DNA is cut in two fragments by *BanI* digestion (470 and 230 bp), while edited DNA is not cut by the restriction enzyme (700 bp band, red arrows). C, Quantification of the mean ( $\pm$  s.d.,  $n = 2$ ) editing efficiency for the three gRNA in N2A cells. D, Schematic representation of editing strategy for gRNA #4 targeting the Rd10 mutation. The HDR strategy was designed to edit the DNA sequence (in red), while introducing a silent mutation in the cutting sequence for *BanI* (in blue). A second silent mutation in the PAM sequence of the gRNA (in green) is included in the repair template in order to avoid further Cas9-mediated cutting on the edited genomic sequence. E, Representative example of an agarose gel electrophoresis of the *BanI* restriction assay for gRNA #4 transfected (T) and control (C) NSC from Rd10 mice. The red arrow indicates the edited DNA that is resistant to *BanI* digestion. F, Quantification of the mean ( $\pm$  s.d.,  $n = 3$ ) editing efficiency for gRNA #4 in Rd10 NSC.



## **Efficient delivery of a reporter gene to photoreceptor cells by *in vivo* electroporation.**

Among the non-viral delivery strategies, electroporation is one of the most efficient for the introduction of DNA into cells and holds a promising therapeutic potential [106–108, 146, 147].

Electrotransfer has been exploited for introducing genetic material and drugs in different tissues and organs and for the treatment of cancer [110, 111]. Moreover, according to *in vitro* reports [112], the size of the plasmid does not have any impact on the transfection efficiency, making the technique suitable for the delivery of large genes that would not fit into AAV viruses.

Electroporation has been widely used to study the mouse retina development [113, 114] but is still under investigation for therapeutic purposes. The only reported use of electroporation on the human eye is in the human ciliary muscle [148]. Albeit it has not yet been applied to the human retina, this delivery technique has been shown to successfully target different retinal cell types, both in young [114, 149] and adult [115] mice. For the above reasons, we chose to use electroporation to deliver our construct to the photoreceptor cells.

The efficiency of electrotransfer depends on various factors such as the cell size, the parameters of the electric pulses, and the phase of the cell cycle. The latter has to be taken into account especially when interested in targeting the highest number of cells and in exploiting the HDR mechanism to achieve gene editing. In order to obtain the highest number of transfected cells without inducing eye defects, we performed pilot experiments to optimise the electroporation protocol and select the best timing for delivery. Although electroporation immediately after birth is potentially more efficient, it can result in eye damage: in our hand, P1 electroporation resulted in more than 50 % of the pups bearing eye defects as adults, while this percentage was reduced at 40 % by performing electroporation at P3 (at the peak of the photoreceptor progenitor cell proliferation curve). For this reason, P3 was selected for the *in vivo* experiments (Fig. 2.2A, dashed line).

Despite the fact that several groups reported efficient retinal electroporation in neonatal mice using five pulses of 50 ms at 80 V (1 Hz) [113, 142], we found this protocol to cause eye defects (possibly affecting visual functions) in 40 % of the adult mice when the electroporation was performed at P3. Thus, based on previous observations in cell cultures [150], we tested a different protocol (Fig. 2.2B) consisting of two short poring pulses at high voltage (5 ms, 100 V, 0.1 Hz) followed by five long transfer pulses at a lower voltage (50 ms, 30 V, 1 Hz). Applying this improved protocol, we obtained an electroporation efficiency comparable to the standard protocol, whereas the number of pups bearing eye defects when adults decreased from 40 to 5 %; those animals were excluded from the experiments. Also, the use of a conductive gel between the electrode plate and the tissue increased the conductivity and avoided burning marks on the cornea.

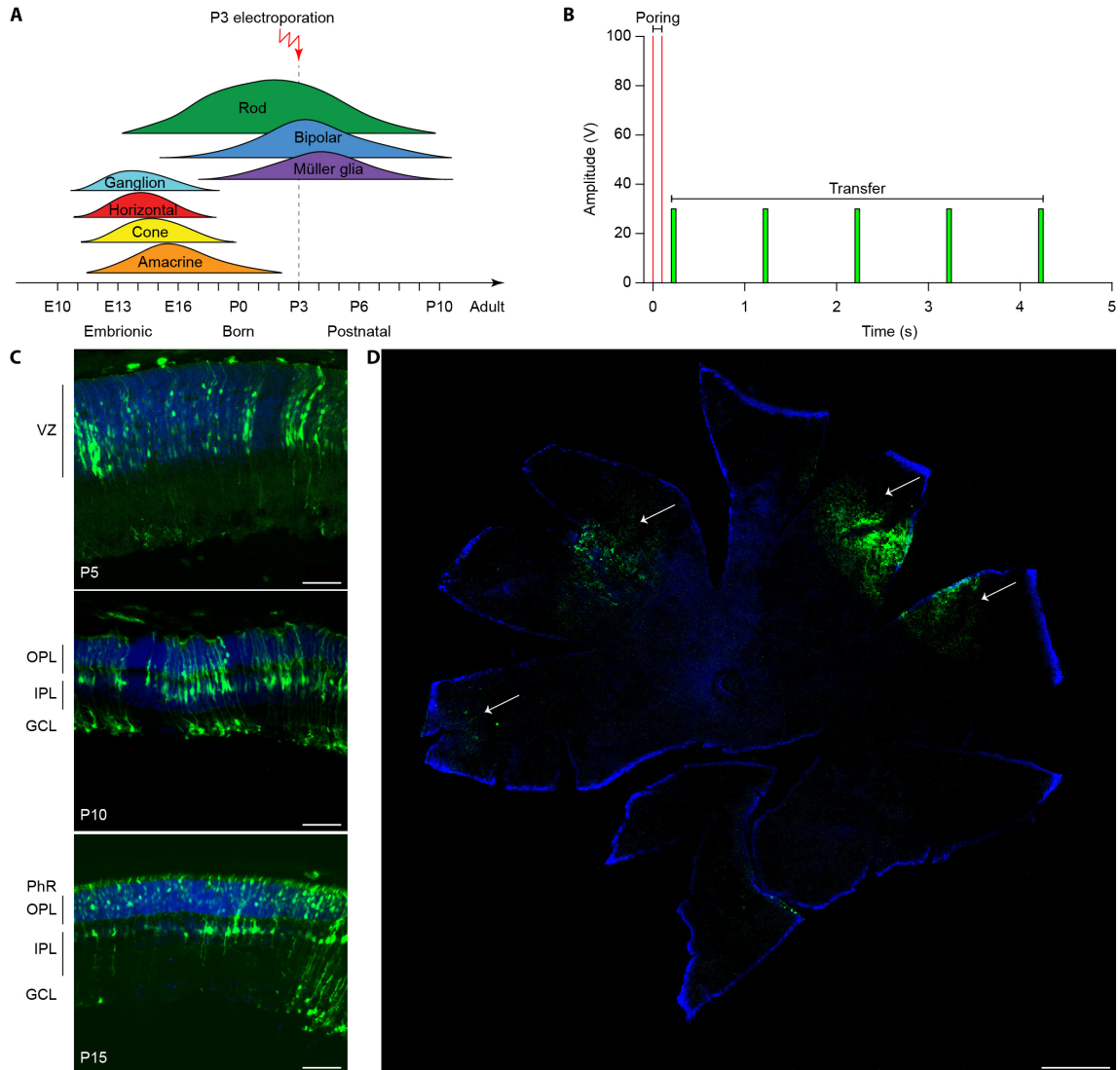


Figure 2.2: Electroporation of photoreceptor progenitor cells *in vivo* at P3. A, The graph shows the proliferation period for all the retinal cell types Sketch redrawn from [151]. The proliferation of rod photoreceptors has a peak at birth (P0-P3) and continues until P10. The electroporation was performed at P3. B, Schematic representation of the protocol used for electroporation. Two high voltage poring pulses (5 ms, 100 V, 0.1 Hz) are followed by five low voltage transfer pulses (50 ms, 30 V, 1 Hz). C, Retinal sections from Rd10 mice electroporated at P3 and collected at different time points, starting from the top: P5, P10, and P15. The scale bar is 60  $\mu\text{m}$ . On the side, the ventricular zone (VZ), the photoreceptor layer (PhR), the outer plexiform layer (OPL), the inner plexiform layer (IPL), and the ganglion cell layer (GCL) are reported. D, Representative wholemount retina electroporated at P3 and collected at P10 illustrating the spread of the electroporation (white arrows). The scale bar is 500  $\mu\text{m}$ .

In order to assess the efficiency of electroporation in targeting the photoreceptor cell progenitors *in vivo*, we delivered a plasmid coding for EGFP to the subretinal space of Rd10 mouse pups with two consecutive subretinal injections followed by electroporation at P3 (Fig. 2.2C). The image sequence shows that EGFP was expressed at all the different stages of retinal development at which the retinas were isolated: P5, P10, and P15 (n = 6 at each time point). At P5, most of the expressing cells were confined to the ventricular zone (VZ), where the photoreceptor progenitors proliferate. At P10, the cells started to migrate towards the photoreceptor layer, which they finally reached by P15. The electroporation targets mostly photoreceptors due to their proximity to the injection site, but it is not completely specific to this cell type; indeed, we observed some bipolar and ganglion cells expressing EGFP. This eventuality does not represent a concern for the outcome of the therapy since the targeted gene is expressed specifically in rod photoreceptors.

To analyse the extension of the electroporated zone, we prepared wholemount retinas from the treated mice (Fig. 2.2D). In a few cases (2 out of 6) the two consecutive injections per eye resulted in two electroporated areas and all the other cases in one area only, with a single area covering up to 25 % of the retina. The localisation of the electroporated cells depends on the orientation of the electric field to the injection site at the moment of the electroporation, which is challenging to control in an animal as small as the mouse, especially at this young age.

### **Significant editing efficiency *in vivo* of the CRISPR/Cas9 editing tool.**

Evaluating editing efficiency in whole retinas *in vivo* is a more challenging task than doing it *in vitro* due to the presence of a mixed population of transfected and non-transfected cells. To this aim, we developed a sensitive ddPCR assay with two fluorescent probes specific for the edited and unedited alleles (Fig. 2.3A).

Rd10 pups were electroporated at P3 with plasmids encoding EGFP, Cas9, gRNA #4, together with the ssODN repair template. Sham electroporation of control retinas in Rd10 pups at P3 was performed by omitting the gRNA. Three days after electroporation, we extracted the gDNA from whole retinas and analysed the editing efficiency at the *Pde6b* gene by ddPCR. We found that the mean ( $\pm$  s.d., n = 10) *in vivo* editing efficiency in Rd10 treated retinas was  $0.22 \pm 0.14$  % and significantly different from Rd10 sham retinas ( $p < 0.05$ , unpaired t-test) that however showed a low but detectable background ( $0.057 \pm 0.050$  %, n = 6) in the assay (Fig. 2.3B). The normalized editing efficiency after subtracting the detectable background is  $0.164 \pm 0.141$  %. Although *in vivo* editing efficiency appeared much lower than *in vitro*, this represents an underestimation because the assay was conducted on gDNA extracted from whole retinas that contained only a relatively small percentage of transfected cells. Moreover, treated retinas showed variable degree of editing, likely due to a difference in electroporation effi-

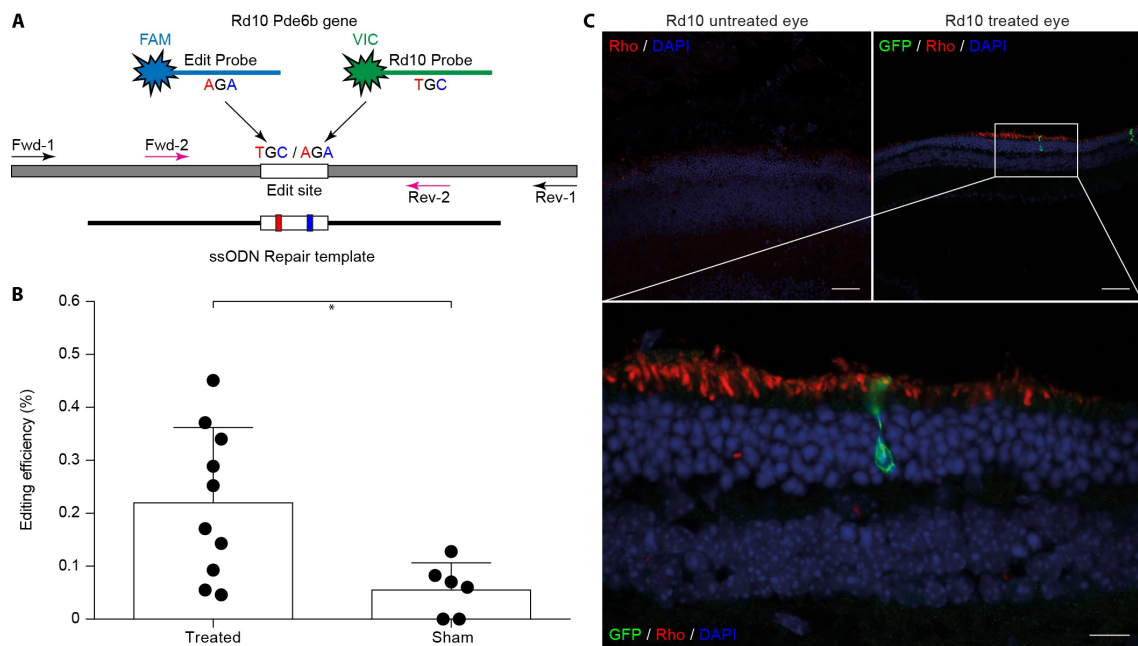


Figure 2.3: Editing efficiency *in vivo*. A, Schematic representation of the ddPCR assay used to quantify *in vivo* editing efficiency. The Pde6b gene is in grey and the ssODN repair template in black (not in scale). The white rectangle represents the target editing region. Black and magenta arrows indicate primers pairs used for the nested-ddPCR. Red and blue letters indicate base mismatches detected by the two specific fluorescent probes for the edited and unedited alleles (blue and green respectively). B, Quantification of the mean ( $\pm$  s.d.) percentage of editing in Rd10 treated retinas. C, Retinal section from P30 Rd10 mice electroporated at P3, collected at P30, and stained for rhodopsin (Rho, red), GFP (green), and DAPI (blue). Scale bars: top left and top right 25  $\mu$ m; bottom 10  $\mu$ m.

ciency. However, even a few functional photoreceptors can make a large difference when it comes to visual performance [68, 152]. We also performed a staining for rhodopsin and GFP on retinal sections from P30 Rd10 mice electroporated at P3. This result shows the preservation of rhodopsin in the outer segment of photoreceptors in the treated eyes in concomitance with electroporated cells 2.3C).

### **Gene editing preserves electroretinograms *ex vivo* and *in vivo*.**

To verify whether the extent of gene editing can translate to improved retinal functionality, we recorded the microelectroretinograms ( $\mu$ ERGs) from explanted retinas of P60 Rd10 mice that were electroporated at P3 (Fig. 2.4A). Untreated Rd10 mice were used as control.

Previous results show that Rd10 retinas are completely degenerated [153] and stop consistently responding to light stimulation at P60 [154]. We recorded simultaneously from all the electrodes of a multielectrode array (MEA) while stimulating using green light pulses (4 ms,  $0.5 \text{ mW mm}^{-2}$ ). In Fig. 2.4B, we present a representative  $\mu$ ERG response from a treated retina, as the average over ten sequential stimulations delivered at 1 Hz of repetition rate. The a-wave peak amplitudes in Rd10 treated retinas are significantly higher ( $p < 0.0001$ , unpaired t-test) than Rd10 untreated retinas (Fig. 2.4C), although some responses can still be detected from the treated retinas. This result supports our hypothesis that the functionality of the retina is preserved in Rd10 treated mice, but were obtained from a limited number of retinas (2 treated and 2 control).

To have a better indicator of the success of the therapy, we then performed ERG recordings *in vivo*. In the Rd10 mouse the degeneration of rod photoreceptors starts at 2 weeks of age and peaks at 4 weeks of age. The thickness of the outer nuclear layer abruptly drops from P20 to P25, which translates into the almost complete absence of ERG responses by P30 [133]. Based on this evidence, we recorded ERGs at P30 in Rd10 mice unilaterally treated (at P3) and WT mice upon Ganzfeld flash stimulation (Fig. 2.4D). In Fig. 2.4E, representative ERG responses (average of 5 sweeps) are shown for the treated (blue) and untreated (black) eyes in Rd10 mice and for both eyes (grey) in WT mice. We then compared the a-wave amplitude in Rd10 mice (Fig. 2.4F) and WT mice (Fig. 2.4G), which correlates directly with the functionality of photoreceptors [119]. These results suggest a preserved photoreceptor functionality in the treated eyes of P3 treated mice compared to the control eye ( $p < 0.01$ , paired t-test). As expected, in WT mice there is no significant difference between the response of the left and right eye ( $p = 0.1969$ , paired t-test).

### **Gene editing preserves visual acuity *in vivo* until P90.**

Next, we assessed the visual acuity of Rd10 unilaterally treated (at P3), Rd10 unilaterally sham-treated (at P3), Rd10 untreated, and WT adult mice using a behavioural assay.

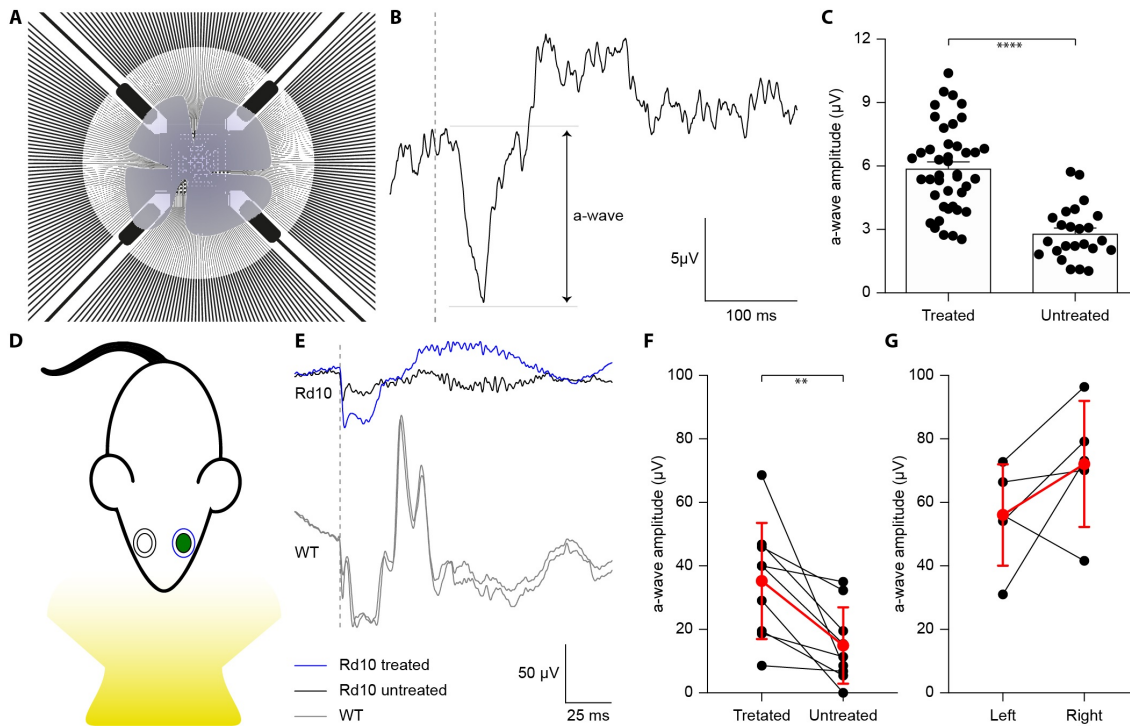


Figure 2.4: Preservation of *ex vivo* microelectroretinograms at P60 and *in vivo* electroretinograms at P30. A, Schematic representation of the *ex vivo* experiment. The retina was dissected and placed on a transparent MEA with the retinal ganglion cell side down in contact with the electrodes. The retina was stimulated using green light pulses coming from the bottom. B, Representative recording from a Rd10 retina treated at P3. C, Quantification of the mean ( $\pm$  s.e.m.) amplitude of the a-wave in the two experimental groups: Rd10 treated ( $5.89 \pm 0.31$ ,  $n = 42$  channels from 2 retinas) and Rd10 untreated ( $2.81 \pm 0.26$ ,  $n = 27$  channels from 2 retinas) retinas. D, Sketch of the recording setup in which the electrode recording from the treated eye (green) is in blue, while the one recording from the untreated eye is in black. E, Representative ERG responses for the treated (blue) and untreated (black) eyes of a Rd10 mouse treated at P3 (top traces) and for the right and left eyes (both in grey) of a WT mouse (bottom panel). The grey dashed lines represent the occurrence of the flash. F, Comparison of the a-wave amplitude of the treated and untreated eyes in Rd10 mice. Mean ( $\pm$  s.d.,  $n = 9$ ) in red. G, Comparison of the a-wave amplitude of the left and right eyes in WT mice. Mean ( $\pm$  s.d.,  $n = 5$ ) in red.

The optomotor test, which measures the integrity of the subcortical visual pathways, uses the amplitude of the optomotor reflex to evaluate the visual acuity of rodents (Fig. 2.5A). In particular, it allows the distinction between right eye-driven and left eye-driven responses, measuring the visual threshold of each eye independently [128]. At P30 (about 1 month after treatment), in Rd10 mice, the treated eye (Fig. 2.5B, white circles) showed a higher visual acuity compared to the paired untreated eye (treated  $0.24 \pm 0.01$  C/°, untreated  $0.14 \pm 0.01$  C/°;  $n = 71$ ,  $p < 0.0001$ , Mann-Whitney test). Conversely, the Rd10 sham-treated eye (light grey circles) did not show any improvement compared to the paired untreated eye (sham  $0.11 \pm 0.01$  C/°, untreated  $0.13 \pm 0.01$  C/°;  $n = 20$ ,  $p = 0.2306$ , unpaired t-test). In both WT (left  $0.41 \pm 0.01$  C/°, right  $0.39 \pm 0.01$  C/°;  $n = 32$ ,  $p = 0.1009$ , Mann-Whitney test; black dots) and Rd10 (left  $0.12 \pm 0.01$  C/°, right  $0.11 \pm 0.01$  C/°;  $n = 47$ ,  $p = 0.4908$ , unpaired t-test; dark grey dots) mice no difference was detected between the left and right eyes (Fig. 2.5B). Measures of the optomotor reflex (Fig. 2.5C) demonstrated that the average visual acuity in the treated eyes of Rd10 mice is significantly higher than the average visual acuity of both Rd10 mice ( $p < 0.0001$ ; One Way ANOVA, Tukey's multiple comparisons test) and sham-treated eyes in Rd10 mice ( $p < 0.0001$ ; One Way ANOVA, Tukey's multiple comparisons test). Sham-treated eyes have a visual acuity not statistically different from Rd10 mice's eyes ( $p = 0.9849$ ; One Way ANOVA, Tukey's multiple comparisons test).

Since it was not measured in dark-adapted conditions, the outcome of the optomotor test is essentially related to the integrity of cone cells and direction-selective retinal ganglion cells. However, the visual acuity measured with this test is reportedly decreasing in Rd10 mice, already starting from P30 [127], which matches our data from control and sham mice. We can thus attribute any further preservation of visual acuity to a protective effect of the treatment. However, the visual acuity, measured with the optomotor test, eventually declined at P90, even in treated mice. We hypothesise that, since the coverage of the injection is not enough to edit the DNA of all the photoreceptor cells, eventually, also the edited cells succumb to the adverse effect of pro-apoptotic factors released by the non-edited dying cells. Multiple cycles of injections followed by electroporation could solve this issue by allowing the gene editing of a higher number of photoreceptors, especially if performed during the progenitor proliferation period.

In vision of a possible translatability of the therapeutic approach, it is way more interesting to investigate what happens at a later stage of photoreceptor differentiation, namely when the differentiation is complete. This is true because in humans it is not possible to perform an *in utero* therapeutic approach and the disease is likely to be discovered at a later stage, when there is no more photoreceptor progenitor cell proliferation.

To this end, we treated mice at P8 (Fig. 2.6A), approximately at the end of the progenitor cell proliferation curve [151]. Electroporation at P8 did not result in

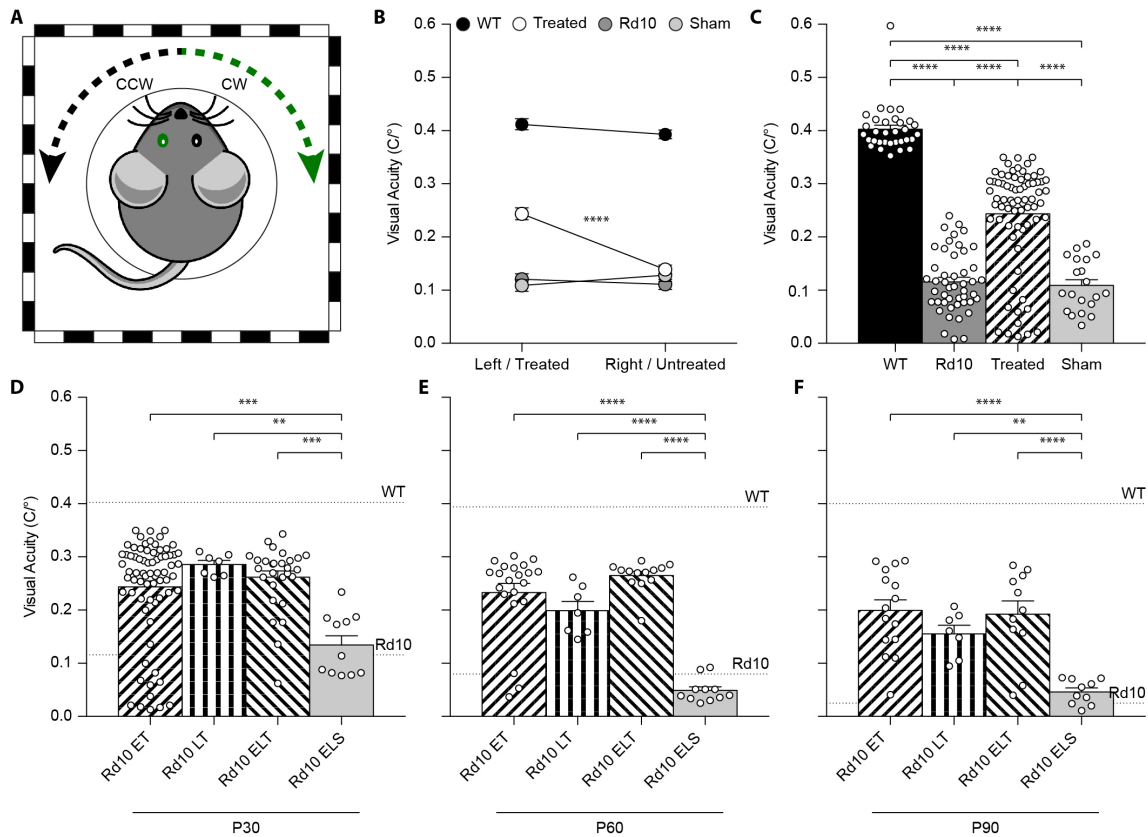


Figure 2.5: Preservation of the visual acuity in Rd10 treated mice. A, For each mouse, both the clock-wise (CW, left eye) and counter clock-wise (CCW, right eye) responses were assessed. The sketch represents a mouse with treatment (green) in the left eye (corresponding to the CW response). B, Mean ( $\pm$  s.e.m.) visual acuity in WT mice (black circles), untreated Rd10 mice (dark grey circles), Rd10 treated mice (white circles), and Rd10 sham-treated mice (light grey circles). C, Statistical comparison among the 4 groups ( $p < 0.0001$ , One Way ANOVA): WT ( $0.40 \pm 0.01$  C/°,  $n = 32$ , averaged left and right responses), Rd10 ( $0.12 \pm 0.01$  C/°,  $n = 47$ , averaged left and right responses), Rd10 treated ( $0.24 \pm 0.01$  C/°,  $n = 71$ ), and Rd10 sham ( $0.11 \pm 0.01$  C/°,  $n = 20$ ). D, Statistical comparison ( $p < 0.001$ , One Way ANOVA) of the mean ( $\pm$  s.e.m.) visual acuity among Rd10 ET ( $0.24 \pm 0.01$  C/°,  $n = 71$ ), Rd10 LT ( $0.29 \pm 0.01$  C/°,  $n = 7$ ), Rd10 ELT ( $0.26 \pm 0.01$  C/°,  $n = 28$ ), and Rd10 ELS ( $0.13 \pm 0.02$  C/°,  $n = 11$ ) at P30. E, Statistical comparison ( $p < 0.0001$ , One Way ANOVA) of the mean ( $\pm$  s.e.m.) visual acuity among Rd10 ET ( $0.23 \pm 0.02$  C/°,  $n = 21$ ), Rd10 LT ( $0.20 \pm 0.02$  C/°,  $n = 7$ ), Rd10 ELT ( $0.26 \pm 0.01$  C/°,  $n = 13$ ), and Rd10 ELS ( $0.05 \pm 0.02$  C/°,  $n = 11$ ) at P60. F, Statistical comparison ( $p < 0.0001$ , One Way ANOVA) of the mean ( $\pm$  s.e.m.) visual acuity among Rd10 ET ( $0.20 \pm 0.02$  C/°,  $n = 15$ ), Rd10 LT ( $0.15 \pm 0.02$  C/°,  $n = 7$ ), Rd10 ELT ( $0.20 \pm 0.03$  C/°,  $n = 11$ ), and Rd10 ELS ( $0.05 \pm 0.02$  C/°,  $n = 10$ ) at P90. In panels C-F, each circle represents a single mouse.



any eye damage. After the electroporation at P8, the EGFP fluorescence could be detected in retinas of P10 and P15 mice (Fig. 2.6B-C).

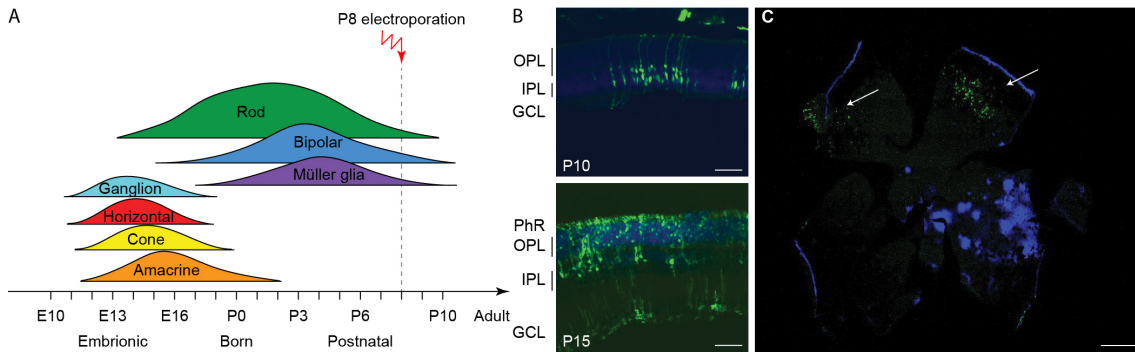


Figure 2.6: Electroporation *in vivo* of photoreceptor progenitor cells at P8. A, Sketch of the late electroporation time point (P8), at the end of the proliferation period. B, Retinal sections from mice electroporated at P8. The sections were collected at two time points after electroporation: P10 and P15. The scale bar is 60  $\mu\text{m}$ . On the side, the PhR layer, the OPL, IPL, and the GCL are reported. C, Wholemount retina electroporated at P8 and collected at P15, illustrating the spread of the electroporation (white arrows). The scale bar is 500  $\mu\text{m}$ .

Based on this result, we assessed the impact of the period of treatment on the optomotor reflex. We compared the optomotor reflex responses of P30 Rd10 mice upon electroporation at P3 (Rd10 Early Treated, ET), P8 (Rd10 Late Treated, LT), or P3 and P8 (Rd10 Early/Late Treated, ELT). We also performed the test in Rd10 control animals (Rd10), WT animals (WT) and P3 and P8 sham treated animals (Rd10 Early/Late Sham, ELS). The first treatment corresponds to the peak of the rod progenitor proliferation curve (P3), the second one to the end of the curve (P8), and the last treatment to the combination of the two (Fig. 2.5D). As for the Rd10 ET mice (Fig. 2.5B), also for the Rd10 LT (Fig. 2.7A) and the Rd10 ELT (Fig. 2.7B), the visual acuity measured in the treated eyes was significantly higher than the visual acuity of the paired untreated eyes. Conversely, in Rd10 Early/Late Sham (Rd10 ELS) treated mice the visual acuity was not different between injected and not injected eyes (Fig. 2.7C).

Notably, we have demonstrated that repeated treatment (at P3 and P8) is not detrimental for the mice, although we cannot conclude that it increases the number of cells targeted or the preservation of visual functions. However, the mouse, especially the pup, is not an ideal model to test this hypothesis, given the tiny size of the eyes: multiple injections and electroporation would damage the eye excessively and it is really difficult to control the injection site or the amount of plasmid delivered, leading to a high variability in the effect of the treatment among subjects.

Last, we verified the long-term preservation of visual acuity by repeating the optomotor test at P60 and P90. Interestingly, while the visual acuity dropped drastically in untreated (Rd10) and sham-treated (ELS) mice at P60, it did not show a significant decline in any of the treated groups (ET, LT, and, ELT; Fig.

2.5E). At P90, the visual acuity eventually decreased also in treated mice, but overall all the treated groups (ET, LT, and ELT) retained about 50 % of their initial value (Fig. 2.5F). This result shows a preserved functionality of subcortical visual pathways up to 3 months in treated mice at both P3 and P8.

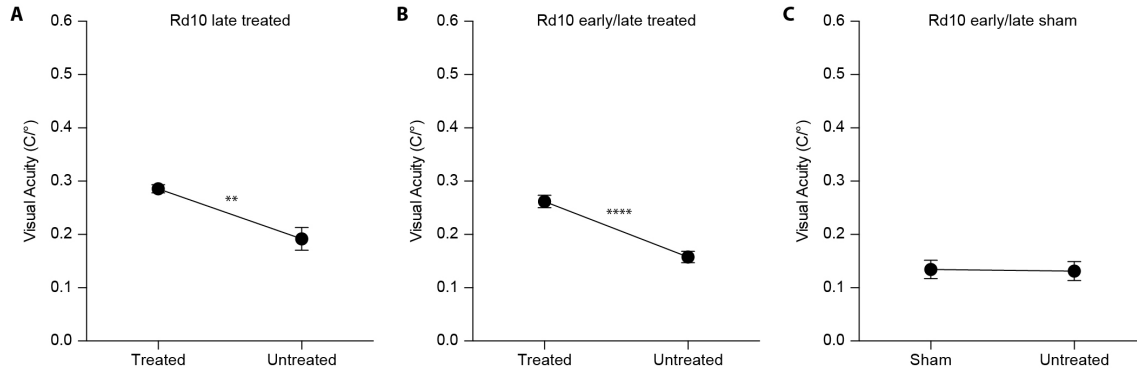


Figure 2.7: Optomotor reflex upon electroporation at P8. A, Mean ( $\pm$  s.e.m.) visual acuity in Rd10 mice treated at P8 (Rd10 LT; treated eye  $0.29 \pm 0.01$  C/°, untreated eye  $0.19 \pm 0.02$  C/°;  $n = 7$ ,  $p < 0.01$ , unpaired t-test). B, Mean ( $\pm$  s.e.m.) visual acuity in Rd10 mice treated at P3 and P8 (Rd10 ELT; treated eye  $0.26 \pm 0.01$  C/°, untreated eye  $0.16 \pm 0.01$  C/°;  $n = 28$ ,  $p < 0.0001$ , unpaired t-test). C, Mean ( $\pm$  s.e.m.) visual acuity in Rd10 mice sham treated at P3 and P8 (Rd10 ELS; sham eye  $0.13 \pm 0.02$  C/°, untreated eye  $0.13 \pm 0.02$  C/°;  $n = 11$ ,  $p = 0.8992$ , unpaired t-test).

### Gene editing preserves flash-evoked cortical responses at P90.

To assess the functionality of the retino-cortical visual pathway, we recorded VEPs from both hemispheres upon flash stimulation. In Fig. 2.8A, we show a representative trace for each experimental group. For treated and sham-treated Rd10 mice, the representative recordings are relative to the cortex contralateral to the injected eye, since in the mouse the majority of the projections decussate at the optic chiasm [155].

Since we cannot exclude completely the input coming from the untreated eye (ipsilateral projection), we compared the results of the treated mice with the ones from Rd10 and sham-treated animals to isolate the contribution of the therapy. The mean prominence of the response's peaks was computed. At P90, Rd10 animals show a complete retinal degeneration with very few spared photoreceptors [133, 156]. Accordingly, we observed an almost flat response in untreated (Rd10) and sham-treated (Rd10 ES and Rd10 ELS) mice. Conversely, when recording from all the treated groups (Rd10 ET, Rd10 LT, and Rd10 ELT), we observed preservation of the peak prominence in the visual response of the contralateral cortex (Fig. 2.8B). This is indicative of a preserved functionality of cortical visual pathways ( $p < 0.0001$ ; Kruskal-Wallis, Dunns multiple comparison test). In the ipsilateral cortex (Fig. 2.8C), the only significant difference was between WT and Rd10 ( $p < 0.01$ ; Kruskal-Wallis, Dunns multiple comparison test). Finally, we

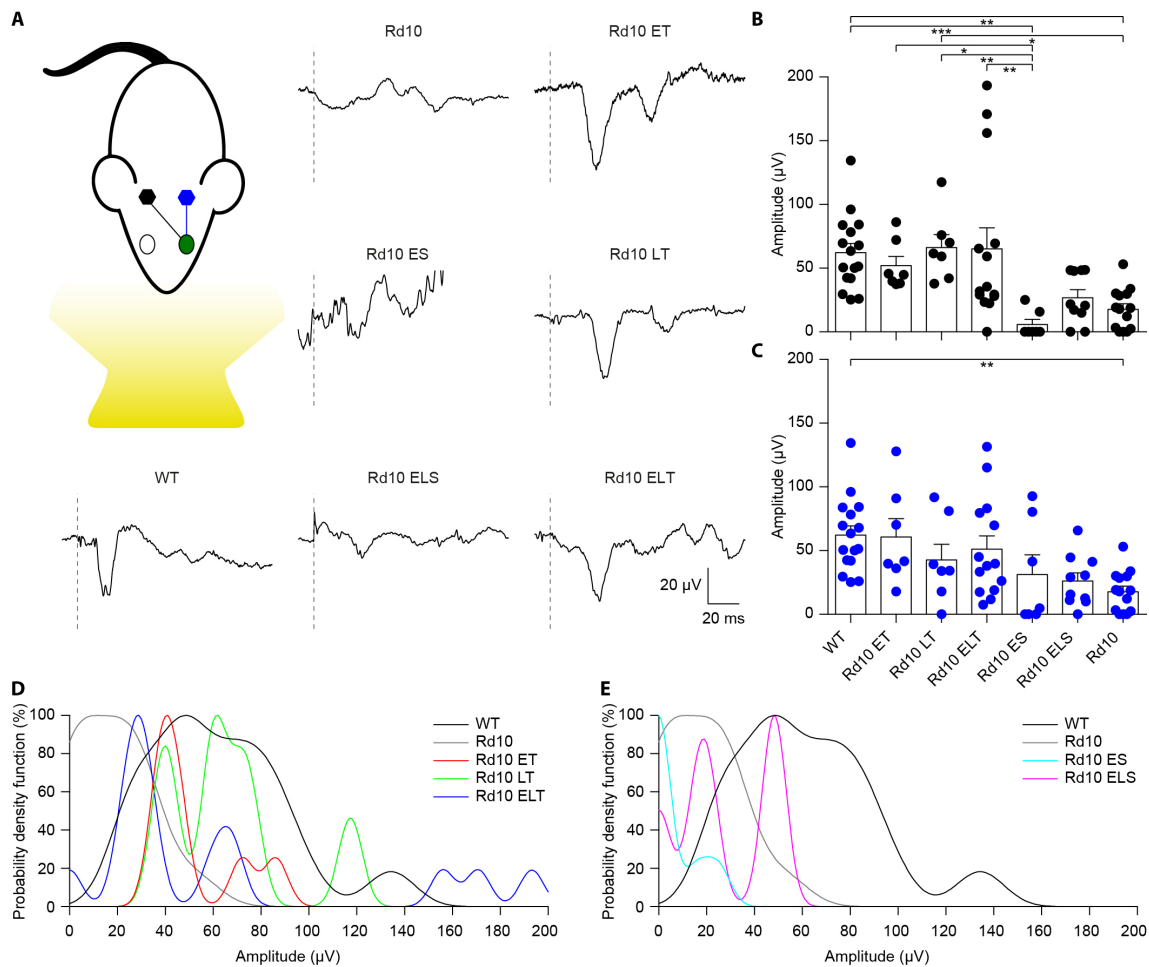


Figure 2.8: Preservation of visually evoked potentials at P90. A, Sketch of the recording setup in which the cortex contralateral to the treated eye (green) is in black, while the ipsilateral is in blue. Representative VEP response for each experimental group. The grey dashed lines are the occurrence of the white light flash (4 ms length). For treated (Rd10 ET, Rd10 LT, and Rd10 ELT) and sham-treated (Rd10 ES and Rd10 ELS) mice, the traces are from the contralateral cortex, while for WT and Rd10 mice the responses of the two cortices were averaged. B, Mean ( $\pm$  s.e.m.) contralateral peak amplitude for all the experimental groups: WT ( $91.7 \pm 11.1 \mu\text{V}$ ,  $n = 16$ ), Rd10 ET ( $62.4 \pm 9.4 \mu\text{V}$ ,  $n = 7$ ), Rd10 LT ( $73.1 \pm 10.8 \mu\text{V}$ ,  $n = 7$ ), Rd10 ELT ( $71.7 \pm 15.2 \mu\text{V}$ ,  $n = 14$ ), Rd10 ES ( $13.7 \pm 8.9 \mu\text{V}$ ,  $n = 7$ ), Rd10 ELS ( $34.4 \pm 7.1 \mu\text{V}$ ,  $n = 10$ ), and Rd10 ( $23.8 \pm 5.5 \mu\text{V}$ ,  $n = 14$ ). C, Mean ( $\pm$  s.e.m.) ipsilateral peak amplitude for all the experimental groups: WT ( $91.7 \pm 11.1 \mu\text{V}$ ,  $n = 16$ ), Rd10 ET ( $69.6 \pm 14.4 \mu\text{V}$ ,  $n = 7$ ), Rd10 LT ( $49.8 \pm 12.8 \mu\text{V}$ ,  $n = 7$ ), Rd10 ELT ( $96.6 \pm 20.7 \mu\text{V}$ ,  $n = 14$ ), Rd10 ES ( $48.0 \pm 21.9 \mu\text{V}$ ,  $n = 7$ ), Rd10 ELS ( $30.8 \pm 7.0 \mu\text{V}$ ,  $n = 10$ ), and Rd10 ( $23.8 \pm 5.5 \mu\text{V}$ ,  $n = 14$ ). In B and C, for WT and Rd10 mice the responses of the two cortices were averaged before computing the peak amplitude; therefore, they are equal. D, Probability density functions fitted using a Kernel distribution of the contralateral response for the treated groups (Rd10 ET, Rd10 LT, and Rd10 ELT) compared to WT and Rd10 mice. E, Probability density functions fitted with a Kernel distribution of the contralateral response for the sham-treated groups (Rd10 ES and Rd10 ELS) mice compared to WT and Rd10 mice.

further compared the scaled probability density functions (pdf, Fig. 2.9) of the VEP prominences in the treated (Fig. 2.8D) and sham-treated (Fig. 2.8E) mice to the ones of WT and Rd10 mice. In WT mice, the pdf was broadly centred at 50  $\mu\text{V}$ . All of the treated groups had a distribution that appeared to be concentrated around 50  $\mu\text{V}$  and narrower than the one of WT mice. In contrast, sham-treated and control group distributions are skewed towards 0, highlighting the higher amount of non-responding mice.

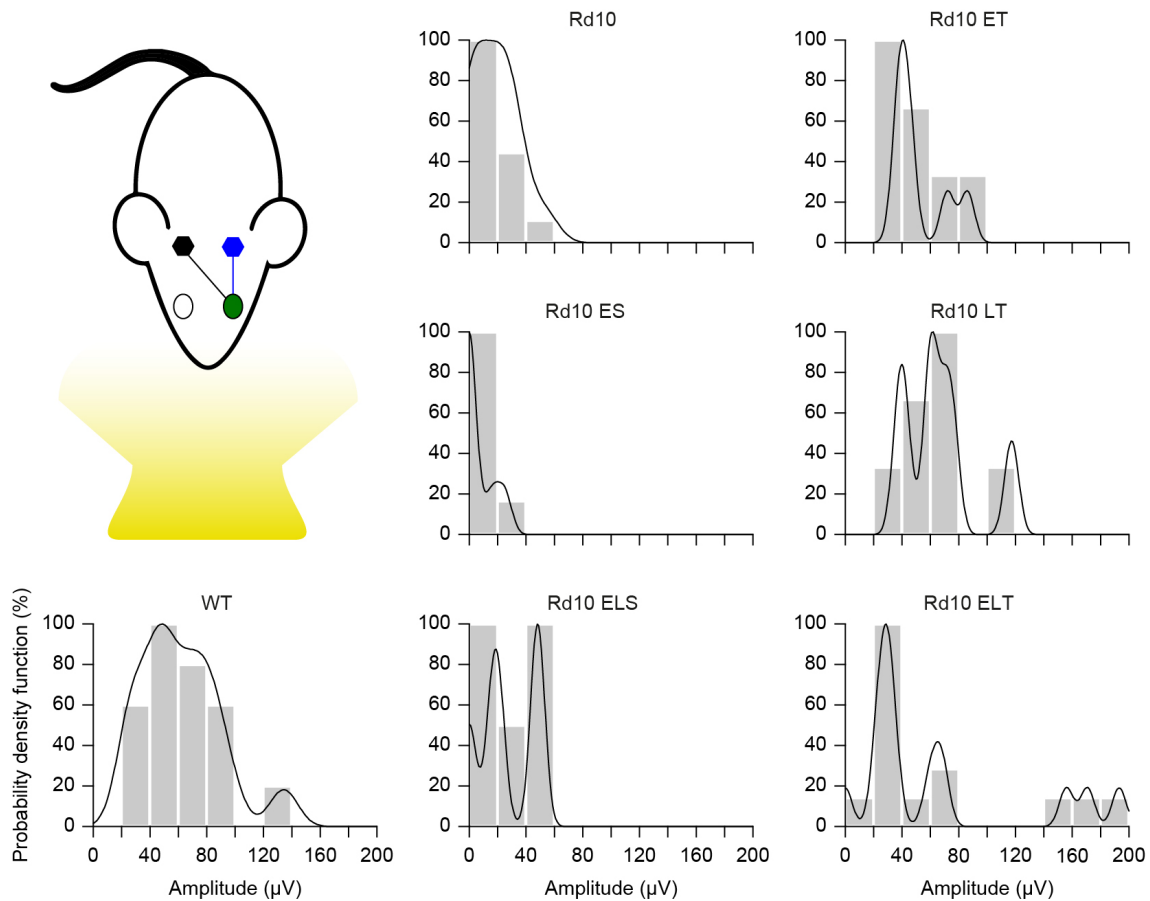


Figure 2.9: Probability density function for the VEP recordings. Each panel shows the histogram (20  $\mu\text{V}$  bins) of the VEP peak amplitude and the fitted Kernel distribution for all the experimental groups. For treated (Rd10 ET, Rd10 LT, and Rd10 ELT) and sham treated (Rd10 ES and Rd10 ELS) mice, the data are from recordings in the cortex (black) contralateral to the treated eye (green).

## 2.4 Conclusions

In conclusion, we used electroporation, a non-viral gene delivery method, to deliver a CRISPR/Cas9 gene editing system to the photoreceptor cells of Rd10 mice. Intervening at the peak of photoreceptor progenitor cell proliferation allowed the approach to be the most effective since it takes advantage of the HDR repair mechanism, which is more active in dividing cells.

Visual functions, relative to both subcortical visual-driven behavioural re-

sponses (optomotor reflex) and cortical visual responses (VEP), were preserved until as late as P90. Overall, the treated mice retained 50 % of the normal visual acuity even three months after the treatment. The visual acuity appears slightly declined at P90, but more long-term experiments are needed to confirm this trend. Possibly, repeating the administration of the therapeutic agent could avoid this problem. Although, as discussed above, the mouse is not the best model to test this hypothesis.

In this study, we provide an example of how CRISPR/Cas9 gene editing can be coupled with electroporation for therapeutic purpose, along with a discussion of the limitations that need to be overcome to translate this approach to the clinics. P3 and, even more so, P8 are considered late timepoints for intervention in mice [139, 140], since P3 is at the beginning of the descending curve of rod proliferation and P8 is at its very end [151]. However, it is currently not possible to translate this approach to human patients given that the available screening methods allow the detection of retinal degeneration only at a late stage and our therapeutic tool is relying on the HDR mechanism, which is much less active in post-mitotic cells. Nevertheless, some future improvements might change this situation. For instance, although we used a standard CRISPR/Cas9 construct, various research groups are working on ways to improve the efficiency of HDR in post-mitotic cells. This has been successfully achieved in different ways: for instance, using molecules that are inhibiting NHEJ [157], exerting temporal control on Cas9 expression [158], and covalently tethering the repair template to the Cas9 protein to increase its concentration on the site of the DNA double-strand break [159]. Moreover, in the future, more advanced diagnostic tools might be available to enable early detection of the degeneration, prior to the onset of the symptoms.

Issues related to the safety of retinal electroporation in large animals, repeatability of the treatment, transfection efficiency, retinal coverage, gene expression levels, and disease stage at the age of injection still need a careful investigation to improve the therapeutic benefits of CRISPR/Cas9-based gene editing strategies. On the other hand, the ease of design of the CRISPR/Cas9 gene editing systems makes them easily tailorable for several mutations in the perspective of a patient-specific therapy. This concept applies particularly when there are small differences in the DNA sequence, as in the case of autosomal recessive mutations.

Our non-viral delivery approach has two main advantages compared to previous reports in small animal models in which retinal degeneration was prevented by viral-mediated delivery of Cas9. First, in perspective of a possible clinical application, it circumvents possible safety issues deriving from viral-based gene therapy. Secondly, plasmid vector delivery by electroporation will result in transient expression of Cas9, therefore limiting the possible occurrence of off-target activity of the nuclease after long-term expression.

3

**Development of a minipig  
chemically-induced model of  
photoreceptor degeneration for  
the *in vivo* testing of retinal  
prostheses**

---

\*Vagni P et al. Manuscript in preparation.

*Contribution:* I performed and analysed *in vivo* electrophysiological experiments, set up the anatomical/histological evaluation, and participated in writing the draft of the manuscript.

## 3.1 Introduction

### The Göttingen minipig as a model of retinal degeneration

The swine is one of the most used animal models in translational research due to the physiological similarity of many organ systems with their human counterparts, which overcomes the principal limitations encountered with smaller animals, such as rodents and rabbits. Notably, the swine is becoming the preferred animal model in translational research for testing surgical procedures and novel implants, including stents, valves, and prostheses [160]. Miniature pigs are also now routinely used: in addition to the human-like anatomy and well-defined genetics, the relatively smaller size makes their manipulation easier [161]. Certain breeds, such as the Göttingen minipig, do not exceed 30-35 Kg of weight in the adulthood and are thus easier to breed in research facilities and manipulate during experiments.

Since the development of Göttingen minipigs in the 1960s, miniature pigs became widely used in ocular research [45] by reason of the size of their eyes being similar to the one of humans [162]. Moreover, like pigs and humans, they have a cone rich part of the retina: the area centralis [43, 163]. These characteristics are extremely valuable in the context of translational studies, as demonstrated by the extensive use of miniature pigs to develop novel implantation techniques, evaluate the safety of new ocular drugs, and test novel biomaterials and implantable ocular devices [164–168].

Specifically, miniature pigs offer a good opportunity for the preclinical testing of retinal prostheses [46]. In recent years, several studies employed miniature pigs [169–174] as well as pigs [175–178]. The challenge behind the use of miniature pigs to validate retinal prostheses lies in the need of a model of blindness, such as photoreceptor degeneration. Such an animal model is not easy to obtain using genetic manipulation in large mammals. Although some miniature pig models of genetic RP have been developed [35, 179], their availability is very limited, especially outside the United States of America.

Retinal degeneration has also been obtained by light exposure, but in this case the procedure is more efficient when performed on albino animals, restricting its use mostly to mice, rats, and rabbits [180]. An alternative approach that does not require genetic manipulation and can be applied to animals that are not albino consists of rapidly inducing photoreceptor degeneration using a chemical substance that interferes with the metabolism of photoreceptor cells. One option is the intravitreal injection of N-metil-N-nitrosurea (MNU), which leads to dose-dependent oxidative stress, resulting in cellular apoptosis. The toxin can be administered to one eye, leaving the other as an internal control. However, the effect of MNU appears to be unpredictable and to leads to an extremely variable degree of photoreceptor degeneration, even in different areas of the same eye. This was documented in studies performed in mice and rabbits [181, 182]. More-

over, MNU has toxic and carcinogenic properties that raise a number of concerns relative to the health of the experimenters and issues related to waste disposal and environmental hazard.

Another well documented strategy of induced photoreceptor degeneration relies on the intravenous injection of iodoacetic acid (IAA) [183, 184]. IAA suppresses glycolysis by inhibiting the function of the glyceraldehyde-3 phosphate dehydrogenase in a concentration dependent way [185]. The effect of IAA was documented in various animal models and, among the medium and large animals, notably in rabbits [186–188] and pigs [189–192]. Long-term studies in rabbits showed a degeneration restricted to the photoreceptor layer, mostly in the ventral retina and visual streak [187]. Further systemic effects are avoided when using an appropriate concentration of IAA, which is toxic for photoreceptors, but not for other cells in the body. Optical coherence tomography (OCT) images revealed the loss of the photoreceptor outer segments and the preservation of the inner segments in the rabbit [188]. Moreover, IAA administration did not lead to extensive remodeling of the surviving retinal cells, contrarily to what is observed in genetic models of inherited retinal degeneration [187]. The effect was stronger in rods than in cones [193] and the magnitude and spread of the degeneration had a certain extent of variability between animals [187].

In pigs, IAA leads to a strong rod degeneration and partial cone inactivation [191]. From the functional point of view, IAA induces a dose-dependent stable decline of full-field flash electroretinogram (ffERG) in both dark- and light-adapted animals. However, the dark-adapted functions are more affected, while the light-adapted responses are partially spared, reflecting the higher susceptibility of rods to the toxin [190]. Although IAA has to be administered via IV injection, hence affecting both eyes, this is at the moment the safest and most reliable option to obtain a light-insensitive large animal model that does not rely on complicated genetic manipulations.

Despite IAA has been previously tested in several animal models, there is a lack of information regarding the reaction to the toxin in the retina of miniature pigs, which cannot be directly inferred from the studies performed in pigs, since there are considerable differences, most notably in size, that can account for diversity in the metabolic response to the toxin. Given the extensive use of miniature pigs as animal models in retinal research, a throughout characterization of the effect of IAA on their retina is needed in view of preclinical applications.

### **Using light-insensitive minipigs to test the POLYRETINA epiretinal prosthesis**

A number of retinal prostheses have been developed in order to fight blindness, a condition that affects an increasing amount of people globally [194]. Several clinical trials have provided positive results, showing recovery of coarse visual functions in blind people using prosthetic devices (e.g. single letter and simple



object discrimination) [195, 196]. Although, many problems still need to be addressed in order to enlarge the visual field and increase the visual acuity above what is considered the threshold for legal blindness (visual acuity lower than 20/200 or visual field smaller than 20 degrees) [197].

The visual field could be enlarged by increasing the surface of the prosthesis [198], but generally the maximum size achievable is given by the size of the aperture (sclerotomy) the surgeon has to make to implant the device. Similarly, while the problem of visual acuity could be tackled using a higher density of electrodes [199], said density is generally limited by the presence of the traces connecting the electrodes to the electronics/stimulator.

In this context, the POLYRETINA epiretinal prosthesis was developed by our laboratory to address the aforementioned problems. This device is a wide field photovoltaic epiretinal prosthesis that can be folded (rolling it on itself), hence minimizing the sclerotomy size needed for its implantation. At the same time, the photovoltaic pixels do not need to be physically connected to any electronics and this allows POLYRETINA to have a higher electrode density [200–202]. Once in the eye, the prosthesis unfolds and can be attached to the ganglion cell side of the retina (Fig. 3.1E).

POLYRETINA is based on poly(dimethylsiloxane) (PDMS) as substrate material, which was chosen because of its transparency, elasticity, low Young's modulus, high strain to failure, and availability as medical grade elastomer. The PDMS–photovoltaic interface (Fig. 3.1A) embeds 2215 stimulating pixels (80 and 130  $\mu\text{m}$  in diameter) distributed on an active area of 12.7 mm (Fig. 3.1C). Each pixel is composed by conjugated polymers and organic semiconductors: PEDOT:PSS (poly(3,4-ethylenedioxythiophene)-poly(styrenesulfonate)) as bottom anode, P3HT:PCBM (regioregular poly(3-hexylthiophene-2,5-diyl), P3HT; [6,6]-phenyl-C61-butyric acid methyl ester, PCBM) as semiconductor layer (also called blend), and titanium (Ti) as top catode (Fig. 3.1B). Another PDMS layer encapsulates the prosthesis, avoiding the delamination of the material (Fig. 3.1D). The photovoltaic reaction, based on the absorbance spectrum of the blend, is best elicited using green light (565 nm).

The POLYRETINA epiretinal prosthesis was extensively tested *in vitro* with positive outcomes [57, 59]. The following step is to test the device *in vivo* using a suitable animal model.

Although retinal prostheses based on micro-electrode arrays coupled to external cameras might not strictly require a blind animal to be tested *in vivo*, the recent development of light-based [195, 204, 205] and photovoltaic [57, 202, 206–208] devices imposes the use of a light-insensitive animal model (ideally lacking the photoreceptor layer) for their functional validation, so as to decouple the effect of the prosthesis activation from the response of remaining retinal photoreceptors. This is where a light-insensitive minipig model of retinal degeneration could be convenient.

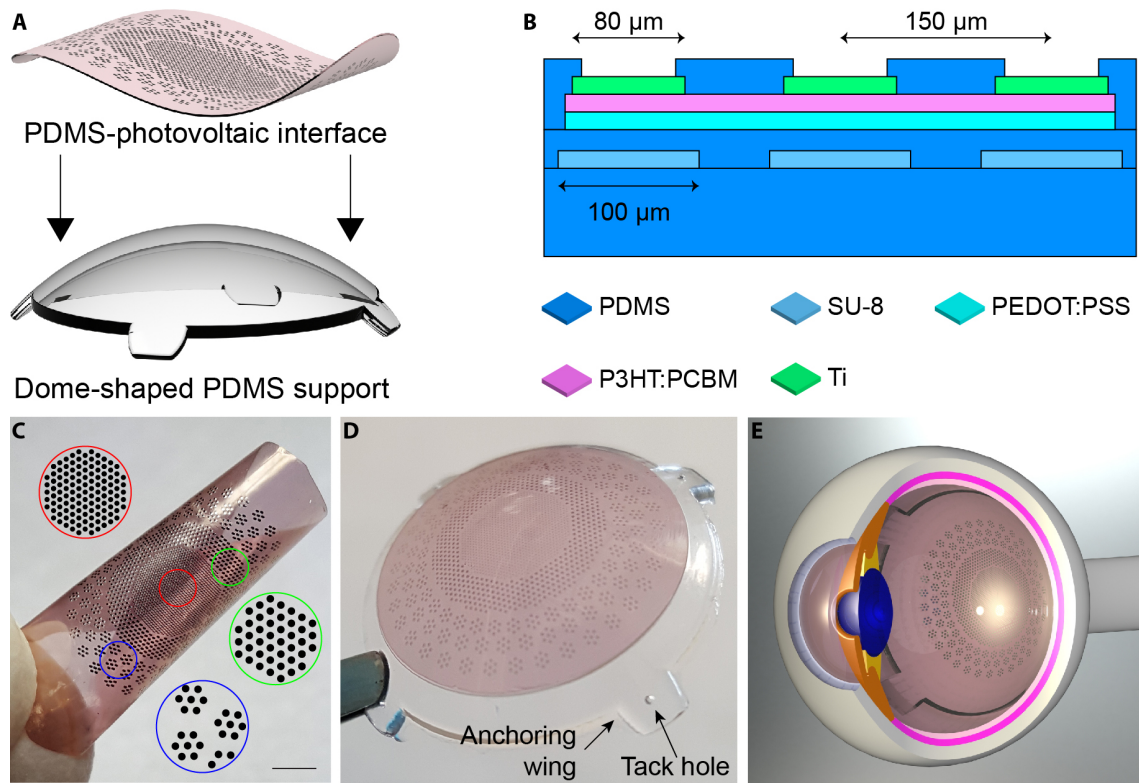


Figure 3.1: The POLYRETINA photovoltaic epiretinal prosthesis. A, 3D model of the fabricated PDMS-interface and of the dome-shaped PDMS support. B, Cross section of the PDMS-photovoltaic interface, including: PDMS ( $50\ \mu\text{m}$ ), a second layer of PDMS ( $10\ \mu\text{m}$ ) embedding SU-8 rigid platforms ( $6\ \mu\text{m}$ ), a layer of PEDOT:PSS ( $50\ \text{nm}$ ), a layer of P3HT:PCBM ( $100\ \text{nm}$ ), titanium cathodes ( $150\ \text{nm}$ ), and a final layer of PDMS ( $4\ \mu\text{m}$ ). Thicknesses are not in scale. C, Fabricated PDMS-photovoltaic interface with pixels arranged in three areas of different sizes and densities: central area (red) with 967 electrodes (electrode diameter  $80\ \mu\text{m}$  and pitch  $150\ \mu\text{m}$ ); first ring (green) with 559 electrodes (electrode diameter  $130\ \mu\text{m}$  and pitch  $250\ \mu\text{m}$ ); second ring (blue) with 719 electrodes (electrode diameter  $130\ \mu\text{m}$ ). Circles show an enlarged view of the pixels distribution. Scale bar = 2.5 mm. D, Picture of POLYRETINA. Four anchoring wings with holes are present for attaching the prosthesis with retinal tacks. E, 3D model after epiretinal placement. Figure and caption adapted from [203].

With the final goal of assessing the functionality of the POLYRETINA epiretinal prosthesis *in vivo*, this chapter describes the anatomical and physiological alterations caused by the systemic injection of IAA in Göttingen minipigs up to three months after the injection. The newly characterized animal model is then applied to the test of this novel photovoltaic epiretinal prosthesis developed by our laboratory.

## 3.2 Methods

### Animals handling and anesthesia

Animal experiments were approved by the Département de l'emploi, des affaires sociales et de la santé (DEAS) and the Direction générale de la santé of the République et Canton de Genève (Switzerland, authorization GE14118). Female Göttingen minipigs (Ellegaard), with a weight between 18 and 25 kg, were used for the experiments. All animals were kept in a 12 h day/night cycle with access to food and water *ad libitum* in a specialized animal facility.

On the day of the scheduled surgical procedures, animals received a prophylactic antibiotic by intramuscular administration of enrofloxacin (Batriol 10 %, 2.5 mg kg<sup>-1</sup>). The antibiotic administration was repeated the two following days, once per day. The minipigs were then premedicated with a mixture of azaperone (0.4 mg kg<sup>-1</sup>), midazolam (0.75 mg kg<sup>-1</sup>), and atropine (40 µg kg<sup>-1</sup>), administered via deep intramuscular injection. Approximately 30 minutes after premedication, anesthesia was induced by inhalation of sevoflurane up to 6 % and an intravenous line was inserted in the ear vein. To facilitate tracheal intubation, atracurium (0.5 mg kg<sup>-1</sup>) was administered intravenously. After intubation, the sevoflurane was stopped and the anesthesia was maintained with continuous intravenous administration of propofol (8 - 10 mg (kg h)<sup>-1</sup>) and ketamine (2 mg (kg h)<sup>-1</sup>), while analgesia was assured via intravenous injection of Fentanyl (2 µg kg<sup>-1</sup>, 5 - 6 ml h<sup>-1</sup>). The minipigs were constantly ventilated using 30 % oxygen fraction, with a tidal volume of 7 ml kg<sup>-1</sup>, and a respiratory rate of 15 per minute. The anaesthesia was provided for the whole duration of the surgical and recording procedures (2-4 hours). The animals were placed on a heating pad to prevent them from hypothermia and continuous monitoring of heart rate, ECG, temperature, blood pressure, end-tidal saturation, and oxygen saturation was performed using a real-time anesthesia monitoring system (Datex, Engstrom). After the procedure, the anesthesia perfusion was interrupted and the oxygen fraction increased to 100 %. The ventilator was set on pressure support to monitor the initiation of spontaneous ventilation. Upon giving signs of spontaneous ventilation, the minipigs were extubated and the respiration was assisted with a mask until signs of awakening were detected. The animals were then returned to their habitat and monitored until complete recovery. Analgesia was provided every 48 hours by patches of buprenorphine (Transtec®, 35 µg h<sup>-1</sup>), applied on

the interscapular area.

### **IAA injection**

IAA (I4386, Sigma-Aldrich) was dissolved in saline solution and injected at the concentration of  $12.5 \text{ mg kg}^{-1}$  intravenously. The injection was performed with a perfusion pump, maintaining a constant flux during 15 minutes. The IAA solution was prepared the same day of the procedure and kept on ice until the moment of injection. A perfusion of 5 minutes with 3 ml of saline solution followed. All the injections were performed at the end of the first day of recordings.

### **Optical coherence tomography**

The pupils were dilated with atropine 0.5 % (Théa Pharma), applied directly on the eye 30 minutes before starting the experiments. Cross-sectional images of the retina were obtained using spectral-domain OCT (SD-OCT). This technique allows the distinction of the different retinal layers. The images were acquired with an ophthalmic imaging system (Leica Bioptigen Envisu™ R2210 VHR SDOIS) with a central wavelength of 840 nm, an optical power  $\leq 750 \mu\text{W}$ , and an axial length of 1.6492 mm in tissues. Each B-scan image (number of repetitions of A-scans) consisted of 100 to 1'000 A-scans at a scanning rate of 32'000 scans  $\text{s}^{-1}$ . The covered area measured 12 x 12 mm, with a depth of 1.6492 mm (1000 x 200 x 1024 pixels). The optic nerve was positioned at the lower boundary of the image to ensure a wide visibility of the retina dorsal to it, which contains the visual streak. OCT scans of each eye were obtained approximately at the following timepoints: prior to IAA injection and one, two, and three months post-injection of IAA. Raw OCT images were exported as TIFF files and the fundus images were used to identify the optic nerve. The dorsal superior margin of the optic disc was identified in the fundus image and defined as the 0 mm landmark. B-scans associated to the 2 mm, 5 mm, and 8 mm dorsal position relative to the 0 mm landmark were imported in ImageJ and processed. The whole retinal thickness was measured from the edge of the RPE layer (defined as the end of the first hyperelective band) to the edge of the ganglion cell's fiber layer (defined as the edge of the most inner hyper reflective layer) in the three chosen locations (2, 5, and 8 mm from the optic nerve) of each B-scan and averaged.

### **Electrophysiological recordings**

As mentioned above, the pupils were dilated with atropin before starting the experiments. Dark adaptation was performed leaving the animal in complete darkness with the eyes covered for 30 minutes. Light adaptation was performed exposing the eye to a continuous light at the intensity of  $20 \text{ cd s m}^{-2}$  for 10 minutes. ERG responses were recorded with lens electrodes (ERG-Jet™, Fabrinol), using conductive gel to make them adhere better to the eye. The ERG responses

were normalized by the activity of the not-stimulated eye, which was kept covered during the entire procedure. To record the VEP responses, the skin was opened to expose the skull, and stainless steel electrodes were implanted on top of the visual cortex (identified in reference to lambda), while another electrode placed on top of the cerebellum served as reference. The electrodes were connected to the headstage using alligator clips. The recordings were acquired simultaneously in 2 channels connected respectively to the lens electrode on the stimulated eye (ERG or corneal potentials when the prosthesis is implanted) and to the screw on the contralateral visual cortex (VEP). White light flashes (4 ms) were delivered using a mini Ganzfeld stimulator (BM6007IL, Biomedica Mangoni) positioned at 1 - 2 cm from the eye and the recorded signals were amplified, filtered (0.1 – 500 Hz), and digitalized (BM623, Biomedica Mangoni). Green light flashes (10 ms, 5 V, 0.1 Hz) were delivered using a LED light (565 nm, Thor Labs) positioned at 15 cm from the eye and controlled with the Pulse Pal pulse train generator (Sanworks). The responses to white and green light were recorded for 500 ms (50 ms pre-stimulus and 450 ms post-stimulus) at 8 kHz using the WinAver program (Biomedica Mangoni). Scotopic responses to increasing white light intensities (from 0.01 to 30 cd s m<sup>-2</sup>, 0.1 Hz) were recorded after dark adaptation. Photopic responses to 30 cd s m<sup>-2</sup> (0.1 Hz) were recorded after light adaptation. Flicker responses to 30 cd s m<sup>-2</sup> train stimuli (30 Hz) were also recorded.

### **Surgical procedure for POLYRETINA implantation**

At the beginning of the surgery, the minipigs were set in lateral decubitus with the head slightly tilted in order to expose the eye to be implanted on a flat plane. The skin surrounding the orbit was disinfected by applying a solution of Povidone Iodine 5 % (Betadine) and let to act for 5 minutes before being wiped off using sterile gauzes. Sterile fields were then laid leaving only the orbit visible. Eyelid retractors were applied and a small incision of 1 - 2 mm was performed on the lateral/dorsal canthus so as to enlarge the access to the sclera. The surgery was performed under a Leica microscope with OCULUS BIOM® 5 lens allowing visibility of both the anterior/posterior chamber and as well the retina. An incision was performed on the limbus and a hydrostatic pressure regulated irrigation tube (Associate® 2500 Compact System from Dutch Ophthalmic, USA) was set in place to maintain ocular pressure throughout the surgery. Two other incisions were performed allowing the insertion of two cannulas (Caliburn 23G Cannulas 1-step, self sealing) enabling easy access to 23G instruments in the orbit. To allow intra-ocular manipulations and insertion of the prosthesis, a phacoemulsification of the lens was performed and was followed by a vitrectomy (Associate® 2500 Compact System from Dutch Ophthalmic, USA). To ensure that the prosthesis would be in close-contact with the retina, Triamcinolone was used to stain and visualize membranes and remaining vitreous ensuring its complete removal. The preparation of the eye was concluded by applying disposable iris retractors leav-

ing the posterior chamber easily accessible and ready to receive the prosthesis. A crescent knife was used to perform a superior corneal tunnel incision which was further enlarged by slit knives up to 6.4 mm. The custom injector containing the pre-rolled prosthesis was inserted into the incision and its piston pushed completely. Once passed the cannula, the flexible wings naturally opened allowing the prosthesis to unroll and to be released in the posterior chamber. Immediately after the injection, the injector was removed and the incision sutured, ensuring a tight seal and a well-controlled ocular pressure. Two custom made stainless steel retinal tacks (LOVIS décolletage, Perrefitte CH) were then inserted through the prosthesis and sclera to keep the device in place. Following the successful delivery and implantation of the prosthesis, the iris retractors were removed and all incisions were sutured. Antibiotic drops of Tobradex were applied and the eyelid retractors removed.

### **Histological and immunofluorescence analysis**

At the end of the last recording session and while still under anesthesia, the animals were euthanized by intravenous injection of pentobarbital (Eskonarkon® 300 mg, 90 mg kg<sup>-1</sup>) and the eyes were enucleated from the orbital cavity and placed in PFA for 1 - 4 hours. They were cryoprotected in sucrose 15 % for 6 hours and then in sucrose 30 % overnight. The eyecups were embedded in optimal cutting temperature compound (Tissue-Tek®), frozen, and stored at -80° C. 30 μm thick sections of the retina were obtained using a Leica cryostat (CM3050S) and placed on microscope slides. The sections were washed in PBS, permeabilised with PBS + Triton 0.1 % (Sigma-Aldrich), blocked with blocking buffer (PBS-T + 5 % Normal Goat Serum), and incubated with primary antibodies (AB5417 Mouse Anti-Rho 1:500 and AB5405 Rabbit Anti-L/Mopsin 1:300, Abcam) overnight at 4° C. The following day, they were incubated with secondary antibodies for 2 hours (Goat Anti Mouse AlexaFluor 488 and Goat Anti Rabbit AlexaFluor 488, 1:500, Thermofisher) and counterstained with DAPI 1:300 (Sigma-Aldrich). Finally, they were mounted with Fluoromount (Sigma-Aldrich) and imaged using a confocal microscope (LSM880, Zeiss).

For the hematoxylin and eosin (H E) staining, the animals were euthanized as described above. The eyes were enucleated, placed in formalin 10 % overnight, dehydrated in increasing concentrations of ethanol, followed by xylene, and finally embedded in paraffin. They were cut with a microtome (HM355S, ThermoScientific). H & E staining was performed on the sections (ST5020, Leica). Images were acquired using a slidescanner microscope (Olympus VS120).

### **Data analysis and statistics**

Data analysis and graphical representation were performed with Matlab and Python for the electrophysiological data. The data of the recordings were extracted as text files and analysed using a custom script in Matlab to calculate

the amplitude of the a- and b-wave for the ERG responses and of the negative wave for the VEP responses. The data from the flicker recordings were analysed using a custom script in Python: the power spectral density of the signal was calculated using Fourier analysis, then the average power content of the 29-33 Hz band was extracted. The histological and OCT data were analysed using ImageJ. The normality test (Shapiro-Wilk normality test) was performed on each dataset to justify the use of a parametric test (t-test). p-values were represented as: \*  $p < 0.05$ , \*\*  $p < 0.01$ , \*\*\*  $p < 0.001$ , and \*\*\*\*  $p < 0.0001$ .

### 3.3 Results and Discussion

#### **Anatomical evidence of complete retinal degeneration in Göttingen minipigs following IAA injection.**

For all the following experiments, we performed an intravenous injection of IAA at the concentration of  $12.5 \text{ mg kg}^{-1}$ , chosen based on previous studies in pigs [190]. We confirmed that this dosage is sub-lethal in minipigs, although a lot of care should be placed after the injection in monitoring the vital parameters of the animal until it recovers, so as to avoid complications.

The first evidence of the complete retinal degeneration in this chemically-induced blind model comes from OCT analyses, performed in minipigs before and after the injection of the toxin. Spectral-domain OCT is a non-invasive, high-resolution technique introduced more than 20 years ago. It is now established as the standard for diagnosing retinal anatomical abnormalities *in situ* such as in several retinal diseases: RP, AMD, and diabetic retinopathies. This technique permits the acquisition of cross-sectional images of the retina showing clearly distinguishable hyper-reflective layers.

We used OCT scans to monitor the retinal thickness before and up to 98 days after the injection of IAA at three locations: 2, 5, and 8 mm from the optic nerve (Fig. 3.2A). To quantify the retinal thickness, we sought to use the common anatomical classification, which divides the retina into an outer and inner part. Although, in the degenerated retinas the different layers become increasingly difficult to localize correctly, hence we arbitrarily redefined the two layers of interest based on the most recognisable structures. As a result, as shown in Fig. 3.2B-C, the inner retina comprises the ganglion cell's fiber layer, the ganglion cell layer, and the inner plexiform layer, while the outer retina includes the remaining layers.

Fig. 3.2D-F show the quantification of the retinal thickness (outer retina, inner retina, and whole retina) in one animal at each of the three locations, up to 98 days post-injection. The loss in thickness seems to leave the INL relatively unaffected and to happen mostly within the first 30 days after the injection. There seems to be a little increase in the thickness of the INL after one month post-injection, but this is probably due to the fact that, being the ONL completely de-

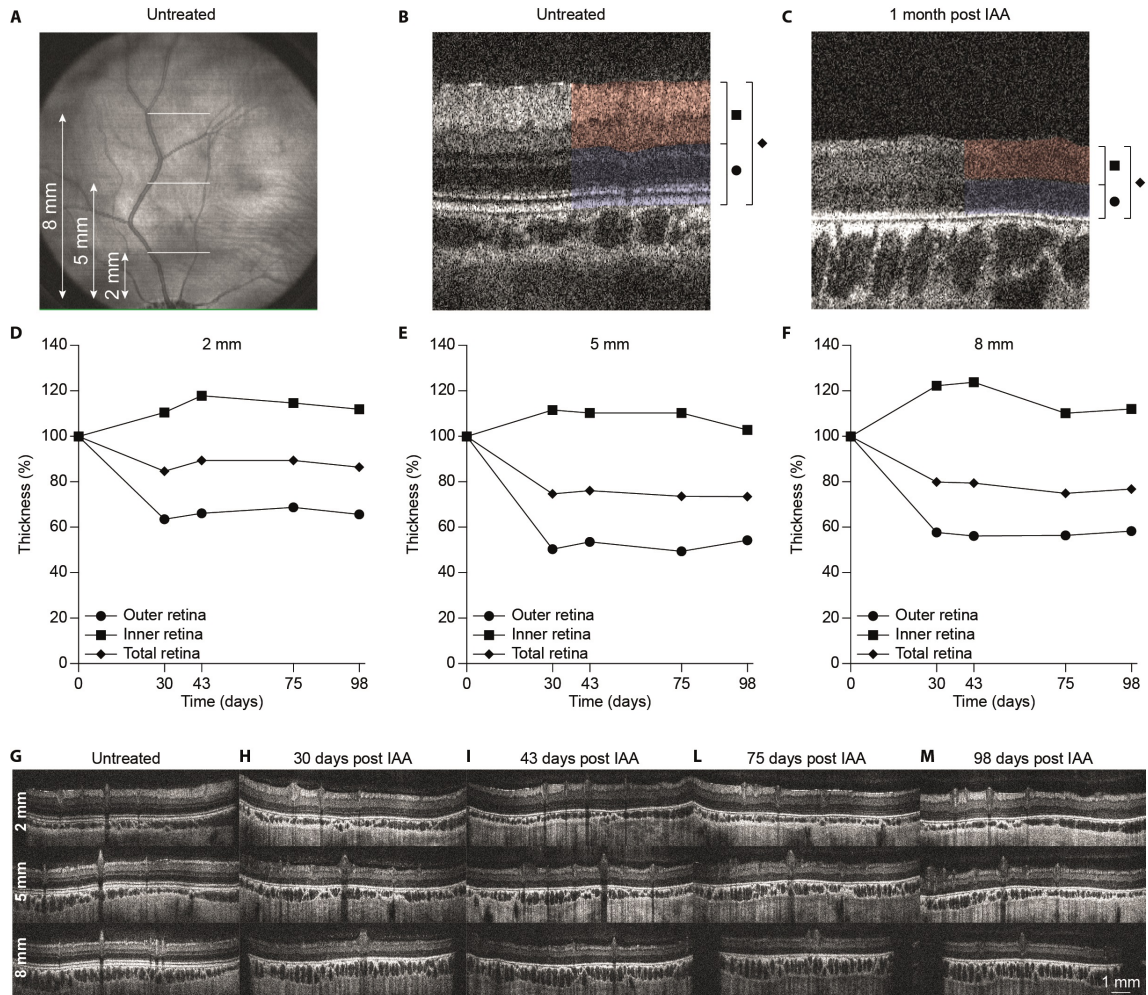


Figure 3.2: Example of quantification of the retinal thickness with OCT in one subject. A, Example of the fundus of the eye before the injection. The images used for the quantification were acquired at 2, 5, and 8 mm from the optic nerve. B-C, Example of OCT scan from untreated and 1 month post-injection of IAA retinas respectively. On the side, the different layers that were considered for the quantification are marked: outer layer (circle), inner layer (square), and total retina (diamond). D-F, Quantification of the retinal thickness from OCT scans before and up to 98 days post-injection. The thickness of the different layers is reported at 2 (D), 5 (E), and 8 mm (F) from the optic nerve and reported as a percentage of the initial value (day 0). G-M, examples of OCT scans of the retina at 2, 5, and 8 mm from the optic nerve before the injection and up to 98 days post-injection.



generated, what remains of it is wrongly identified together with the INL, slightly increasing the thickness of the latter. Fig. 3.2G-M show examples of OCT scans at each time point for the three locations.

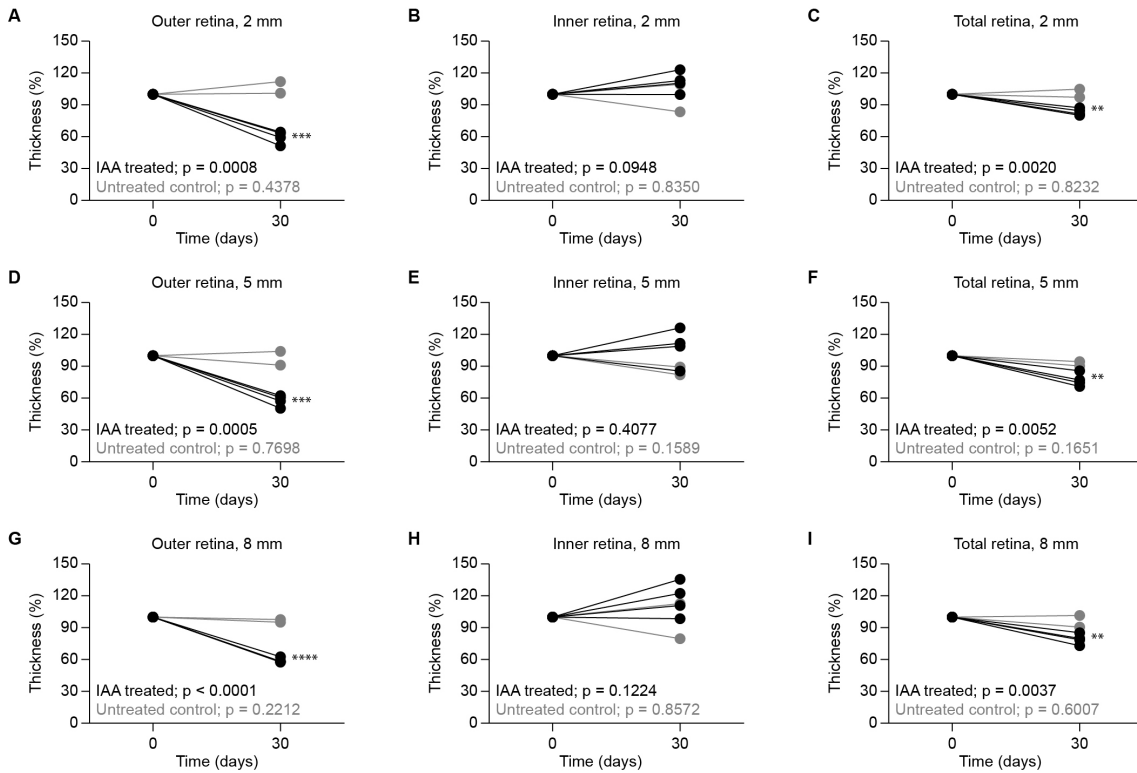


Figure 3.3: Quantification of the retinal thickness in control (gray,  $n = 2$ ) and treated (black,  $n = 4$ ) eyes before and one month after the injection of IAA. A-C, Thickness measured at 2 mm from the optic nerve. From A to C: outer retina, inner retina, and total retina. D-F, Thickness of the same layers measured at 5 mm from the optic nerve. G-I, Thickness of the same layers measured at 8 mm from the optic nerve. Each point represents one eye. For each eye, the thickness is showed as percentage of the initial value (day 0). Paired t-test: values reported in the figure.

Fig. 3.3 shows the thickness of the retinal layers (inner retina, outer retina, and total retina) measured from the OCT images for each of the pigs analysed. The retinal layers of interest were defined as described above. The data points (one point represents the value for one eye) were obtained before and one month after the injection of IAA at the three chosen locations: 2 mm (3.3A-C), 5 mm (3.3D-F), and 8 mm (3.3G-I) from the optic nerve. Notably, the thickness of the outer retina decreases drastically in treated eyes one month after the injection of IAA (2 and 5 mm, Fig. 3.3A and D;  $n = 4$ ; paired t-test) and the effect appears to increase slightly further away from the optic nerve (8 mm, Fig. 3.3G;  $n = 4$ ; paired t-test). Conversely, the thickness of the inner retina seems unaffected by the injection of IAA (Fig. 3.3B, E, and H;  $n = 4$ ; paired t-test). As expected, the thickness of all the retinal layers remains constant in the control eyes (gray, Fig. 3.3;  $n = 2$ ; paired t-test).

To obtain a better idea of the morphological changes induced by the injection of IAA, we performed histological examinations of the retina before and after the injection of the toxin. Hematoxylin and Eosin (H & E) staining before and up to 3 months after IAA injection shows that the outer segments of PhRs, clearly visible in the control sample and one hour after the injection, are completely absent in the injected eye starting from the first timepoint tested (2 months post-injection). Due to experimental constraints, we do not have any post-mortem data prior to two months post-injection. Although, based on the OCT results, it could be hypothesized that the changes we see at two months post-injection of IAA would be fairly similar to what is already observable at one month post-injection.

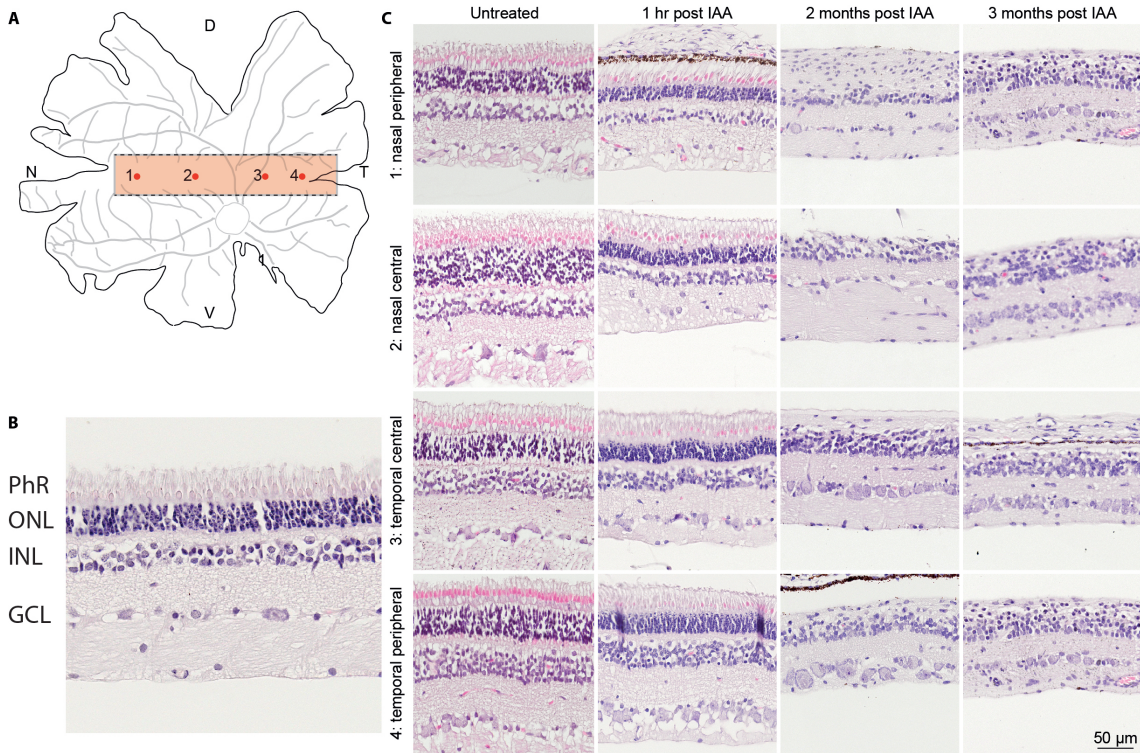


Figure 3.4: H & E staining on retinal sections in the visual streak. A, Schematic representation of the retina. D = dorsal, N = nasal, V = ventral, T = temporal. The sections were prepared from the zone of the visual streak (in red). B, Layers of the retina that can be recognized in the images: photoreceptor layer (PhR), outer nuclear layer (ONL), inner nuclear layer (INL), and ganglion cell layer (GCL). C, Sections of minipig retinas before, 1 hour post-injection, 2 months post-injection, and 3 months post-injection. Images are acquired at four different locations: nasal peripheral (1), nasal central (2), temporal peripheral (3), and temporal central (4).

We acquired images of the samples at two different locations: the zone in close proximity to the visual streak (Fig. 3.4), and the zone adjacent to the optic nerve (Fig. 3.5). For each location, we present examples of the temporal and nasal areas of both central and peripheral retina. The ONL, where the bodies of photoreceptor cells are located, is still recognizable at two and three months post-injection, but the cells lack their outer segment. Conversely, the INL of the retina

looks less affected by the toxin, even though it seems to undergo a certain extent of reorganization. This is in line with other reports on the effect of IAA in rabbits and pigs [186, 189, 191] and is explained by the fact that, being photoreceptors highly metabolically active cells, they are more prone to be damaged by the administration of IAA, which interferes with cell metabolism. No clear evidence of further degeneration is visible at three months post-injection when compared to two months post-injection, which is expected since the photoreceptors have already degenerated at this stage.

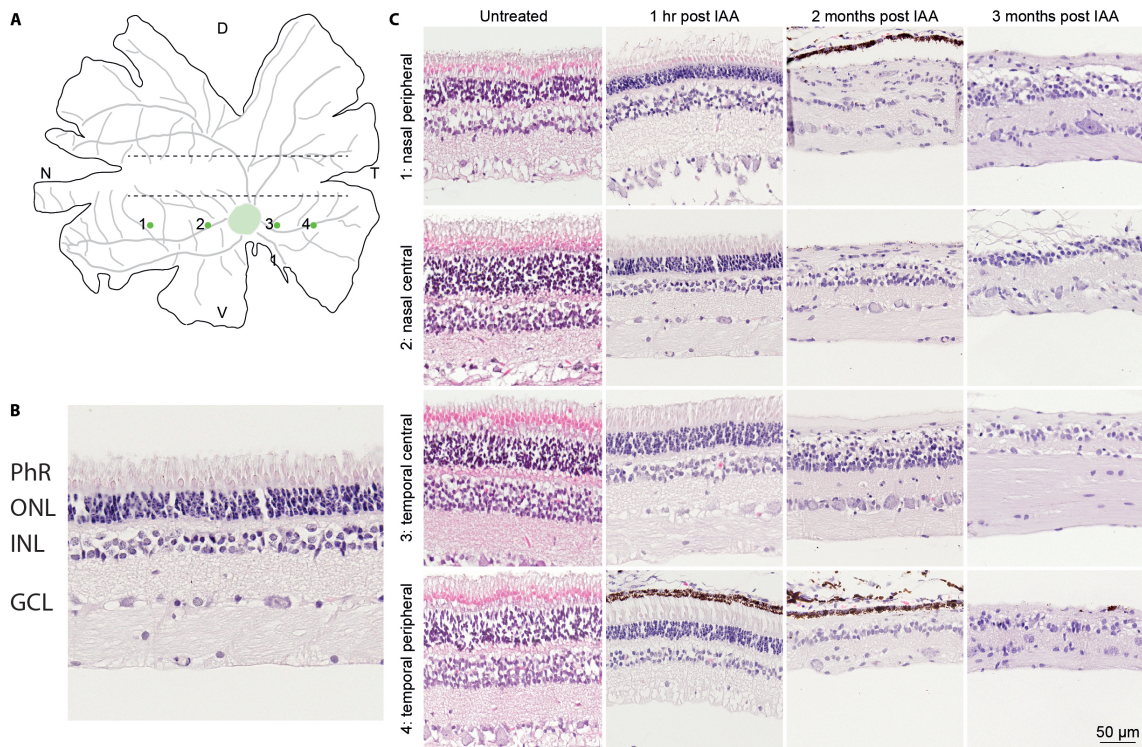


Figure 3.5: H & E staining on retinal sections in the zone adjacent to the optic nerve. A, Schematic representation of the retina. D = dorsal, N = nasal, V = ventral, T = temporal. The sections were prepared from the zone adjacent to the optic nerve (in green). B, Layers of the retina that can be recognised in the images: PhR layer, ONL, INL, and GCL. C, Sections of minipig retinas before, 1 hour post-injection, 2 months post-injection, and 3 months post-injection. Images are acquired at four different locations: nasal peripheral (1), nasal central (2), temporal peripheral (3), and temporal central (4).

The toxin does not seem to have any impact on the RGCs, at least at the tested timepoints. Nevertheless, we can hypothesize that ganglion cells will eventually die as a consequence of the degeneration of photoreceptors and the retina will undergo extensive remodeling, as it happens normally in advanced stage retinal degeneration [34]. Although, this cannot be completely confirmed using histological techniques at the time points tested, but it would be more likely to be detected at a much later stage (around one year after the injection).

To further investigate which cells are most affected by the toxin, we performed fluorescent immunohistochemistry (IHC/IF) on retinal samples before and up

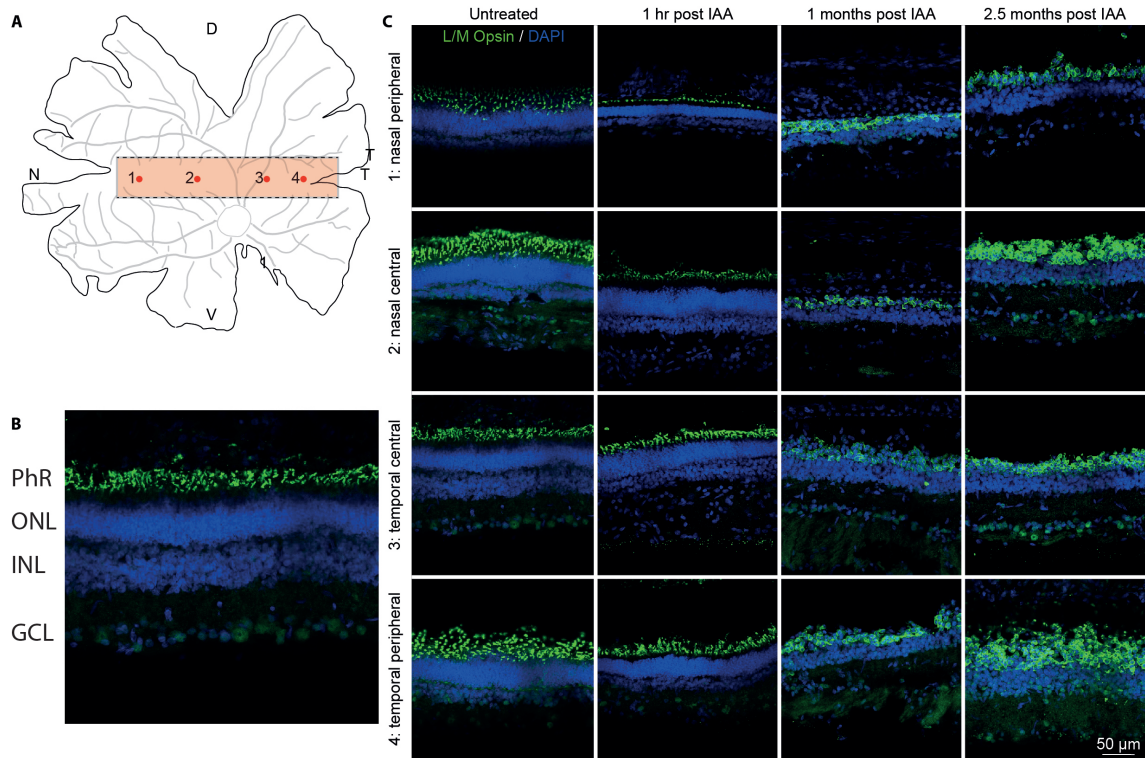


Figure 3.6: IHC/IF for L/M opsin on retinal sections in the visual streak. A, Schematic representation of the retina. D = dorsal, N = nasal, V = ventral, T = temporal. The sections were prepared from the zone of the visual streak (in red). B, Layers of the retina that can be recognised in the images: PhR layer, ONL, INL, and GCL. C, Sections of minipig retinas before, 1 hour post-injection, 1 month post-injection and 2.5 months post-injection. Images are acquired at four different locations: nasal peripheral (1), nasal central (2), temporal peripheral (3), and temporal central (4). Staining for L/M opsin (green) and DAPI (blue).

to 2.5 months after IAA injection. We used antibodies against L/M opsin and Rho to identify cone and rod photoreceptors respectively. As explained above, we analysed a number of different retinal locations. In Fig. 3.6 we present the results for the visual streak (2 mm dorsal from the optic nerve) and in Fig. 3.7 the results for the zone adjacent to the optic nerve, both stained for L/M opsin.

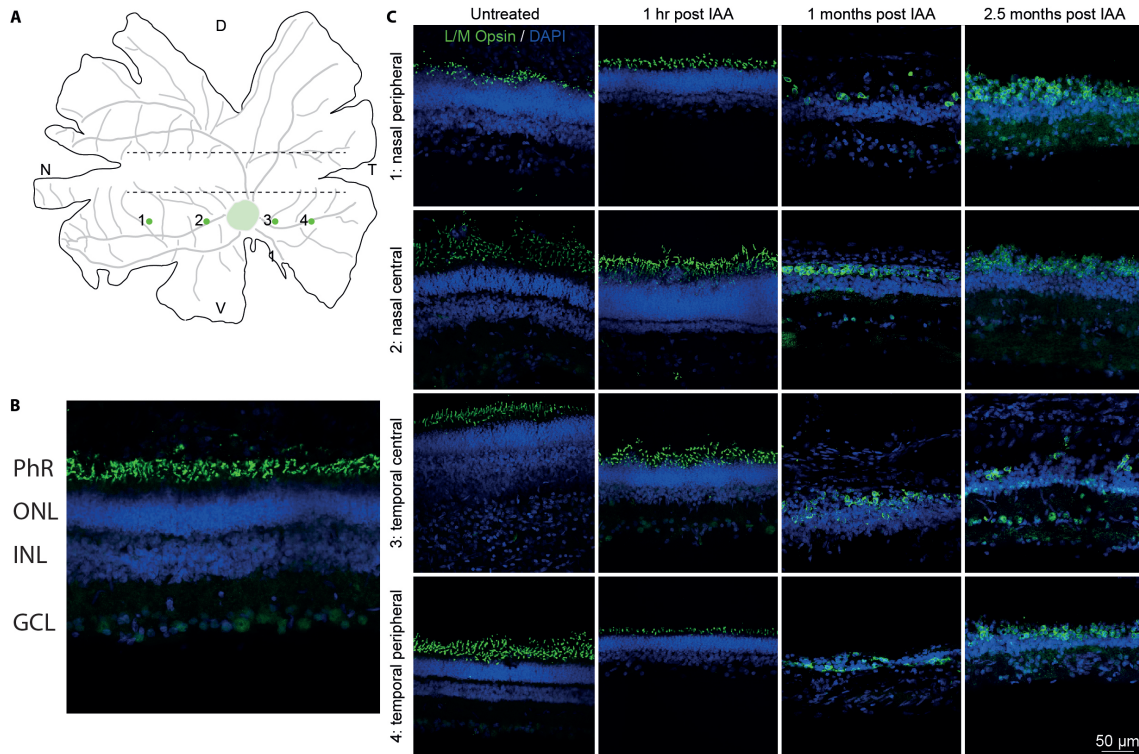


Figure 3.7: IHC/IF for L/M opsin on retinal sections in the zone adjacent to the optic nerve. A, Schematic representation of the retina. D = dorsal, N = nasal, V = ventral, T = temporal. The sections were prepared from the zone adjacent to the optic nerve (in green). B, Layers of the retina that can be recognised in the images: PhR layer, ONL, INL, and GCL. C, Sections of minipig retinas before, 1 hour post-injection, 1 month post-injection, and 2.5 months post-injection. Images are acquired at four different locations: nasal peripheral (1), nasal central (2), temporal peripheral (3), and temporal central (4). Staining for L/M opsin (green) and DAPI (blue).

Previous accounts on the effect of IAA on the retina show that rod photoreceptors lose their outer segment first, with translocation of rhodopsin in the inner segment of the remaining cells. The same happens to a lesser extent in cone photoreceptors which were in general less affected by the toxin [191]. In our case, the immunostaining shows that there are no rod photoreceptors, clearly visible up to one hour after the injection, left two months after the injection in both central and peripheral retina (Fig. 3.8, only one example is presented here since rod photoreceptors were not detectable in any of the areas tested). On the other hand, some cones survive, although they lack the outer segment (Fig. 3.6C and Fig. 3.7C), which is clearly visible up to one hour after injection. As a consequence of the complete absence of rod photoreceptors, we have no way to verify the translo-

cation of rhodopsin to the inner segment of degenerating cells, which probably happens at an earlier stage. Moreover, some fluorescence is detectable outside the outer nuclear layer in these samples (when stained for L/M opsin), but this effect can most likely be attributed to autofluorescence and it not indicative of the presence of displaced cone photoreceptors, although we will investigate this aspect further.

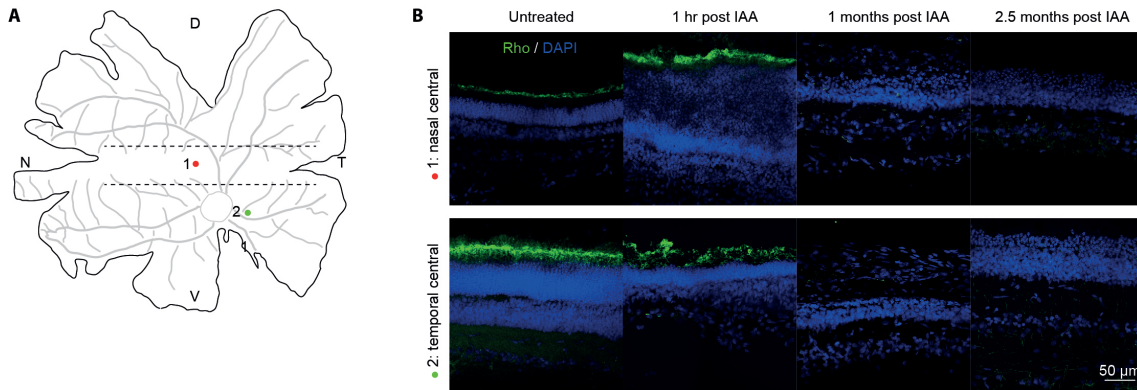


Figure 3.8: IHC/IF for Rho on retinal sections. A, Schematic representation of the retina. D = dorsal, N = nasal, V = ventral, T = temporal. The sections used for the examples are marked: section 1 on the visual streak and section 2 close to the optic nerve. B, Sections of minipig retinas before, 1 hour post-injection, 1 month post-injection, and 2.5 months post-injection. The two locations are presented as examples since there was no detectable rhodopsin in any of the areas inspected. Staining for Rho (green) and DAPI (blue).

Collectively, these observations show photoreceptor death and degeneration in this minipig model of IAA-induced retinal degeneration, which would make it suitable to test photovoltaic retinal prostheses. We can hypothesize that the degeneration is happening within the first few days after the injection of the toxin since there is no notable evidence of cell degeneration at one hour after the injection, but extensive cell death is obvious at one month post injection.

To confirm that the degeneration observed in the retina translates to a complete loss of visual functions, we performed some electrophysiological tests of the visual system.

### **Electrophysiological responses in the retina and visual cortex of the Göttingen minipig following IAA injection**

First, we recorded ERG responses using a lens-shaped electrode (JET) placed on the cornea of the stimulated eye (Fig. 3.9A) and, as a reference, the same type of electrode placed on the other eye (kept covered for the duration of the stimulation). To obtain ERG recordings in scotopic conditions, which isolate the response of rod photoreceptors, we performed 30 minutes of dark adaptation keeping the animal in complete darkness prior to the recording session. We recorded the response to stimuli of increasing intensity (0.01 to 30 cd s m<sup>-2</sup>, Fig. 3.9B) in dark adapted animals. The lower intensities of light allow us to assess the functionality

of rod photoreceptors, which are really sensitive to dim conditions after undergoing dark adaptation. Starting from the intensity of  $3 \text{ cd s m}^{-2}$ , the observed response comes from a combination of rod and cone activity and represents the functionality of the whole retina [121]. In the experiments hereafter, we consider each eye as an individual subject since IAA can have a different effect on the two eyes of the same animal, preventing us from coupling them in the analysis.

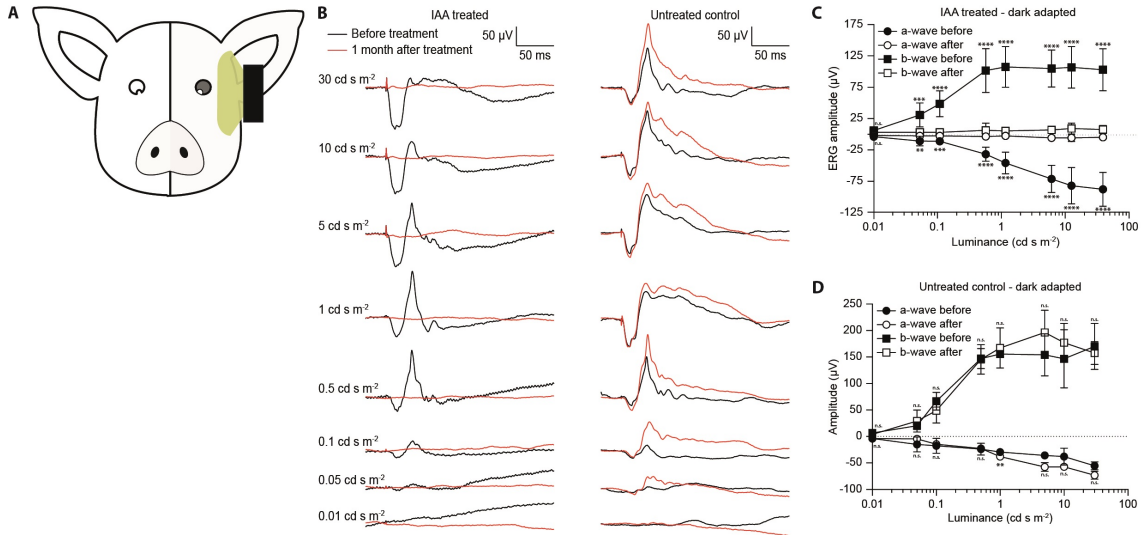


Figure 3.9: ERG recordings in control and blind animals after dark adaptation. A, Schematic representation of the experiment. The recording electrode (in gray) is a lens placed on the stimulated eye, while the reference electrode (in white) is placed on the other eye. The recordings are performed after 30 minutes of dark adaptation. 5 flashes (4 ms duration) for each luminance are presented at the frequency of 0.1 Hz and the response is averaged. B, Left panel: example of recording before (black) and one month after (red) the injection of IAA at each luminance tested. Right panel: example of recordings in a control animal at comparable timepoints. C, Mean ( $\pm$  s.d.) amplitude of the a- (circle) and b-wave (square) along the different luminances tested in treated eyes before (filled marker,  $n = 10$ ) and one month after IAA injection (empty marker,  $n = 10$ ). Paired t-test a-wave:  $0.01 \text{ cd s m}^{-2}$  ( $p = 0.1047$ ),  $0.05/0.1 \text{ cd s m}^{-2}$  ( $p < 0.01$ ),  $0.5/1/5/10/30 \text{ cd s m}^{-2}$  ( $p < 0.0001$ ). Paired t-test b-wave:  $0.01 \text{ cd s m}^{-2}$  ( $p = 0.1212$ ),  $0.05 \text{ cd s m}^{-2}$  ( $p < 0.01$ ),  $0.1 \text{ cd s m}^{-2}$  ( $p < 0.001$ ),  $0.5/1/5/10/30 \text{ cd s m}^{-2}$  ( $p < 0.0001$ ). D, Mean ( $\pm$  s.d.) amplitude of the a- and b-wave in control eyes at comparable timepoints: the day of the first experiment ( $n = 2$ ) and one month after ( $n = 2$ ). Paired t-test a-wave:  $0.01 \text{ cd s m}^{-2}$  ( $p = 0.9805$ ),  $0.05 \text{ cd s m}^{-2}$  ( $p = 0.5747$ ),  $0.1 \text{ cd s m}^{-2}$  ( $p = 0.8641$ ),  $0.5 \text{ cd s m}^{-2}$  ( $p = 0.9306$ ),  $1 \text{ cd s m}^{-2}$  ( $p < 0.01$ ),  $5 \text{ cd s m}^{-2}$  ( $p = 0.0723$ ),  $10 \text{ cd s m}^{-2}$  ( $p = 0.2465$ ),  $30 \text{ cd s m}^{-2}$  ( $p = 0.3467$ ). Paired t-test b-wave:  $0.01 \text{ cd s m}^{-2}$  ( $p = 0.4366$ ),  $0.05 \text{ cd s m}^{-2}$  ( $p = 0.5310$ ),  $0.1 \text{ cd s m}^{-2}$  ( $p = 0.1654$ ),  $0.5 \text{ cd s m}^{-2}$  ( $p = 0.9739$ ),  $1 \text{ cd s m}^{-2}$  ( $p = 0.7461$ ),  $5 \text{ cd s m}^{-2}$  ( $p = 0.5972$ ),  $10 \text{ cd s m}^{-2}$  ( $p = 0.7184$ ),  $30 \text{ cd s m}^{-2}$  ( $p = 0.8278$ ).

In Fig. 3.9B the examples show that the response to all the light intensities tested is flat in the treated animal one month after the injection of IAA (left), while it remains constant in the control animal (right) at comparable timepoints. The slightly different responses of the example control animal at one month compared

to day 0 are due to the fact that new electrodes were placed at the beginning of each experiment, hence it was not possible to reproduce the exact conditions of day 0 recordings. The mean ( $\pm$  s.d.) amplitude of the a- and b-wave is significantly lower in treated eyes one month after the injection of IAA for all the intensities tested, except the lowest one (Fig. 3.9C;  $n = 10$ ; paired t-test). On the contrary, the mean ( $\pm$  s.d.) amplitude of both a- and b- waves remains constant in control eyes for all the intensities tested, except for the a-wave at  $1 \text{ cd s m}^{-2}$  (Fig. 3.9D;  $n = 2$ ; paired t-test).

ERG recordings in photopic conditions are useful to isolate the functionality of cone photoreceptors. To this end, the eye was exposed to bright light ( $20 \text{ cd s m}^{-2}$ ) for 10 minutes, after which we recorded the response to bright light flashes ( $30 \text{ cd s m}^{-2}$ , 4 ms duration) presented at 0.1 Hz (Fig. 3.10A). We observed some residual cone functionality, which was expected since cones appear to be relatively spared (compared to rods) in IAA-induced retinal degeneration, although both the a- and b-wave are significantly reduced in treated eyes (Fig. 3.10C;  $n = 6$ ; paired t-test). Conversely, Fig. 3.10D shows that in control eyes tested at comparable timepoints the response remains constant ( $n = 2$ ; paired t-test).

Furthermore, we performed the flicker ERG analysis after light adaptation. This response is driven by cones and tests their capability to respond to a high frequency stimulus (delivered at 30 Hz, Fig. 3.11A). The analysis of the Fourier transforms of the signal results in a power spectral density with a peak around 30 Hz, coherently with the frequency of the stimulus (black, Fig. 3.11B). On the other hand, one month after the injection of IAA the power content of the signal does not show any prominent peak (red, Fig. 3.11B). The average power content of the frequency band between 29 and 33 Hz was calculated and compared between treated and control eyes. The quantification in Fig. 3.11C shows that the power of the 29-33 Hz band significantly decreases in treated eyes one month after the injection of IAA (red;  $n = 6$ ; paired t-test), while it stays constant in control animals (black;  $n = 4$ ; paired t-test). Although in Fig. 3.10 we could observe some residual cone response when stimulating at 0.1 Hz after light adaptation, it is evident from the negligible power content of the flicker ERG response that there is an important loss of cone functionality in animals injected with IAA.

In addition to the experiment described above, which are related to the functionality of retinal circuits, we also measured the VEPs from the primary visual cortex in response to white light flashes delivered at 0.1 Hz. VEPs are the result of the activation of both the retina and of higher parts of the visual system. Our application for this animal model is to test the POLYRETINA epiretinal prosthesis, which is stimulating the retinal ganglion cell layer, bypassing the degenerated photoreceptor layer. In this case, an ERG electrode would only show the corneal potential produced by the activation of the prosthesis itself (as will be shown after) and, although this ensures the correct functionality of the device, it does not provide any information about the effective activation of the visual pathways.



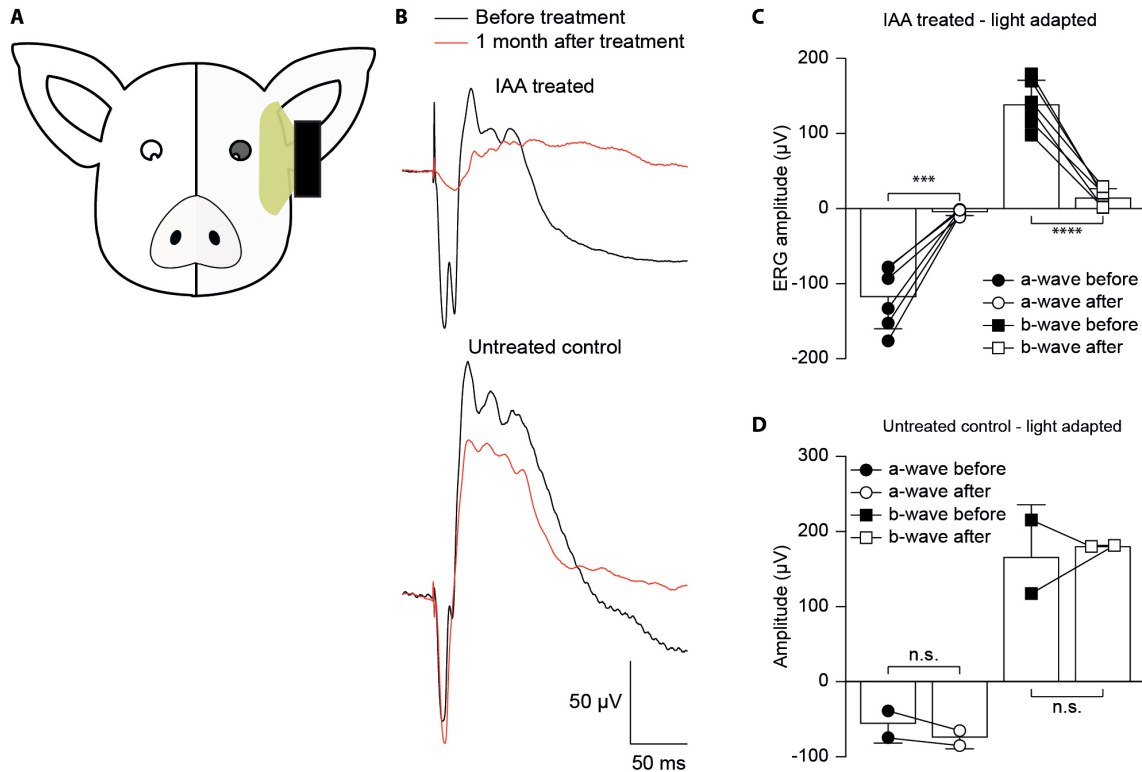


Figure 3.10: ERG recordings in control and blind animals following light adaptation. A, Schematic representation of the experiment. The recording electrode (in gray) is a lens placed on the stimulated eye, while the reference electrode (in white) is placed on the other eye. The recordings are performed after 10 minutes of light adaptation at  $20 \text{ cd s m}^{-2}$ . 30 flashes ( $30 \text{ cd s m}^{-2}$ , 4 ms duration) are presented at the frequency of 0.1 Hz and the response is averaged. B, Top panel: example of response in treated animals before (black) and one month after IAA injection (red). Bottom panel: example of response in the untreated control at comparable timepoints. C, Mean ( $\pm$  s.d.) amplitude of the a- (circle) and b-wave (square) in the treated eyes before (filled markers; a-wave:  $-118.49 \pm 37.72 \mu\text{V}$ ; b-wave:  $139.54 \pm 28.61 \mu\text{V}$ ;  $n = 6$ ) and one month after IAA injection (empty markers; a-wave:  $-5.38 \pm 3.55 \mu\text{V}$ ; b-wave:  $15.38 \pm 10.29 \mu\text{V}$ ;  $n = 6$ ). Paired t-test: a-wave ( $p < 0.001$ ), b-wave ( $p < 0.0001$ ). D, Mean ( $\pm$  s.d.) amplitude of the a- and b-wave in control eyes at comparable timepoints: the day of the first experiment (a-wave:  $-56.44 \pm 17.87 \mu\text{V}$ ; b-wave:  $166.63 \pm 48.9 \mu\text{V}$ ;  $n = 2$ ) and one month after (a-wave:  $-75 \pm 10.15 \mu\text{V}$ ; b-wave:  $180.94 \pm 0.47 \mu\text{V}$ ;  $n = 2$ ). Paired t-test: a-wave ( $p = 0.1255$ ), b-wave ( $p = 4102$ ).

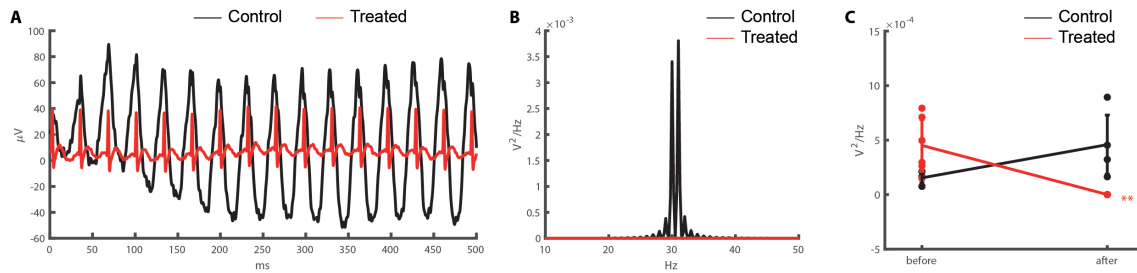


Figure 3.11: Flicker ERG in control and blind animals. A, Example of flicker ERG before (black) and one month after the injection of IAA (red). The stimulus was delivered at 30 Hz. B, Power spectral density of the response to 30 Hz stimulation before (black) and one month after the injection of IAA (red). C, Quantification of the power content of the band between 29 and 33 Hz in treated ( $n = 6$ , paired t-test:  $p < 0.01$ ) and control eyes ( $n = 2$ , paired t-test:  $p = 0.1201$ ).

For this reason, our primary goal in recording VEPs was to relate them to the ERG activity and to make sure they completely disappear in the light-insensitive animal model, so that, after the implantation of the device, we can attribute any further signal detected in the visual cortex to the stimulation performed by the prosthesis.

For this experiment, two electrodes were placed through the bone above the two visual cortices and the responses were recorded from the electrode contralateral to the stimulated eye (Fig. 3.12A). The responses were then normalized by a reference electrode implanted outside the visual cortex (Fig. 3.12C, r: reference electrode, e: recording electrodes). We recorded from the contralateral visual cortex since minipigs, as other lateral-eyed mammals, have the majority of connections in the optic nerve decussating at the level of the optic chiasm and forming synapses with the contralateral hemisphere.

The response becomes undetectable starting from one month after the injection, as seen in the example provided in Fig. 3.12B. The quantification in Fig. 3.12D (left panel) shows a significant decrease of the mean ( $\pm$  s.d.) amplitude of the negative wave of the VEP one month after the injection of IAA ( $n = 6$ ; paired t-test). Conversely, in control eyes the response remains constant at comparable timepoints, as shown in the right panel of Fig. 3.12D ( $n = 2$ ; paired t-test). Notably, the VEP signals seem to disappear when ERG signals are still somehow detectable. This discrepancy could be attributed to the easier detectability of responses coming directly from the retina, while a stronger signal is needed in the visual cortex to be identified by the VEP electrodes.

In conclusion, IAA is interfering with the metabolism of cells and, given their high metabolic rate, photoreceptors are especially sensitive to it. This allows us to induce a fast retinal degeneration without relying on complicated genetic manipulations, which can be difficult to perform in large animals. We could obtain flat or extremely reduced responses from the retina and the visual cortex in minipigs when administering IAA at the concentration of  $12.5 \text{ mg kg}^{-1}$  (the

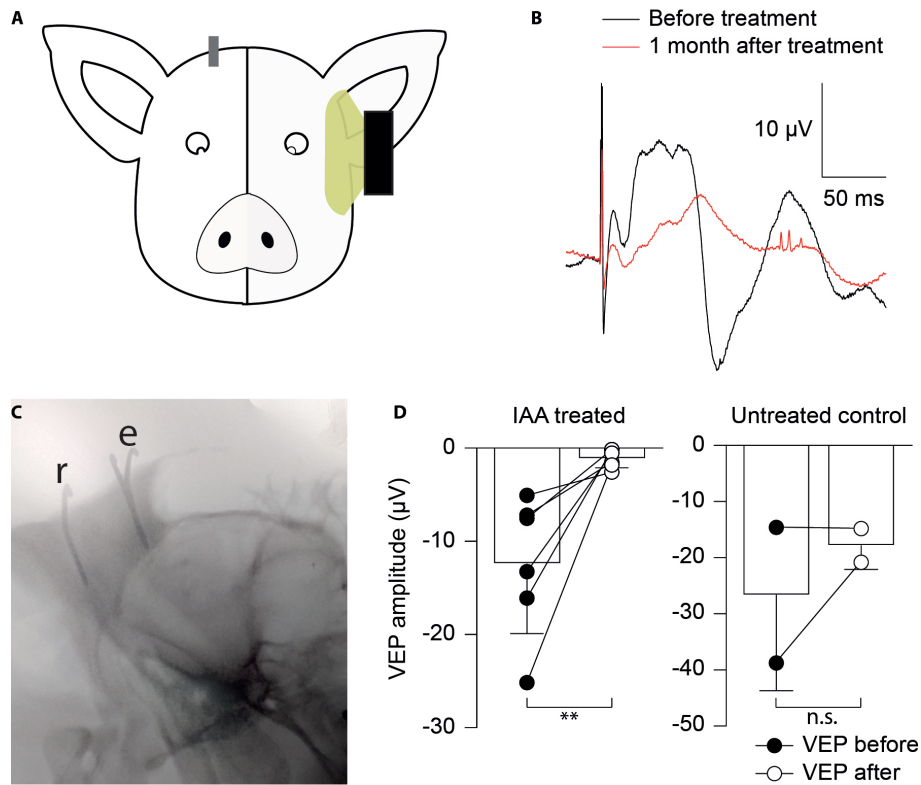


Figure 3.12: VEP recordings from the primary visual cortex. A, Schematic representation of the experiment. The recording electrode (in gray) is placed on the cortex contralateral to the stimulated eye, while the reference electrode is placed outside the visual cortex. 30 flashes ( $30 \text{ cd s m}^{-2}$ , 4 ms duration) are presented at the frequency of 0.1 Hz and the response is averaged. B, Example of VEP recordings in treated animals before (black) and one month after IAA injection (red). C, Radiography showing the position of the recording electrodes (e) and the reference electrode (r). D, Left panel: mean ( $\pm$  s.d.) amplitude of the negative wave of the VEPs before (filled markers;  $-12.38 \pm 6.85$ ;  $n = 6$ ) and one month after IAA injection (empty markers;  $-1.12 \pm 0.9$ ;  $n = 6$ ). Paired t-test:  $p < 0.01$ . Right panel: mean ( $\pm$  s.d.) amplitude of the negative wave of the VEP in control eyes at comparable timepoints: the day of the first experiment ( $-23.86 \pm 9.27$ ;  $n = 2$ ) and one month after ( $-14.73 \pm 7.03$ ;  $n = 2$ ). Paired t-test:  $p = 0.0767$ .

same concentration showed to reliably cause retinal degeneration in pigs), as demonstrated from the recordings in scotopic and photopic conditions. These results are corroborated by the histological evidence showing the lack of the entire photoreceptor layer. All considered, this light-insensitive animal is an ideal model to test the POLYRETINA epiretinal prosthesis.

### **Electrophysiological responses in the retina and visual cortex of blind Göttingen minipigs implanted with POLYRETINA: preliminary results**

Following the characterization of the minipig model of IAA-induced retinal degeneration, we applied it to the *in vivo* testing of the POLYRETINA epiretinal prosthesis that our laboratory has developed in the past years. The surgical procedure is very innovative and relies on the fact that the prosthesis (Fig. 3.13A) is foldable and can be rolled (Fig. 3.13B-C) into a custom-made injector (Fig. 3.13D-E). This allows the surgeon to open an extremely small tunnel (< 7 mm) in the cornea (at the level of the limbus), through which they can insert the injector and then push the prosthesis inside the eye (Fig. 3.13G-I). Once in the eye, the prosthesis unfolds automatically (Fig. 3.13F) and sits on the ganglion cell layer. The surgeon can then place two retinal tacks through the prosthesis to keep the device in place and the photovoltaic pixels in contact with the retina. This procedure was developed in order to minimize traumatic manipulation and the size of the opening needed to insert the prosthesis in the eye. Once the POLYRETINA is implanted and fixed using the tacks, the little opening on the cornea is sutured and the minipig can recover in a short period of time.

In the first part of the project, we characterized a minipig model of IAA-induced retinal degeneration and optimized the implantation and recording procedure. We are currently in the process of testing the device in minipigs. Fig. 3.14 shows the results for the first implanted animal, obtained 2 weeks after the implantation of the device. The photovoltaic reaction in the pixels is best elicited by green light, hence a green LED (565 nm,  $\approx 1 \text{ mV mm}^{-2}$ ) was used for this experiment. All the recordings in the figure were obtained by stimulating the same eye, before (Fig. 3.14B-C) and two weeks after (Fig. 3.14D) the implantation of the POLYRETINA prosthesis. Except for the color of the light, the protocol used was the same as explained earlier for both ERG and VEP recordings (Fig 3.14A). The response to green light in normal sighted animals is similar to the one obtained using white light (black, Fig. 3.14B-C). and appears extremely reduced one month after the injection of IAA (red, Fig. 3.14B-C). When the retinal prosthesis is implanted, what is measured with the lens electrodes is no longer an ERG, but the voltage produced by the activation of the photovoltaic pixels. This response will be referred hereafter as corneal potential and can be used to confirm the activation of the retinal prosthesis: the duration of the response is consistent with the duration of the flash (Fig. 3.14D, top panel). In the top panel of Fig. 3.14D we can notice a little remaining ERG response from the control eye (also noticeable in

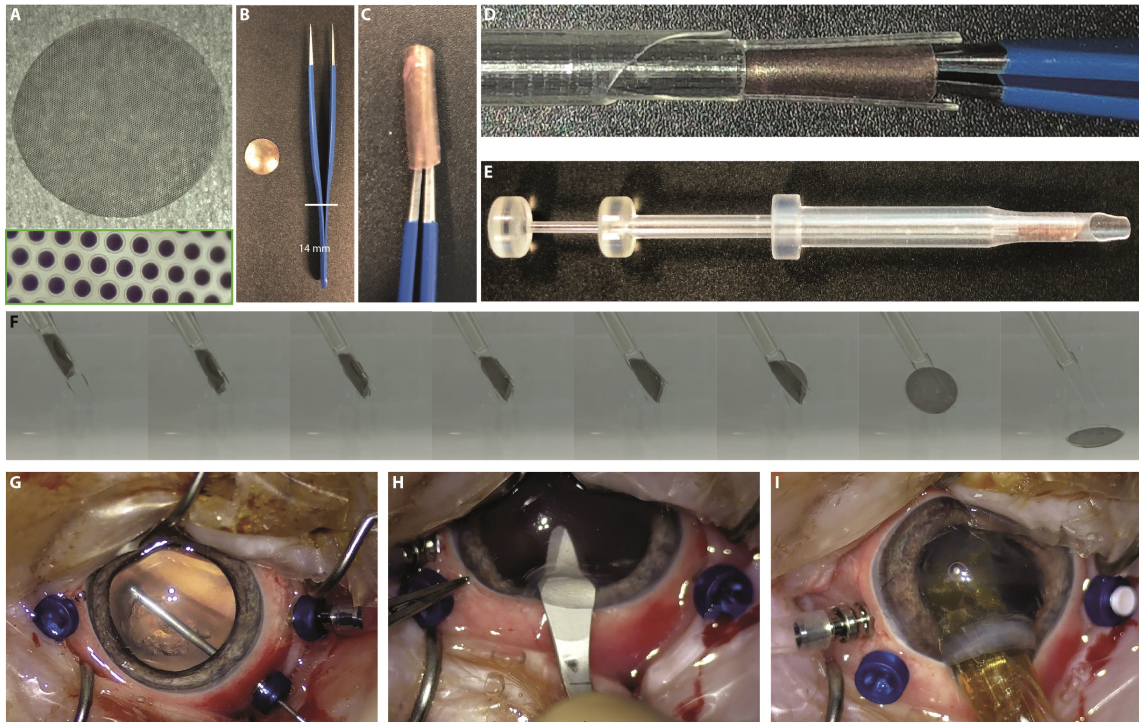


Figure 3.13: Surgical procedure for the implantation of the POLYRETINA epiretinal prosthesis. A, The POLYRETINA epiretinal prosthesis (top) with a zoom on the photovoltaic pixels (bottom). B, Normal forceps can be used to roll the prosthesis. C, The POLYRETINA prosthesis rolled around the forceps. D, The rolled device is introduced in the tip of a custom-made syringe. E, The custom-made syringe with the POLYRETINA loaded in the tip. F, Sequence of images representing the unfolding process. The device is pushed out of the tip of the syringe and automatically unfolds inside the eye. G, Setup for the surgical implantation. The vitreous is removed and replaced by an aqueous solution and the lens is removed by aspiration. H, The surgeon opens a small tunnel in the cornea using a scalpel. I, The tip of the syringe can be inserted in the tunnel and the surgeon pushes the prosthesis inside the eye.

Fig. 3.14B), probably due to the activation of the remaining cone photoreceptors by the green light. Although, this response does not change shape when increasing the length of the stimulus and retains the b-wave. Conversely, the corneal potentials elicited by the activation of the prosthesis have the same duration as the stimulus and lack the b-wave.

At the same time, the VEPs elicited by green light are almost absent one month after the injection of IAA (red, Fig. 3.14C), but a response can be detected in the visual cortex 2 weeks after implanting the retinal prosthesis (Fig. 3.14D, bottom panel, blue tracing). This response appears reliably as an N75 wave (arrow), independently from the duration of the stimulus. A less reliable response appears in the control eye. We need to repeat the experiment in more subjects to undoubtedly attribute the responses to the activation of the POLYRETINA epiretinal prosthesis since these results presented here were obtained from a single animal.

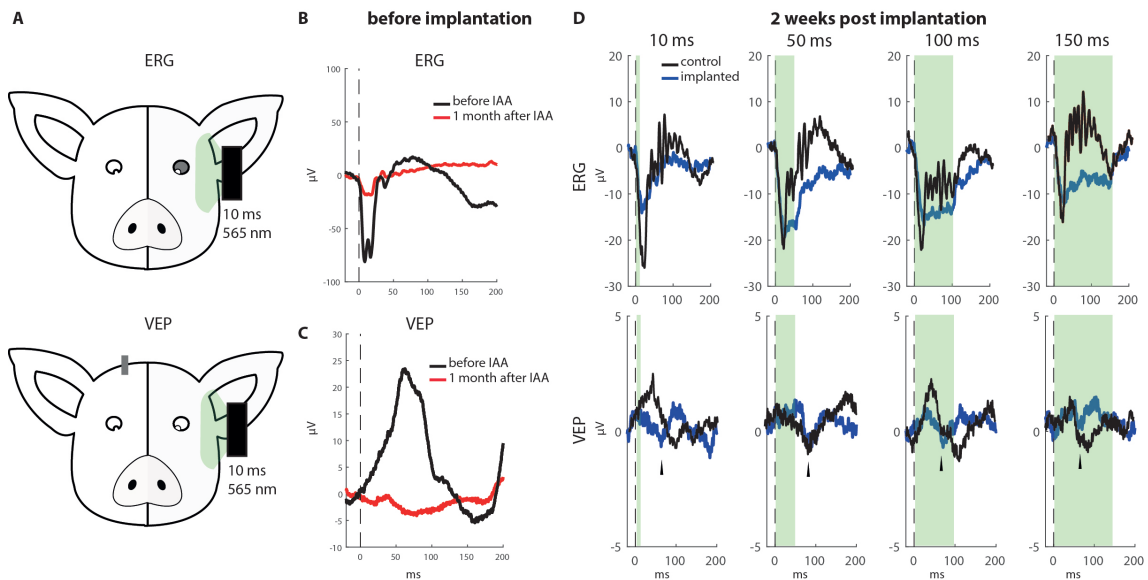


Figure 3.14: ERG/corneal potentials and VEP responses 2 weeks after POLYRETINA implantation. A, Schematic representation of the experiments. Top: corneal potentials/ERGs were recorded from the stimulated eye (in gray). Bottom: cortical evoked potentials/VEPs were recorded from the contralateral visual cortex (in gray). B, Example of ERG responses to green light flashes (565 nm, 10 ms duration) before (black) and one month after the injection of IAA (red). C, Example of VEP responses to green light flashes (565 nm, 10 ms duration) in the same eye as in B and C before (black) and one month after the injection of IAA (red). D, Corneal potentials/ERGs (top) and cortical evoked potentials/VEPs (bottom) responses for different duration of the flash (green area, from left to right: 10, 50, 100, and 150 ms) recorded two weeks after the implantation of the prosthesis from the implanted (blue) and control (black) eye. Arrow: N75 wave. The results were all obtained from the same animal.

In this subject, we noticed retinal detachment below the implanted device, which is not ideal for the stimulation. There are two main things that could have contributed to this situation: the incomplete insertion of the tacks through the sclera (they will come off after a certain period of time) and the mismatch between

the curvature of the prosthesis and the one of the pig eye. Both these problems will be addressed in future experiments.

### **3.4 Conclusions and Future Work**

We are currently in the process of replicating the results obtained in the first animal in more subjects. To address the problem of retinal detachment, part of the LNE team is working on a new mold for the POLYRETINA prosthesis which resembles more closely the curvature of the eye in the minipig. In fact, the unmatched curvature probably results in the prosthesis pulling the retina and causing its detachment. Moreover, during the next surgeries, the surgeon will punch slightly the sclera prior to introducing the tacks to facilitate their insertion. Hopefully, these details will allow us to obtain reliable results for a longer period of time from implanted animals, without encountering the retinal detachment problem.

The responses recorded after stimulation of the POLYRETINA prosthesis (Fig. 3.14) were obtained from a single animal and a couple of details need to be adjusted for future experiments. First, the implant should block approximately half of the light. Hence, it would be more accurate to compare the results obtained from the stimulation of the implanted eye with the results obtained stimulating a control eye corrected taking into consideration the fraction of the light intensity which is supposed to reach the retina through the prosthesis. Second, the lens is removed during the surgical procedure, which makes it difficult to compare the results before and after the implantation. We will solve this problem by removing the lens in the eye that is not implanted (control) in order to obtain comparable conditions. Doing so would allow us to test the amplitude and latency of the response in control vs implanted eye of the same animal and to perform statistical analysis on the results. Overall, in view of these observations, the results presented in Fig. 3.14D are even more encouraging.

An important aspect to take into consideration is that the toxin, which is administered systemically and is interfering with the cell metabolism, has the potential to cause complications in the initial phase after the injection is complete, which we observed in two subjects during the first batch of experiments we conducted. This slightly stronger reaction (respiratory complications) to IAA observed in minipigs, with respects to what was reported in swines, might be due to their smaller size, which might allow the toxin to reach the retina at a higher concentration before being metabolized. Although, we found that these occurrences could be completely avoided just supervising the animal for a couple of hours after the injection, maintaining it under anesthesia by inhalation while monitoring the vital parameters. Moreover, we do not have any definite prove that the reaction was caused by the injection of IAA and not only by anaesthesia itself.

In conclusion, here we tested a chemically-induced model of retinal degeneration which appears to be comparable to the swine, with the clear advantage of

being easier to manipulate because of the smaller size. The next step will be to reproduce the results from the first animal in more subjects and to obtain reliable and comparable responses that can be clearly attributed to the POLYRETINA epiretinal prosthesis. This project will lead to important preclinical results in view of further studies in primates and clinical trials.



# **Discussion and Outlook**

In this thesis, I discussed two different approaches to vision restoration, both representing a valuable contribution to the research in the field of ophthalmology. The two strategies presented lie at the opposite extremities of the spectrum of therapeutic options for vision restoration. Gene editing is best utilized to correct genetic mutations in the early stages of the retinal degeneration, when the photoreceptors are still alive. On the other hand, retinal prostheses represent an essential approach for later stages of photoreceptor degeneration since they bypass the lost photoreceptor layer, relying on the stimulation of the inner circuits of the retina to restore visual perception.

Although many advances have appeared in the last decade, a sight-restoring therapy is still a major unmet medical need for many of the known IRDs. Moreover, with the constant aging of the population, we can expect blindness to become more prevalent, which increases the need for optimizing the current therapeutic options and finding new solutions.

The heterogeneous nature of IRDs negates the possibility for a common therapy. Even just considering a single disease, the number of mutations that can lead to the symptoms can be overwhelming. A clear example of this is RP, with more than 50 causative mutations identified to date. What this means in practice is that researchers and clinicians should work together towards the development and optimization of new approaches to vision restoration. A decision about which one can be applied to the specific patient can be taken only upon analysing each individual situation, and the more options are available, the higher will be the probability of a positive outcome.

The result of clinical interventions depends in large part on the preclinical research, like the work showed in this thesis, which is conducted *in vitro* and on animal models. Proof-of-concept studies in mice can help us understand if the designed approach has the desired functional outcome, in which case it is possible to move the study to larger animal models such as pigs or primates. For certain therapeutic methods, such as retinal prostheses, there is the necessity to use a larger animal model almost immediately in the preclinical phase, because the eye size is closer to the one of humans, which can help in studying the surgical procedure and device functionality.

The second chapter of the thesis introduced a technique for *in vivo* gene editing in the retina of mice carrying a mutation that leads to retinal degeneration. Because of its anatomical configuration and accessibility, the eye has always been at the forefront of gene therapy research, leading to several proof-of-concept studies in animal models of IRDs. Some of these findings have been transferred to the clinics during the years and are now being tested on patients. Those clinical trials have been overall successful, but have also raised a series of challenges that need to be overcome in order to move further with retinal therapies. For instance, as already discussed, the safe delivery of viral vectors to the outer segment of the retina still needs to be addressed, as well as the selection of the right IRDs and

patients in order to maximise the effect of the the specific treatment. With the high number of diverse mutations involved, a technique such as CRISPR/Cas9 can be really useful since it allows to easy tailor the therapy to the specific needs of the patient.

Moreover, another interesting concept presented in the second chapter of this thesis is the use of non-viral delivery methods to introduce genes into the retina. These alternative approaches are less widely accepted than the current standard (viral vectors) because of the lacking of tests in human patients, but are worth our consideration and further research. Since viral approaches are not risk free, finding feasible alternatives could be extremely beneficial for the field.

The third chapter focused on retinal prostheses, which have been studied for several years, although obtaining a functional form of vision that is above what is considered the threshold for blindness still represents a challenge. Retinal prostheses are probably the most adopted therapeutic option for patients in late stages of retinal degeneration. At this point, sometimes using electrical stimulation is the only hope left for the patient. In this scenario, it is of foremost importance to come up with new technologies to achieve a better outcome for the patient. Hopefully, neuroprotective strategies, discussed in the introduction of this thesis, could be used in the future together with retinal prostheses to preserve the inner circuits of the retina for a longer time.

With the amount of therapeutic options available at the moment, it is easy to imagine to combine them to obtain a synergic result. Some recent advances that could improve the outcome of genetic approaches to vision restoration are retinal regeneration strategies and photoreceptor transplantation. A lot of research is currently being conducted to understand the mechanisms by which cells regenerate and to recreate functional networks of cells *in vitro* using progenitor or stem cells, with the idea of implanting them in the host. In this context, we could envisage *in vitro* gene editing approaches that could eliminate most of the issues related with the introduction of DNA in cells *in vivo*. For instance, the cells could be taken directly from the patient, the mutation corrected *in vitro*, and the cell re-implanted in the same patient. Although, for this strategy to be efficient, we need to understand how transplanted cells can best integrate in the host tissue, which is another emerging line of research in ophthalmology.

In the frame of this discussion, we must keep in mind that the overarching goal is to improve the quality of life of patients that suffered from vision loss. Hence, the priority should be to explore every possibility in order to increase our chances to find the right treatment for each disease. Besides, it is becoming increasingly clear that one single approach is not going to work for all the patients, even though they are affected by the same condition, raising the need for personalized and combinatorial approaches.

An area in which an advance could greatly improve the outcome of retinal therapies is the development of new and more reliable diagnostic methods. In fact,

being able to understand early enough the mutations responsible for the disease in a specific subject would make it easier to choose the right therapeutic strategy, maximizing the possibility for a positive outcome. To this end, researchers and clinicians from different fields must combine their insights to build on the current knowledge and come up with innovative ideas and ways to test them.

Ultimately, the hope is that the retinal research of the future will combine different techniques and therapeutic strategies with the final goal of maximising vision restoration for the benefit of the patients. Although a lot remains to be done to fulfil this goal, the situation looks promising if we consider that, in a few years, we made enormous steps forward in the field of retinal therapies. Those new alternatives, considered impossible not long ago, represent a great advance towards finally accomplishing a long-term objective of medicine: restoring vision in blind people.

## References

1. Coffey, M., Coufopoulos, A. & Kinghorn, K. Barriers to employment for visually impaired women. *International Journal of Workplace Health Management*. ISSN: 1753836X. doi:10.1108/IJWHM-06-2013-0022 (2014).
2. Cumberland, P. M. & Rahi, J. S. Visual function, social position, and health and life chances the UK Biobank study. *JAMA Ophthalmology*. ISSN: 21686165. doi:10.1001/jamaophthamol.2016.1778 (2016).
3. Hernandez Trillo, A. & Dickinson, C. M. The impact of visual and nonvisual factors on quality of life and adaptation in adults with visual impairment. *Investigative Ophthalmology and Visual Science*. ISSN: 01460404. doi:10.1167/iovs.12-9580 (2012).
4. Senra, H., Vieira, C. R., Nicholls, E. G. & Leal, I. Depression and experience of vision loss in group of adults in rehabilitation setting: Mixed-methods pilot study. *Journal of Rehabilitation Research and Development*. ISSN: 0748-7711. doi:10.1682/jrrd.2012.08.0138 (2014).
5. Frick, K. D. & Foster, A. The magnitude and cost of global blindness: An increasing problem that can be alleviated. *American Journal of Ophthalmology*. ISSN: 00029394. doi:10.1016/S0002-9394(02)02110-4 (2003).
6. Köberlein, J., Beifus, K., Schaffert, C. & Finger, R. P. The economic burden of visual impairment and blindness: A systematic review. *BMJ Open*. ISSN: 20446055. doi:10.1136/bmjopen-2013-003471 (2013).
7. Chakravarthy, U. *et al.* The Economic Impact of Blindness in Europe. *Ophthalmic Epidemiology*. ISSN: 17445086. doi:10.1080/09286586.2017.1281426 (2017).
8. Flaxman, S. R. *et al.* Global causes of blindness and distance vision impairment 1990–2020: a systematic review and meta-analysis. *The Lancet Global Health*. ISSN: 2214109X. doi:10.1016/S2214-109X(17)30393-5 (2017).
9. Kolb, H. How the Retina Works. *American Scientist*. ISSN: 0003-0996. doi:10.1511/2003.1.28 (2003).
10. Sung, C. H. & Chuang, J. Z. *The cell biology of vision* 2010. doi:10.1083/jcb.201006020.
11. Masland, R. H. *The Neuronal Organization of the Retina* 2012. doi:10.1016/j.neuron.2012.10.002.
12. Simó, R., Villarroel, M., Corraliza, L., Hernández, C. & Garcia-Ramírez, M. The Retinal Pigment Epithelium: Something More than a Constituent of the Blood-Retinal Barrier—Implications for the Pathogenesis of Diabetic Retinopathy. *Journal of Biomedicine and Biotechnology*. ISSN: 1110-7243. doi:10.1155/2010/190724 (2010).

13. Provis, J. M., Diaz, C. M. & Dreher, B. Ontogeny of the primate fovea: A central issue in retinal development. *Progress in Neurobiology*. ISSN: 03010082. doi:10.1016/S0301-0082(97)00079-8 (1998).
14. Molday, R. S. & Moritz, O. L. Photoreceptors at a glance. *Journal of Cell Science*. ISSN: 0021-9533. doi:10.1242/jcs.175687 (2015).
15. Baccus, S. A. Timing and Computation in Inner Retinal Circuitry. *Annual Review of Physiology*. ISSN: 0066-4278. doi:10.1146/annurev.physiol.69.120205.124451 (2006).
16. Liew, G., Michaelides, M. & Bunce, C. A comparison of the causes of blindness certifications in England and Wales in working age adults (16-64 years), 1999-2000 with 2009-2010. *BMJ Open*. ISSN: 20446055. doi:10.1136/bmjopen-2013-004015 (2014).
17. Broadgate, S., Yu, J., Downes, S. M. & Halford, S. *Unravelling the genetics of inherited retinal dystrophies: Past, present and future 2017*. doi:10.1016/j.preteyeres.2017.03.003.
18. Simunovic, M. P. & Moore, A. T. The cone dystrophies. *Eye (Basingstoke)*. ISSN: 14765454. doi:10.1038/eye.1998.145 (1998).
19. Mitchell, P., Liew, G., Gopinath, B. & Wong, T. Y. *Age-related macular degeneration 2018*. doi:10.1016/S0140-6736(18)31550-2.
20. Armstrong, R. A. & Mousavi, M. Overview of Risk Factors for Age-Related Macular Degeneration (AMD). *Journal of stem cells* **10**, 171–91. ISSN: 1556-8539 (2015).
21. Ferrari, S. *et al.* Retinitis Pigmentosa: Genes and Disease Mechanisms. *Current Genomics* **12**, 238–249. ISSN: 1389-2029 (2011).
22. Narayan, D. S., Wood, J. P. M., Chidlow, G. & Casson, R. J. A review of the mechanisms of cone degeneration in retinitis pigmentosa. *Acta Ophthalmologica*. ISSN: 1755-3768. doi:10.1111/aos.13141. <<http://dx.doi.org/10.1111/aos.13141>> (2016).
23. Ali, M. U., Rahman, M. S. U., Cao, J. & Yuan, P. X. Genetic characterization and disease mechanism of retinitis pigmentosa; current scenario. *3 Biotech* **7**, 251. ISSN: 2190-572X (Aug. 2017).
24. Takkar, B., Bansal, P. & Venkatesh, P. Leber's Congenital Amaurosis and Gene Therapy. *The Indian Journal of Pediatrics* **85**, 237–242. ISSN: 0019-5456 (Mar. 2018).
25. Hamel, C. P. Cone rod dystrophies. *Orphanet journal of rare diseases* **2**, 7. ISSN: 1750-1172 (Feb. 2007).
26. Altschwager, P., Ambrosio, L., Swanson, E. A., Moskowitz, A. & Fulton, A. B. Juvenile Macular Degenerations. *Seminars in Pediatric Neurology*. ISSN: 15580776. doi:10.1016/j.spen.2017.05.005 (2017).

27. Mitsios, A., Dubis, A. M. & Moosajee, M. Choroideremia: from genetic and clinical phenotyping to gene therapy and future treatments. *Therapeutic advances in ophthalmology* **10**, 2515841418817490. issn: 2515-8414 (2018).
28. Veleri, S. *et al.* Biology and therapy of inherited retinal degenerative disease: insights from mouse models. *Disease Models & Mechanisms*. issn: 1754-8403. doi:10.1242/dmm.017913 (2015).
29. Chang, B. *et al.* Retinal degeneration mutants in the mouse. *Vision Research* **42**, 517–525. issn: 0042-6989 (2002).
30. Strauss, O., Stumpff, F., Mergler, S., Wienrich, M. & Wiederholt, M. The Royal College of Surgeons Rat: An Animal Model for Inherited Retinal Degeneration with a Still Unknown Genetic Defect. *Cells Tissues Organs*. issn: 1422-6405. doi:10.1159/000046474 (1998).
31. Han, J. *et al.* Review: the history and role of naturally occurring mouse models with Pde6b mutations. *Molecular vision* **19**, 2579–89. issn: 1090-0535 (Dec. 2013).
32. Petersen-Jones, S. M. & Komáromy, A. M. Dog Models for Blinding Inherited Retinal Dystrophies. *Human Gene Therapy Clinical Development*. issn: 2324-8637. doi:10.1089/humc.2014.155 (2015).
33. LaVail, M. M. *et al.* Phenotypic characterization of P23H and S334ter rhodopsin transgenic rat models of inherited retinal degeneration. *Experimental Eye Research*. issn: 10960007. doi:10.1016/j.exer.2017.10.023 (2018).
34. Jones, B. W. *et al.* Retinal remodeling in the Tg P347L rabbit, a large-eye model of retinal degeneration. *Journal of Comparative Neurology*. issn: 00219967. doi:10.1002/cne.22703 (2011).
35. Ross, J. W. *et al.* Generation of an inbred miniature pig model of retinitis pigmentosa. *Investigative Ophthalmology and Visual Science*. issn: 01460404. doi:10.1167/iovs.11-8784 (2012).
36. Dancinger, M. *et al.* Mutations in the PDE6B Gene in Autosomal Recessive Retinitis Pigmentosa. *Genomics* **30**, 1–7. issn: 0888-7543 (1995).
37. McLaughlin, M. E., Ehrhart, T. L., Berson, E. L. & Dryja, T. P. Mutation spectrum of the gene encoding the beta subunit of rod phosphodiesterase among patients with autosomal recessive retinitis pigmentosa. *Proceedings of the National Academy of Sciences* **92**, 3249–3253. issn: 0027-8424 (1995).
38. Ulshafer, R. J., Garcia, C. A. & Hollyfield, J. G. Sensitivity of photoreceptors to elevated levels of cGMP in the human retina. *Investigative ophthalmology & visual science* **19**, 1236–1241. issn: 0146-0404 (1980).

39. Chang, B. *et al.* Two mouse retinal degenerations caused by missense mutations in the  $\beta$ -subunit of rod cGMP phosphodiesterase gene. **47**, 624–633. ISSN: 0042-6989 (2007).
40. Bowes, C. *et al.* Retinal degeneration in the rd mouse is caused by a defect in the  $\beta$  subunit of rod cGMP-phosphodiesterase. *Nature*. ISSN: 00280836. doi:10.1038/347677a0 (1990).
41. Safran, A. B. *et al.* A review of in vivo animal studies in retinal prosthesis research. *Graefe's Archive for Clinical and Experimental Ophthalmology* **246**, 1505–1517. ISSN: 0721-832X (2008).
42. Mollon, J. D. & Bowmaker, J. K. The spatial arrangement of cones in the primate fovea. *Nature*. ISSN: 00280836. doi:10.1038/360677a0 (1992).
43. Chandler, Smith, Samuelson & Mackay. Photoreceptor density of the domestic pig retina. *Veterinary Ophthalmology* **2**, 179–184. ISSN: 1463-5216 (Sept. 1999).
44. Beattie, J. R., Brockbank, S., McGarvey, J. J. & Curry, W. J. Raman microscopy of porcine inner retinal layers from the area centralis. *Molecular vision*. ISSN: 1090-0535 (2007).
45. Shrader, S. M. & Greentree, W. F. Göttingen Minipigs in Ocular Research. *Toxicologic Pathology* **46**, 403–407. ISSN: 0192-6233 (June 2018).
46. Bertschinger, D. R. *et al.* A review of in vivo animal studies in retinal prosthesis research 2008. doi:10.1007/s00417-008-0891-7.
47. Llonch, S., Carido, M. & Ader, M. *Organoid technology for retinal repair* 2018. doi:10.1016/j.ydbio.2017.09.028.
48. Lechner, J., O'Leary, O. E. & Stitt, A. W. The pathology associated with diabetic retinopathy. *Vision Research* **139**, 7–14. ISSN: 0042-6989 (Oct. 2017).
49. Petit, L., Khanna, H. & Punzo, C. Advances in Gene Therapy for Diseases of the Eye. *Human gene therapy* **27**, 563–79. ISSN: 1557-7422 (2016).
50. Auricchio, A., Smith, A. J. & Ali, R. R. The future looks brighter after 25 years of retinal gene therapy. *Human Gene Therapy*. ISSN: 1043-0342. doi:10.1089/hum.2017.164. <<http://dx.doi.org/10.1089/hum.2017.164>> (2017).
51. Scholl, H. P. N. *et al.* Emerging therapies for inherited retinal degeneration. *Science translational medicine* **8**, 368rv6. ISSN: 1946-6242 (Dec. 2016).
52. Jacobson, S. G. & Cideciyan, A. V. Treatment Possibilities for Retinitis Pigmentosa. *The New England Journal of Medicine* **363**, 1669–1671. ISSN: 0028-4793 (2010).



53. Pardue, M. T. & Allen, R. S. Neuroprotective strategies for retinal disease. *Progress in Retinal and Eye Research*. ISSN: 18731635. doi:10.1016/j.preteyeres.2018.02.002 (2018).
54. Wubben, T. J., Besirli, C. G., Johnson, M. W. & Zacks, D. N. Retinal Neuroprotection: Overcoming the Translational Roadblocks. *American Journal of Ophthalmology* **192**, xv–xxii. ISSN: 0002-9394 (Aug. 2018).
55. Marc, R. E., Jones, B. W., Watt, C. B. & Strettoi, E. *Neural remodeling in retinal degeneration 2003*. doi:10.1016/S1350-9462(03)00039-9.
56. Yue, L., Weiland, J. D., Roska, B. & Humayun, M. S. *Retinal stimulation strategies to restore vision: Fundamentals and systems 2016*. doi:10.1016/j.preteyeres.2016.05.002.
57. Ferlauto, L. *et al.* Design and validation of a foldable and photovoltaic wide-field epiretinal prosthesis. *Nature Communications* **9**, 992. ISSN: 2041-1723 (2018).
58. Harris, J. *et al.* Photovoltaic restoration of sight with high visual acuity. *Nature Medicine* **21**, 476–482. ISSN: 1078-8956 (2015).
59. Chenais, N. A. L., Airaghi Leccardi, M. J. I. & Ghezzi, D. Capacitive-like photovoltaic epiretinal stimulation enhances and narrows the network-mediated activity of retinal ganglion cells by recruiting the lateral inhibitory network. *Journal of Neural Engineering*. ISSN: 1741-2560. doi:10.1088/1741-2552/ab3913 (2019).
60. Ho, A. C. *et al.* Long-Term Results from an Epiretinal Prosthesis to Restore Sight to the Blind. *Ophthalmology*. ISSN: 15494713. doi:10.1016/j.ophtha.2015.04.032 (2015).
61. Duebel, J., Marazova, K. & Sahel, J.-A. Optogenetics. *Current opinion in ophthalmology* **26**, 226–32. ISSN: 1531-7021 (May 2015).
62. Klapoetke, N. C. *et al.* Independent optical excitation of distinct neural populations. *Nature Methods*. ISSN: 15487105. doi:10.1038/nmeth.2836 (2014).
63. Busskamp, V., Picaud, S., Sahel, J. A. & Roska, B. Optogenetic therapy for retinitis pigmentosa. *Gene Therapy* **19**, 169–175. ISSN: 0969-7128 (2012).
64. Sahel, J.-A. & Roska, B. Gene Therapy for Blindness. *Annual Review of Neuroscience*. ISSN: 0147-006X. doi:10.1146/annurev-neuro-062012-170304 (2013).
65. Wan, J. & Goldman, D. *Retina regeneration in zebrafish 2016*. doi:10.1016/j.gde.2016.05.009.
66. Karl, M. O. *et al.* Stimulation of neural regeneration in the mouse retina. *Proceedings of the National Academy of Sciences*. ISSN: 0027-8424. doi:10.1073/pnas.0807453105 (2008).

67. Da Cruz, L. *et al.* Phase 1 clinical study of an embryonic stem cell-derived retinal pigment epithelium patch in age-related macular degeneration. *Nature Biotechnology*. ISSN: 15461696. doi:10.1038/nbt.4114 (2018).
68. MacLaren, R. E. *et al.* Retinal repair by transplantation of photoreceptor precursors. *Nature* **444**, nature05161. ISSN: 1476-4687 (2006).
69. Lamba, D. A., Gust, J. & Reh, T. A. Transplantation of human embryonic stem cell-derived photoreceptors restores some visual function in Crx-deficient mice. *Cell stem cell* **4**, 73–9. ISSN: 1875-9777 (Jan. 2009).
70. Klassen, H. J. *et al.* Multipotent Retinal Progenitors Express Developmental Markers, Differentiate into Retinal Neurons, and Preserve Light-Mediated Behavior. *Investigative Ophthalmology & Visual Science* **45**, 4167. ISSN: 1552-5783 (Nov. 2004).
71. Yao, K. *et al.* Restoration of vision after de novo genesis of rod photoreceptors in mammalian retinas. *Nature* **560**, 484–488. ISSN: 0028-0836 (Aug. 2018).
72. Michael E. Cheetham, P. J. C. e., G. Astrid Limb, R. R. A. & Alison J. Hardcastle, R. A. P. Stem cells for retinal biology, disease modelling and repair. *Nature*. <<https://www.nature.com/magazine-assets/d42473-018-00099-9/d42473-018-00099-9.pdf>> (2018).
73. Hilton, B. J. & Bradke, F. Can injured adult CNS axons regenerate by recapitulating development? *Development* **144**, 3417–3429. ISSN: 0950-1991 (2017).
74. Hunt, N. C. *et al.* 3D culture of human pluripotent stem cells in RGD-alginate hydrogel improves retinal tissue development. *Acta Biomaterialia* **49**, 329–343. ISSN: 17427061 (Feb. 2017).
75. Ballios, B. G., Cooke, M. J., van der Kooy, D. & Shoichet, M. S. A hydrogel-based stem cell delivery system to treat retinal degenerative diseases. *Biomaterials* **31**, 2555–2564. ISSN: 01429612 (Mar. 2010).
76. Liu, Y. *et al.* The application of hyaluronic acid hydrogels to retinal progenitor cell transplantation. *Tissue engineering. Part A* **19**, 135–42. ISSN: 1937-335X (Jan. 2013).
77. Tang, Z. *et al.* Mussel-inspired injectable hydrogel and its counterpart for actuating proliferation and neuronal differentiation of retinal progenitor cells. *Biomaterials*. ISSN: 18785905. doi:10.1016/j.biomaterials.2018.12.015 (2019).
78. Sahel, J.-A. & Roska, B. Gene Therapy for Blindness. *Annual Review of Neuroscience* **36**, 467–488. ISSN: 0147-006x (2012).

79. Cideciyan, A. V. *et al.* Human gene therapy for RPE65 isomerase deficiency activates the retinoid cycle of vision but with slow rod kinetics. *Proceedings of the National Academy of Sciences*. ISSN: 0027-8424. doi:10.1073/pnas.0807027105 (2008).
80. Maguire, A. M. *et al.* Safety and efficacy of gene transfer for Leber's congenital amaurosis. *The New England journal of medicine*. ISSN: 1533-4406. doi:10.1056/NEJMoa0802315 (2008).
81. Bainbridge, J. W. B. *et al.* Effect of gene therapy on visual function in Leber's congenital amaurosis. *The New England journal of medicine*. ISSN: 1533-4406. doi:10.1056/NEJMoa0802268 (2008).
82. Bainbridge, J. W. *et al.* Long-term effect of gene therapy on Leber's congenital amaurosis. *New England Journal of Medicine*. ISSN: 15334406. doi:10.1056/NEJMoa1414221 (2015).
83. Jacobson, S. G. *et al.* Improvement and decline in vision with gene therapy in childhood blindness. *New England Journal of Medicine*. ISSN: 15334406. doi:10.1056/NEJMoa1412965 (2015).
84. Heidenreich, M. & Zhang, F. Applications of CRISPR-Cas systems in neuroscience. *Nature Reviews Neuroscience* **17**, 36–44. ISSN: 1471-003x (2016).
85. Ran, A. F. *et al.* Genome engineering using the CRISPR-Cas9 system. **8**, 2281–2308. ISSN: 1754-2189 (2013).
86. Saleh-Gohari, N. & Helleday, T. Conservative homologous recombination preferentially repairs DNA double-strand breaks in the S phase of the cell cycle in human cells. *Nucleic Acids Research* **32**, 3683–3688. ISSN: 0305-1048 (2004).
87. Colella, P., Cotugno, G. & Auricchio, A. Ocular gene therapy: current progress and future prospects. *Trends in Molecular Medicine* **15**, 23–31. ISSN: 1471-4914 (2009).
88. Venkatesh, A., Ma, S., Langellotto, F., Gao, G. & Punzo, C. Retinal gene delivery by rAAV and DNA electroporation. *Current Protocols in Microbiology*. ISSN: 19348525. doi:10.1002/9780471729259.mc14d04s28 (2013).
89. Allocca, M. *et al.* Novel Adeno-Associated Virus Serotypes Efficiently Transduce Murine Photoreceptors. *Journal of Virology* **81**, 11372–11380. ISSN: 0022-538X (2007).
90. Trapani, I. in *Methods in molecular biology (Clifton, N.J.)* 153–175 (2018). doi:10.1007/978-1-4939-7522-8\_{\\_}11. <<http://www.ncbi.nlm.nih.gov/pubmed/29188512>&20[http://link.springer.com/10.1007/978-1-4939-7522-8\\_11](http://link.springer.com/10.1007/978-1-4939-7522-8_11)>.
91. Trapani, I. *et al.* Effective delivery of large genes to the retina by dual AAV vectors. *EMBO Molecular Medicine* **6**, 194–211. ISSN: 1757-4684 (2014).

92. Rossidis, A. C. *et al.* In utero CRISPR-mediated therapeutic editing of metabolic genes. *Nature Medicine* **24**, 1513–1518. ISSN: 1078-8956 (Oct. 2018).
93. Kumar-Singh, R. Barriers for retinal gene therapy: Separating fact from fiction. *Vision Research* **48**, 1671–1680. ISSN: 0042-6989 (July 2008).
94. Trapani, I., Puppo, A. & Auricchio, A. Vector platforms for gene therapy of inherited retinopathies. *Progress in Retinal and Eye Research* **43**, 108–128. ISSN: 1350-9462 (Nov. 2014).
95. Baum, C., Kustikova, O., Modlich, U., Li, Z. & Fehse, B. Mutagenesis and Oncogenesis by Chromosomal Insertion of Gene Transfer Vectors. *Human Gene Therapy* **17**, 253–263. ISSN: 1043-0342 (2006).
96. Thomas, C. E., Ehrhardt, A. & Kay, M. A. Progress and problems with the use of viral vectors for gene therapy. *Nature Reviews Genetics* **4**, 346–358. ISSN: 1471-0056 (2003).
97. Worgall, S. *et al.* Treatment of late infantile neuronal ceroid lipofuscinosis by CNS administration of a serotype 2 adeno-associated virus expressing CLN2 cDNA. TL - 19. *Human gene therapy* **19 VN - r**, 463–474. ISSN: 1043-0342 (2008).
98. Yoshioka, Y. *et al.* Recombinant AAV-Transduced Iris Pigment Epithelial Cell Transplantation May Transfer Vector to Native RPE but Suppress Systemic Dissemination TL - 47. *Investigative Ophthalmology & Visual Science* **47 VN - r**, 745–752. ISSN: 1552-5783 (2006).
99. Niidome, T. & Huang, L. Gene Therapy Progress and Prospects: Nonviral vectors. *Gene Therapy* **9**, 3301923. ISSN: 1476-5462 (2002).
100. Andrieu-Soler, C. *et al.* Single-stranded oligonucleotide-mediated in vivo gene repair in the rd1 retina. **13**, 692–706. ISSN: 1090-0535 (2007).
101. Bainbridge, J. W. B., Tan, M. H. & Ali, R. R. Gene therapy progress and prospects: the eye. *Gene Therapy* **13**, 1191–1197. ISSN: 0969-7128 (2006).
102. Han, Z., Conley, S. M. & Naash, M. I. AAV and Compacted DNA Nanoparticles for the Treatment of Retinal Disorders: Challenges and Future Prospects. *Investigative Ophthalmology & Visual Science* **52**, 3051–3059. ISSN: 1552-5783 (2011).
103. Al-Dosari, M. S. & Gao, X. Nonviral Gene Delivery: Principle, Limitations, and Recent Progress. *The AAPS Journal* **11**, 671–681 (2009).
104. Endoh, M. *et al.* Fetal gene transfer by intrauterine injection with microbubble-enhanced ultrasound. *Molecular Therapy*. ISSN: 15250016. doi:10.1006/mthe.2002.0577 (2002).
105. Adijanto, J. & Naash, M. I. Nanoparticle-based technologies for retinal gene therapy. *European Journal of Pharmaceutics and Biopharmaceutics*. ISSN: 18733441. doi:10.1016/j.ejpb.2014.12.028 (2015).

106. Cancedda, L. *et al.* High-performance and reliable site-directed in vivo genetic manipulation of mouse and rat brain by in utero electroporation with a triple-electrode probe. *Protocol Exchange*. issn: 2043-0116. doi:10.1038/protex.2013.089. <<http://www.nature.com/protocolexchange/protocols/2889>> (Dec. 2013).
107. Cwetsch, A. W., Pinto, B., Savardi, A. & Cancedda, L. In vivo methods for acute modulation of gene expression in the central nervous system. *Progress in Neurobiology* **168**, 69–85. issn: 03010082 (Sept. 2018).
108. Dal Maschio, M. *et al.* High-performance and site-directed in utero electroporation by a triple-electrode probe. *Nature Communications* **3**, 960. issn: 2041-1723 (Jan. 2012).
109. Szczurkowska, J. *et al.* Increased performance in genetic manipulation by modeling the dielectric properties of the rodent brain in 2013 35th Annual International Conference of the IEEE Engineering in Medicine and Biology Society (EMBC) (IEEE, July 2013), 1615–1618. isbn: 978-1-4577-0216-7. doi:10.1109/EMBC.2013.6609825. <<http://ieeexplore.ieee.org/document/6609825/>>.
110. Gothelf, A., Mir, L. M. & Gehl, J. Electrochemotherapy: results of cancer treatment using enhanced delivery of bleomycin by electroporation. *Cancer Treatment Reviews* **29**, 371–387. issn: 0305-7372 (2003).
111. Lambrecht, L. *et al.* Clinical potential of electroporation for gene therapy and DNA vaccine delivery. *Expert Opinion on Drug Delivery* **13**, 295–310. issn: 1742-5247 (2015).
112. Hornstein, B. D., Roman, D., Arévalo-Soliz, L. M., Engevik, M. A. & Zechiedrich, L. Effects of Circular DNA Length on Transfection Efficiency by Electroporation into HeLa Cells TL - 11. *PLOS ONE* **11 VN - r**. issn: 1932-6203. doi:10.1371/journal.pone.0167537. <<http://dx.doi.org/10.1371/journal.pone.0167537>> (2016).
113. Matsuda, T. & Cepko, C. L. Electroporation and RNA interference in the rodent retina in vivo and in vitro. *Proceedings of the National Academy of Sciences* **101**, 16–22. issn: 0027-8424 (2004).
114. Matsuda, T. & Cepko, C. L. Controlled expression of transgenes introduced by *in vivo* electroporation. *Proceedings of the National Academy of Sciences* **104**, 1027–1032. issn: 0027-8424 (Jan. 2007).
115. Touchard, E. *et al.* Suprachoroidal Electrotransfer: A Nonviral Gene Delivery Method to Transfect the Choroid and the Retina Without Detaching the Retina. *Molecular Therapy* **20**, 1559–1570. issn: 1525-0016 (2012).
116. Pinto, L. H. & Enroth-Cugell, C. Tests of the mouse visual system. *Mammalian genome : official journal of the International Mammalian Genome Society* **11**, 531–6. issn: 0938-8990 (July 2000).

117. Leinonen, H. Vision in laboratory rodents—Tools to measure it and implications for behavioral research. *Behavioural Brain Research* **352**, 172–182. ISSN: 0166-4328 (Oct. 2018).
118. Frishman, L. J. & Wang, M. H. *Electroretinogram of Human, Monkey and Mouse* tech. rep. (). <[https://pdfs.semanticscholar.org/3b68/b18d9866e82603fed3f69e52c000pdf?\\_ga=2.73757979.881182567.1558515176-1174553544.1558515176](https://pdfs.semanticscholar.org/3b68/b18d9866e82603fed3f69e52c000pdf?_ga=2.73757979.881182567.1558515176-1174553544.1558515176)>.
119. Pinto, L. H., Invergo, B., Shimomura, K., Takahashi, J. S. & Troy, J. B. Interpretation of the mouse electroretinogram. *Documenta Ophthalmologica* **115**, 127–136. ISSN: 0012-4486 (Oct. 2007).
120. Stett, A. *et al. Biological application of microelectrode arrays in drug discovery and basic research* 2003. doi:10.1007/s00216-003-2149-x.
121. McCulloch, D. L. *et al. ISCEV Standard for full-field clinical electroretinography (2015 update). Documenta Ophthalmologica.* ISSN: 15732622. doi:10.1007/s10633-014-9473-7 (2015).
122. Kremers, J. & Tanimoto, N. in *Methods in molecular biology (Clifton, N.J.)* 27–40 (2018). doi:10.1007/978-1-4939-7720-8\_{\\_}2. <[http://www.ncbi.nlm.nih.gov/pubmed/29564779%20http://link.springer.com/10.1007/978-1-4939-7720-8\\_2](http://www.ncbi.nlm.nih.gov/pubmed/29564779%20http://link.springer.com/10.1007/978-1-4939-7720-8_2)>.
123. Kraut, M. A., Arezzo, J. C. & Vaughan, H. G. Intracortical generators of the flash VEP in monkeys. *Electroencephalography and Clinical Neurophysiology/ Evoked Potentials.* ISSN: 01685597. doi:10.1016/0168-5597(85)90007-3 (1985).
124. Ducati, A., Fava, E. & Motti, E. D. F. Neuronal generators of the visual evoked potentials: intracerebral recording in awake humans. *Electroencephalography and Clinical Neurophysiology/ Evoked Potentials.* ISSN: 01685597. doi:10.1016/0168-5597(88)90010-X (1988).
125. Creel, D. *Visually Evoked Potentials* (1995).
126. Strain, G. M. & Tedford, B. L. Flash and pattern reversal visual evoked potentials in C57BL/6J and B6CBAF1/J mice. *Brain Research Bulletin* **32**, 57–63. ISSN: 03619230 (1993).
127. Prusky, G. T., Alam, N. M., Beekman, S. & Douglas, R. M. Rapid Quantification of Adult and Developing Mouse Spatial Vision Using a Virtual Optomotor System. *Investigative Ophthalmology & Visual Science* **45**, 4611–4616. ISSN: 0146-0404 (2004).
128. Douglas, R. M. *et al.* Independent visual threshold measurements in the two eyes of freely moving rats and mice using a virtual-reality optokinetic system. *Visual Neuroscience* **22**, 677–684. ISSN: 1469-8714 (2005).
129. Kretschmer, F., Tariq, M., Chatila, W., Wu, B. & Badea, T. C. Comparison of optomotor and optokinetic reflexes in mice. *Journal of Neurophysiology.* ISSN: 0022-3077. doi:10.1152/jn.00055.2017 (2017).

130. Abdeljalil, J. *et al.* The optomotor response: A robust first-line visual screening method for mice. *Vision Research* **45**, 1439–1446. ISSN: 00426989 (2005).
131. Kretschmer, F., Kretschmer, V., Kunze, V. P. & Kretzberg, J. OMR-arena: Automated measurement and stimulation system to determine mouse visual thresholds based on optomotor responses. *PLoS ONE* **8**, 1–12. ISSN: 19326203 (2013).
132. Mohand-Said, S., Hicks, D., Dreyfus, H. & Sahel, J. A. Selective Transplantation of Rods Delays Cone Loss in a Retinitis Pigmentosa Model. *Archives of Ophthalmology* **118**, 807–811. ISSN: 0003-9950 (2000).
133. Gargini, C., Terzibasi, E., Mazzoni, F. & Strettoi, E. Retinal organization in the retinal degeneration 10 (rd10) mutant mouse: A morphological and ERG study. *Journal of Comparative Neurology* **500**, 222–238. ISSN: 1096-9861 (2007).
134. Bennett, J., Wilson, J., Sun, D., Forbes, B. & Maguire, A. Adenovirus vector-mediated in vivo gene transfer into adult murine retina. *Investigative ophthalmology & visual science* **35**, 2535–2542. ISSN: 0146-0404 (1994).
135. Jomary, C., Vincent, K. A., Grist, J., Neal, M. J. & Jones, S. E. Rescue of photoreceptor function by AAV-mediated gene transfer in a mouse model of inherited retinal degeneration. *Gene Therapy* **4**, 3300440. ISSN: 1476-5462 (1997).
136. Pang, J.-j. *et al.* AAV-Mediated Gene Therapy for Retinal Degeneration in the rd10 Mouse Containing a Recessive PDE $\beta$  Mutation. **49**, 4278–4283. ISSN: 0146-0404 (2008).
137. Pang, J.-J. *et al.* AAV-mediated gene therapy in mouse models of recessive retinal degeneration. *Current molecular medicine* **12**, 316–330 (2012).
138. Giannelli, S. G. *et al.* Cas9/sgRNA selective targeting of the P23H Rhodopsin mutant allele for treating Retinitis Pigmentosa by intravitreal AAV9.PHP.B-based delivery. *Human Molecular Genetics* **27**, 761–779. ISSN: 0964-6906 (2017).
139. Latella, M. *et al.* In vivo Editing of the Human Mutant Rhodopsin Gene by Electroporation of Plasmid-based CRISPR/Cas9 in the Mouse Retina. *Molecular Therapy - Nucleic Acids* **5**, e389. ISSN: 2162-2531 (2016).
140. Bakondi, B. *et al.* In Vivo CRISPR/Cas9 Gene Editing Corrects Retinal Dystrophy in the S334ter-3 Rat Model of Autosomal Dominant Retinitis Pigmentosa. **24**, 556–563. ISSN: 1525-0016 (2016).
141. Pacey, L., Stead, S., Gleave, J., Tomczyk, K. & Doering, L. Neural Stem Cell Culture: Neurosphere generation, microscopical analysis and cryopreservation. *Protocol Exchange*. ISSN: 2043-0116. doi:10.1038/nprot.2006.215. <<http://www.nature.com/protocolexchange/protocols/77>> (Aug. 2006).

142. Melo, J. d. & Blackshaw, S. In vivo Electroporation of Developing Mouse Retina. *Journal of Visualized Experiments*. ISSN: 1940-087X. doi:10.3791/2847. <<http://dx.doi.org/10.3791/2847>> (2011).
143. Lipinski, D. M. *et al.* CNTF Gene Therapy Confers Lifelong Neuroprotection in a Mouse Model of Human Retinitis Pigmentosa. *Molecular Therapy* **23**. ISSN: 15250024. doi:10.1038/mt.2015.68 (2015).
144. Smith, A. J., Bainbridge, J. & Ali, R. R. Gene supplementation therapy for recessive forms of inherited retinal dystrophies. *Gene Therapy* **19**, gt2011161. ISSN: 1476-5462 (2012).
145. Yu, W. *et al.* Nr1 knockdown by AAV-delivered CRISPR/Cas9 prevents retinal degeneration in mice. *Nature Communications* **8**. ISSN: 20411723. doi:10.1038/ncomms14716 (2017).
146. Gehl, J. Electroporation: theory and methods, perspectives for drug delivery, gene therapy and research. *Acta Physiologica Scandinavica* **177**, 437–447. ISSN: 1365-201X (2003).
147. Szczurkowska, J. *et al.* High-performance and reliable site-directed *in vivo* genetic manipulation of mouse and rat brain by *in utero* electroporation with a triple-electrode probe. Dec. 2013.
148. Touchard, E. *et al.* Effects of ciliary muscle plasmid electrotransfer of TNF- $\alpha$  soluble receptor variants in experimental uveitis. *Gene Therapy* **16**, 862–873. ISSN: 0969-7128 (July 2009).
149. Wang, S., Sengel, C., Emerson, M. M. & Cepko, C. L. A Gene Regulatory Network Controls the Binary Fate Decision of Rod and Bipolar Cells in the Vertebrate Retina. *Developmental Cell* **30**, 513–527. ISSN: 1534-5807 (2014).
150. Bureau, M. F., Gehl, J., Deleuze, V., Mir, L. M. & Scherman, D. Importance of association between permeabilization and electrophoretic forces for intramuscular DNA electrotransfer. *Biochimica et Biophysica Acta (BBA) - General Subjects* **1474**, 353–359. ISSN: 0304-4165 (2000).
151. Zhang, X., Serb, J. M. & Greenlee, H. M. Mouse Retinal Development: a Dark Horse Model for Systems Biology Research. *Bioinformatics and Biology Insights* **5**, 99–113 (2011).
152. Tucker, B. A. *et al.* Transplantation of Adult Mouse iPS Cell-Derived Photoreceptor Precursors Restores Retinal Structure and Function in Degenerative Mice. *PLoS ONE* **6**, e18992 (2011).
153. Jae, S. A. *et al.* Electrophysiological and Histologic Evaluation of the Time Course of Retinal Degeneration in the *rd10* Mouse Model of Retinitis Pigmentosa. *The Korean Journal of Physiology & Pharmacology* **17**, 229. ISSN: 1226-4512 (June 2013).



154. Stasheff, S. F., Shankar, M. & Andrews, M. P. Developmental time course distinguishes changes in spontaneous and light-evoked retinal ganglion cell activity in *rd1* and *rd10* mice. *Journal of Neurophysiology* **105**, 3002–3009. ISSN: 0022-3077 (June 2011).
155. Coleman, J. E., Law, K. & Bear, M. F. Anatomical origins of ocular dominance in mouse primary visual cortex. *Neuroscience* **161**, 561–571. ISSN: 0306-4522 (2009).
156. Pennesi, M. E. *et al.* Long-Term Characterization of Retinal Degeneration in *rd1* and *rd10* Mice Using Spectral Domain Optical Coherence TomographySD-OCT Imaging of *rd1* and *rd10* Mice. *Investigative Ophthalmology & Visual Science* **53**, 4644–4656. ISSN: 1552-5783 (2012).
157. Chu, V. T. *et al.* Increasing the efficiency of homology-directed repair for CRISPR-Cas9-induced precise gene editing in mammalian cells. *Nature Biotechnology* **33**, 543–548. ISSN: 1087-0156 (May 2015).
158. Lin, S., Staahl, B. T., Alla, R. K. & Doudna, J. A. Enhanced homology-directed human genome engineering by controlled timing of CRISPR/Cas9 delivery. *eLife* **3**, e04766. ISSN: 2050-084X (Dec. 2014).
159. Aird, E. J., Lovendahl, K. N., St. Martin, A., Harris, R. S. & Gordon, W. R. Increasing Cas9-mediated homology-directed repair efficiency through covalent tethering of DNA repair template. *Communications Biology* **1**, 54. ISSN: 2399-3642 (Dec. 2018).
160. Swindle, M. M., Makin, A., Herron, A. J., Clubb, F. J. & Frazier, K. S. Swine as Models in Biomedical Research and Toxicology Testing. doi:10.1177/0300985811402846. <<http://vet.sagepub.com>>.
161. Stricker-Krongrad, A., Shoemaker, C. R. & Bouchard, G. F. The Miniature Swine as a Model in Experimental and Translational Medicine. *Toxicologic Pathology* **44**, 612–623. ISSN: 15331601 (2016).
162. Shrader, S. M. & Mowry, R. N. Histomorphometric evaluation of the Göttingen minipig eye. *Veterinary Ophthalmology*, vop.12665. ISSN: 1463-5216 (2019).
163. De Schaepdrijver, L., Lauwers, H., Simoens, P. & de Geest, J. P. Development of the retina in the porcine fetus. A light microscopic study. *Anatomia, histologia, embryologia* **19**, 222–35. ISSN: 0340-2096 (Sept. 1990).
164. Bayouth, W., Carstesen, D., Walter, P. & Weinberger, A. W. A. Intraocular silicone implant to treat chronic ocular hypotony: an in vivo trial. *Graefe's Archive for Clinical and Experimental Ophthalmology* **255**, 1947–1955. ISSN: 0721-832X (Oct. 2017).

165. Koss, M. J. *et al.* Subretinal implantation of a monolayer of human embryonic stem cell-derived retinal pigment epithelium: a feasibility and safety study in Yucatán minipigs. *Graefe's Archive for Clinical and Experimental Ophthalmology* **254**, 1553–1565. ISSN: 0721-832X (Aug. 2016).
166. Schopf, L. R. *et al.* Topical ocular drug delivery to the back of the eye by mucus-penetrating particles. *Translational Vision Science and Technology*. ISSN: 21642591. doi:10.1167/tvst.4.3.11 (2015).
167. De Smet, M. D., Lynch, J. L., Dejneka, N. S., Keane, M. & Khan, I. J. A subretinal cell delivery method via suprachoroidal access in minipigs: Safety and surgical outcomes. *Investigative Ophthalmology and Visual Science*. ISSN: 15525783. doi:10.1167/iovs.17-22233 (2018).
168. Daull, P., Paterson, C. A., Kuppermann, B. D. & Garrigue, J. S. A preliminary evaluation of dexamethasone palmitate emulsion: A novel intravitreal sustained delivery of corticosteroid for treatment of macular Edema. *Journal of Ocular Pharmacology and Therapeutics*. ISSN: 10807683. doi:10.1089/jop.2012.0044 (2013).
169. Hämmerle, H. *et al.* Biostability of micro-photodiode arrays for subretinal implantation. *Biomaterials*. ISSN: 01429612. doi:10.1016/S0142-9612(01)00185-5 (2002).
170. Laube, T. *et al.* Chronically implanted epidural electrodes in Göttinger minipigs allow function tests of epiretinal implants. *Graefe's Archive for Clinical and Experimental Ophthalmology*. ISSN: 0721832X. doi:10.1007/s00417-003-0758-x (2003).
171. Montezuma, S. R., Loewenstein, J., Scholz, C. & Rizzo, J. F. Biocompatibility of materials implanted into the subretinal space of Yucatan pigs. *Investigative Ophthalmology and Visual Science*. ISSN: 01460404. doi:10.1167/iovs.06-0106 (2006).
172. Sachs, H. G. *et al.* Implantation of stimulation electrodes in the subretinal space to demonstrate cortical responses in Yucatan minipig in the course of visual prosthesis development. *European Journal of Ophthalmology*. ISSN: 11206721 (2005).
173. Schwahn, H. N. *et al.* Studies on the feasibility of a subretinal visual prosthesis: Data from Yucatan micropig and rabbit. *Graefe's Archive for Clinical and Experimental Ophthalmology*. ISSN: 0721832X. doi:10.1007/s004170100368 (2001).
174. Laube, T. *et al.* Development of surgical techniques for implantation of a wireless intraocular epiretinal retina implant in Göttingen minipigs. *Graefe's Archive for Clinical and Experimental Ophthalmology* **250**, 51–59. ISSN: 0721832X (2012).

175. Gekeler, F. *et al.* Compound subretinal prostheses with extra-ocular parts designed for human trials: Successful long-term implantation in pigs. *Graefe's Archive for Clinical and Experimental Ophthalmology*. ISSN: 0721832X. doi:10.1007/s00417-006-0339-x (2007).
176. Johnson, L. *et al.* Impedance-based retinal contact imaging as an aid for the placement of high resolution epiretinal prostheses. *Journal of Neural Engineering*. ISSN: 17412560. doi:10.1088/1741-2560/4/1/S03 (2007).
177. Sachs, H. G., Schanze, T., Brunner, U., Sailer, H. & Wiesenack, C. *Transscleral implantation and neurophysiological testing of subretinal polyimide film electrodes in the domestic pig in visual prosthesis development in Journal of Neural Engineering* (2005). doi:10.1088/1741-2560/2/1/008.
178. Schanze, T., Sachs, H. G., Wiesenack, C., Brunner, U. & Sailer, H. Implantation and testing of subretinal film electrodes in domestic pigs. *Experimental Eye Research*. ISSN: 00144835. doi:10.1016/j.exer.2005.07.007 (2006).
179. Scott, P. A. *et al.* Progression of Pro23His Retinopathy in a Miniature Swine Model of Retinitis Pigmentosa. *Translational Vision Science & Technology*. ISSN: 2164-2591. doi:10.1167/tvst.6.2.4 (2017).
180. Grimm, C. & Remé, C. E. in *Methods in molecular biology (Clifton, N.J.)* 87–97 (2012). doi:10.1007/978-1-62703-080-9\_6. <<http://www.ncbi.nlm.nih.gov/pubmed/23150362>><[http://link.springer.com/10.1007/978-1-62703-080-9\\_6](http://link.springer.com/10.1007/978-1-62703-080-9_6)>.
181. Rösch, S. *et al.* Selective photoreceptor degeneration by intravitreal injection of N-methyl-N-nitrosourea. *Investigative Ophthalmology and Visual Science*. ISSN: 01460404. doi:10.1167/iovs.13-13242 (2014).
182. Rösch, S., Werner, C., Müller, F. & Walter, P. Photoreceptor degeneration by intravitreal injection of N-methyl-N-nitrosourea (MNU) in rabbits: a pilot study. *Graefe's Archive for Clinical and Experimental Ophthalmology*. ISSN: 1435702X. doi:10.1007/s00417-016-3531-7 (2017).
183. Noell, W. K. Experimentally Induced Toxic Effects on Structure and Function of Visual Cells and Pigment Epithelium. *American Journal of Ophthalmology* **36**, 103–116. ISSN: 0002-9394 (June 1953).
184. Noell, W. K. The effect of iodoacetate on the vertebrate retina. *Journal of Cellular and Comparative Physiology* **37**, 283–307. ISSN: 0095-9898 (Apr. 1951).
185. Winkler, B. S., Sauer, M. W. & Starnes, C. A. Modulation of the Pasteur effect in retinal cells: Implications for understanding compensatory metabolic mechanisms. *Experimental Eye Research* **76**, 715–723. ISSN: 00144835 (2003).

186. Orzalesi, N., Calabria, G. A. & Grignolo, A. Experimental degeneration of the rabbit retina induced by iodoacetic acid: A study of the ultrastructure, the rhodopsin cycle and the uptake of <sup>14</sup>C-labeled iodoacetic acid. *Experimental Eye Research* **9**, 246–253. ISSN: 0014-4835 (Apr. 1970).
187. Liang, L. *et al.* Long-term cellular and regional specificity of the photoreceptor toxin, iodoacetic acid (IAA), in the rabbit retina. *Visual Neuroscience* **25**, 167–177. ISSN: 09525238 (2008).
188. Yamauchi, Y. *et al.* Correlation between high-resolution optical coherence tomography (OCT) images and histopathology in an iodoacetic acid-induced model of retinal degeneration in rabbits. *British Journal of Ophthalmology*. ISSN: 00071161. doi:10.1136/bjo.2010.186718 (2011).
189. Scott, P. A., Kaplan, H. J. & Sandell, J. H. Anatomical evidence of photoreceptor degeneration induced by iodoacetic acid in the porcine eye. *Experimental Eye Research* **93**, 513–527. ISSN: 00144835 (2011).
190. Noel, J. M. *et al.* Iodoacetic acid, but not sodium iodate, creates an inducible swine model of photoreceptor damage. *Experimental Eye Research* **97**, 137–147. ISSN: 00144835 (2012).
191. Wang, W. *et al.* Selective rod degeneration and partial cone inactivation characterize an iodoacetic acid model of swine retinal degeneration. *Investigative Ophthalmology and Visual Science* **52**, 7917–7923. ISSN: 01460404 (2011).
192. Elmi, A. *et al.* H NMR Spectroscopy Characterization of Porcine Vitreous Humor in Physiological and Photoreceptor Degeneration Conditions (2019).
193. Lasansky, A. & Robertis, E. D. Submicroscopic Changes in Visual Cells of the Rabbit Induced by Iodoacetate. *The Journal of Cell Biology* **5**, 245–250. ISSN: 0021-9525 (Mar. 1959).
194. Bourne, R. R. *et al.* Causes of vision loss worldwide, 1990-2010: A systematic analysis. *The Lancet Global Health*. ISSN: 2214109X. doi:10.1016/S2214-109X(13)70113-X (2013).
195. Stingl, K. *et al.* Interim results of a multicenter trial with the new electronic subretinal implant alpha AMS in 15 patients blind from inherited retinal degenerations. *Frontiers in Neuroscience*. ISSN: 1662453X. doi:10.3389/fnins.2017.00445 (2017).
196. Luo, Y. H. L. & da Cruz, L. *The Argus® II Retinal Prosthesis System* 2016. doi:10.1016/j.preteyeres.2015.09.003.
197. WHO. WHO | *International Classification of Diseases, 11th Revision (ICD-11)* 2019.

198. Dagnelie, G. *et al.* Real and virtual mobility performance in simulated prosthetic vision. *Journal of Neural Engineering*. ISSN: 17412560. doi:10.1088/1741-2560/4/1/S11 (2007).
199. Pérez Fornos, A., Sommerhalder, J., Rappaz, B., Safran, A. B. & Pelizzone, M. Simulation of artificial vision, III: Do the spatial or temporal characteristics of stimulus pixelization really matter? *Investigative Ophthalmology and Visual Science*. ISSN: 01460404. doi:10.1167/iovs.04-1173 (2005).
200. Ghezzi, D. *et al.* A hybrid bioorganic interface for neuronal photoactivation. *Nature Communications*. ISSN: 20411723. doi:10.1038/ncomms1164 (2011).
201. Ghezzi, D. *et al.* A polymer optoelectronic interface restores light sensitivity in blind rat retinas. *Nature Photonics*. ISSN: 17494885. doi:10.1038/nphoton.2013.34 (2013).
202. Antognazza, M. R. *et al.* Characterization of a Polymer-Based, Fully Organic Prosthesis for Implantation into the Subretinal Space of the Rat. *Advanced Healthcare Materials*. ISSN: 21922659. doi:10.1002/adhm.201600318 (2016).
203. Ferlauto, L. *et al.* Development and characterization of PEDOT:PSS/alginate soft microelectrodes for application in neuroprosthetics. *Frontiers in Neuroscience*. ISSN: 1662453X. doi:10.3389/fnins.2018.00648 (2018).
204. Edwards, T. L. *et al.* Assessment of the Electronic Retinal Implant Alpha AMS in Restoring Vision to Blind Patients with End-Stage Retinitis Pigmentosa. *Ophthalmology*. ISSN: 15494713. doi:10.1016/j.ophtha.2017.09.019 (2018).
205. Stingl, K. *et al.* Subretinal Visual Implant Alpha IMS - Clinical trial interim report. *Vision Research*. ISSN: 18785646. doi:10.1016/j.visres.2015.03.001 (2015).
206. Maya-Vetencourt, J. F. *et al.* A fully organic retinal prosthesis restores vision in a rat model of degenerative blindness. *Nature Materials* **16**, 681–689. ISSN: 1476-1122 (June 2017).
207. Ghezzi, D. Retinal prostheses: progress toward the next generation implants. *Frontiers in neuroscience* **9**, 290. ISSN: 1662-4548 (2015).
208. Lorach, H. *et al.* Photovoltaic restoration of sight with high visual acuity. *Nature Medicine*. ISSN: 1546170X. doi:10.1038/nm.3851 (2015).

## List of Abbreviations

AAV	Adeno-associated Virus
AMD	Age-related Macular Degeneration
Cas	CRISPR-associated Gene
CHD	Choroideremia
CRD	Cone-rod Dystrophy
CRISPR	Clustered Regularly Interspaced Short Palindromic Repeats
gDNA	Genomic DNA
DSB	Double Strand Break
EGFP	Enhanced Green Fluorescent Protein
$\mu$ ERGs	Microelectroretinograms
fERG	Flash Electroretinography
prERG	Pattern-reversal Electroretinography
ELS	Early/Late Sham Rd10 Mice
ELT	Early/Late Treated Rd10 Mice
ES	Early Sham Rd10 Mice
ET	Early Treated Rd10 Mice
FACS	Fluorescent Activated Cell Sorting
GCL	Ganglion Cell Layer
GFP	Green Fluorescent Protein
cGMP	Cyclic Guanosine Monophosphate
HDR	Homologous Direct Repair
IAA	Iodoacetic Acid
IHC	Immunohistochemistry
indels	Insertions and Deletions
IPL	Inner Plexiform Layer
IRD	Inherited Retinal Disease
JMD	Juvenile Macular Degeneration
LCA	Leber Congenital Amaurosis
LT	Late Treated Rd10 Mice
MEA	Multi-electrode Array
MNU	N-metil-N-nitrosurea
N2A	Neuro 2A Cells
H&E	Hematossilin and Eosin Staining
NHEJ	Non-homologous End Joining
NSCs	Neural Stem Cells
OCT	Optical Coherence Tomography
ssODN	Single-stranded Oligonucleotide
OM	Optomotor
OPL	Outer Plexiform Layer
P(n)	Postnatal Day (n)

P3HT	Regioregular Poly(3-hexylthiophene-2,5-diyl)
PCBM	[6,6]-phenyl-C61-butyric Acid Methyl Ester
ddPCR	Droplet-digital Polymerase Chain Reaction
PDE6B	$\beta$ -domain of the Phosphodiesterase 6
PDMS	Poly(dimethylsiloxane)
PEDOT:PSS	Poly(3,4-ethylenedioxythiophene)-poly(styrenesulfonate)
PhR	Photoreceptors
Rd(n)	Retinal Degeneration (n) Mouse Model
Rho	Rhodopsin
gRNA	Guide RNA
RP	Retinitis Pigmentosa
RPE	Retinal Pigmented Epithelium
SFM	Serum Free Medium
VEGF	Vascular Endothelial Growth Factor
fVEP	Flash Visually Evoked Potentials
prVEP	Pattern-reversal Visually Evoked Potentials
VZ	Ventricular Zone
WT	Wild Type

## List of Publications with Detailed Contribution

### Peer-reviewed publications:

1. **Vagni P**, Perlini LE, Chenais NAL, Marchetti T, Parrini M, Contestabile A, Cancedda L, Ghezzi D. Gene editing preserves visual functions in a mouse model of retinal degeneration. *Front. Neurosci.* 2019.  
[DOI: 10.3389/fnins.2019.00945](https://doi.org/10.3389/fnins.2019.00945).  
*Contribution:* I performed all the experiments and wrote the manuscript.
2. Gaillet V\*, Cutrone A\*, Artoni F\*, **Vagni P**, Romero Pinto SA, Lipucci Di Paola D, Micera S, Ghezzi D. Spatially selective activation of the visual cortex via intraneural stimulation of the optic nerve. *Nat. Biomed. Eng.* 2019.  
[DOI: 10.1038/s41551-019-0446-8](https://doi.org/10.1038/s41551-019-0446-8).  
*Contribution:* I performed the *in vivo* validation of the device (surgeries and recordings), the histological experiments, and the statistical analysis of the fibre diameter distribution in the optic nerve.
3. Airaghi Leccardi MJL, **Vagni P**, Ghezzi D. Multilayer 3D electrodes for neural implants. *J. Neural. Eng.* 2019.  
[DOI: 10.1088/1741-2552/aae191](https://doi.org/10.1088/1741-2552/aae191).  
*Contribution:* I performed the surgeries and set-up the visually evoked potential experiment and the data analysis for the *in vivo* validation of the device. I also performed the clarity and whole brain imaging.
4. Ferlauto L, D'Angelo AN, **Vagni P**, Airaghi Leccardi MJI, Mor FM, Cuttaz EA, Heuschkel MO, Stoppini L, Ghezzi D. Development and Characterization of PEDOT:PSS/Alginate Soft Microelectrodes for Application in Neuroprosthetics. *Front. Neurosci.* 2018.  
[DOI: 10.3389/fnins.2018.00648](https://doi.org/10.3389/fnins.2018.00648).  
*Contribution:* I performed the surgeries and set-up the visually evoked potential experiment and the data analysis for the *in vivo* validation of the device.
5. Ferlauto L\*, Airaghi Leccardi MJI\*, Chenais NAL\*, Gilliéron SCA, **Vagni P**, Bevilacqua M, Wolfensberger TJ, Sivula K, Ghezzi D. Design and validation of a foldable and photovoltaic wide-field epiretinal prosthesis. *Nat. Commun.* 2018.  
[DOI: 10.1038/s41467-018-03386-7](https://doi.org/10.1038/s41467-018-03386-7).  
*Contribution:* I performed the simulated surgeries on pig eyes.

### Publications in preparation:

1. Ferlauto L\*, **Vagni P\***, Zollinger EG, Fanelli A, Paolicelli RC, Ghezzi D. Towards polymer-based transient devices for applications in neuroprosthetics. Manuscript in preparation.



*Contribution:* I performed and analysed *in vivo* experiments, set up the anatomical/histological evaluation, and participated in writing the manuscript.

2. **Vagni P** et al. Manuscript in preparation.

*Contribution:* I performed and analysed *in vivo* electrophysiological experiments, set up the anatomical/histological evaluation, and participated in writing the manuscript.

# PAOLA VAGNI *Curriculum Vitae*

ADDRESS Boulevard des Philosophes 16, 1205 Geneva, Switzerland

PHONE +41 78 810 77 67

EMAIL [paola.vagni@epfl.ch](mailto:paola.vagni@epfl.ch); [paola.vagni@protonmail.ch](mailto:paola.vagni@protonmail.ch)

NATIONALITY Italian

ORCID ID <https://orcid.org/0000-0003-1107-0947>

## LANGUAGES

---

ITALIAN Native

ENGLISH Fluent

FRENCH B2

## EDUCATION

---

BACHELOR IN BIOTECHNOLOGY (2008-2011)

University of Pavia, Italy

MASTER IN NEUROBIOLOGY (2011-2013)

University of Pavia, Italy

RESEARCH INTERNSHIP (2014-2015)

Istituto Italiano di Tecnologia, Genova, Italy

PhD IN NEUROSCIENCE (2015-present)

EPFL Medtronic Chair in Neuroengineering, Geneva, Switzerland

## SKILLS

---

### IT SKILLS :

- Microsoft Office (Word, PowerPoint, Excel).
- Matlab: data manipulation, plotting, and statistics.
- Adobe Illustrator: images and posters.
- Imaging software: ImageJ, Nikon, Imaris.
- Biomedical software for electrophysiological recordings: WinAver, MCRack.
- Biomedical software for behavioural experiments: Cerebral Mechanics.
- LaTeX for scientific papers and documents.

### TECHNICAL SKILLS :

- Experience with handling and experimental procedures on different animal models: mice, rats, rabbits, and minipigs.
- Surgeries on brain and retina (injections, implants, lesions etc.).
- Setup and validation of electrophysiological recordings *in vivo*: VEPs and ERGs.
- Setup and validation of visual behavioural tests: Prusky water maze and Optomotor test.
- Histological techniques: tissue preparation, slicing, and IHC.

- Molecular and cellular biology techniques: primary cell cultures, PCR analysis, restriction analysis, DNA purification, cloning.
- Imaging techniques: bright field, fluorescence, confocal, slide scanner, clarity techniques, and whole brain imaging.

#### TRANSFERABLE SKILLS :

- Supervision of Bachelor and Master students.
- Teaching assistance in several courses at the Bachelor and Master level: Biomaterials, Laboratory of Physiology, Literature Analysis in Bioengineering.
- Course of Scientific Writing (Language Center, EPFL).
- Experience in the presentation of scientific results to a large specialized audience.

#### PEER REVIEWED PUBLICATIONS

---

1. **Vagni P**, Perlini LE, Chenais NAL, Marchetti T, Parrini M, Contestabile A, Cancedda L, Ghezzi D. Gene editing preserves visual functions in a mouse model of retinal degeneration. *Front. Neurosci.* 2019. <https://doi.org/10.3389/fnins.2019.00945>.
2. Gaillet V\*, Cutrone A\*, Artoni F\*, **Vagni P**, Romero Pinto SA, Lipucci Di Paola D, Micera S, Ghezzi D. Spatially selective activation of the visual cortex via intraneural stimulation of the optic nerve. *Nat. Biomed. Eng.* 2019. <https://doi.org/10.1038/s41551-019-0446-8>.
3. Airaghi Leccardi MJL, **Vagni P**, Ghezzi D. Multilayer 3D electrodes for neural implants. *J. Neural. Eng.* 2018. <https://doi.org/10.1088/1741-2552/aae191>.
4. Ferlauto L, D'Angelo AN, **Vagni P**, Airaghi Leccardi MJI, Mor FM, Cuttaz EA, Heuschkel MO, Stoppini L, Ghezzi D. Development and Characterization of PEDOT:PSS/Alginate Soft Microelectrodes for Application in Neuroprosthetics. *Front. Neurosci.* 2018. <https://doi.org/10.3389/fnins.2018.00648>.
5. Ferlauto L\*, Airaghi Leccardi MJI\*, Chenais NAL\*, Gilliron SCA, **Vagni P**, Bevilacqua M, Wolfensberger TJ, Sivula K, Ghezzi D. Design and validation of a foldable and photovoltaic wide-field epiretinal prosthesis. *Nat. Commun.* 2018. <https://doi.org/10.1038/s41467-018-03386-7>.

#### CONFERENCE PRESENTATIONS

---

1. Gene Editing in Photoreceptor Progenitors Prevents Visual Function Loss in a Mouse Model of Retinal Degeneration. Poster Presentation. ARVO (Association for Research in Vision and Ophthalmology) Annual Meeting. Baltimore (USA), May 2017.
2. Preventing Visual Function Loss in the Rd10 Mouse Model of *Retinitis Pigmentosa* using gene editing. Talk. ERM (European Retina Meeting). Paris (France), October 2017.
3. Gene editing preserves visual function in a mouse model of retinal degeneration. Poster Presentation. FENS (Forum European Neuroscience Society). Berlin (Germany), July 2018.

#### REFERENCES

---

Prof. Diego Ghezzi [diego.ghezzi@epfl.ch](mailto:diego.ghezzi@epfl.ch)  
 Medtronic Chair in Neuroengineering, EPFL (Geneva, Switzerland)

Dr. Andrea Contestabile [andrea.contestabile@iit.it](mailto:andrea.contestabile@iit.it)  
 Department of Neuroscience and Brain Technologies, IIT (Genova, Italy)

Dr. Laura Cancedda [laura.cancedda@iit.it](mailto:laura.cancedda@iit.it)  
 Department of Neuroscience and Brain Technologies, IIT (Genova, Italy)